12-9-2016

Characterization of Microparticles through Digital Holography

Nava Raj Subedi

Characterization of microparticles through digital holography

By

Nava Raj Subedi

A Dissertation
Submitted to the Faculty of
Mississippi State University
in Partial Fulfillment of the Requirements
for the Degree of Doctor of Philosophy
in Applied Physics
in the Bagley College of Engineering

Mississippi State, Mississippi

December 2016

Characterization of microparticles through digital holography

By

Nava Raj Subedi

Approved:

_____

Matthew J. Berg
(Major Professor)

_____

Chuji Wang
(Committee Member)

_____

Donna M. Pierce
(Committee Member)

_____

Yaroslav Koshka
(Committee Member)

_____

Hendrik F. Arnoldus
(Committee Member/ Graduate Coordinator)

_____

Jason M. Keith
Dean
Bagley College of Engineering

Name: Nava Raj Subedi

Date of Degree: December 9, 2016

Institution: Mississippi State University

Major Field: Applied Physics

Major Professor: Matthew J. Berg

Title of Study: Characterization of microparticles through digital holography

Pages in Study: 118

Candidate for Degree of Doctor of Philosophy

In this work, digital holography (DH) is extensively utilized to characterize microparticles. Here, "characterization" refers to the determination of a particle's shape, size, and, in some cases, its surface structure. A variety of microparticles, such as environmental dust, pollen, volcanic ash, clay, and biological samples, are thoroughly analyzed. In this technique, the microscopically fine interference pattern generated by the coherent superposition of an object and a reference wave fields is digitally recorded using an optoelectronic sensor, in the form of a hologram, and the desired particle property is then computationally extracted by performing a numerical reconstruction to form an image of the particle.

The objective of this work is to explore, develop, and demonstrate the feasibility of different experimental arrangements to reconstruct the image of various arbitrary-shaped particles. Both forward- and backward-scattering experimental arrangements are constructed and calibrated to quantify the size of several micron-sized particles. The performance and implications of the technique are validated using the National Institute of Standards and Technology (NIST)-traceable borosilicate glass microspheres of various diameters and a Thorlabs resolution plate. After successful validation and calibration of

the system, the resolution limit of the experimental setup is estimated, which is ~10 microns. Particles smaller than 10 microns in size could not be imaged well enough to ensure that what appeared like a single particle was not in fact a cluster. The forward- and backward-scattering holograms of different samples are recorded simultaneously and images of the particles are then computationally reconstructed from these recorded holograms. Our results show that the forward- and backward-scattering images yield different information on the particle surface structure and edge roughness, and thus, reveal more information about a particle profile. This suggests that the two image perspectives reveal aspects of the particle structure not available from a more commonly used forward-scattering based image alone. The results of this work could be supportive to insight more on the particles' morphology and subsequently important for the advancement of contact-free particle characterization technique.

DEDICATION

To my parents,

Padam Lal Subedi and *Sushila Subedi*

whose blessings have always strengthened me at every step of my life.

To my wife,

Sabita

for all of her love, care, and support.

To my son

Shuvam

for all of his curiosity, incentive, and inspiration to do something better.

ACKNOWLEDGEMENTS

I would like to express my sincere indebtedness to Dr. Matthew J. Berg for his patient guidance throughout the work as a major advisor in my doctoral research. His endless support, continued encouragement, and invaluable assistance at all times has been of immense value in the successful accomplishment of this dissertation work. My long, daring journey of pursuing my Ph.D. in the United States would not have been so smooth without his inspiration, devoted time, and readiness to support in each and every step. He is the one who has taught me the ways to work and survive in the realm of experimental physics. He has not only guided me through this uppermost level of education, but more meaningfully, he has instilled in me his infectious passion for physics research that I will carry forward with me and feast among my peers.

I would like to extend my sincere gratitude to Dr. Henk F. Arnoldus for his exemplary role as a teacher and graduate coordinator during this journey. I would like to further extend my indebtedness to Dr. Chuji Wang, Dr. Donna M. Pierce, and Dr. Yaroslav Koshka for readily accepting to serve as a committee member of my dissertation committee and providing me valuable suggestions and encouragement throughout the work.

I would also like to express my earnest appreciation to Dr. Mark A. Novotny (Head, Department of Physics and Astronomy) and other faculty members of our department for their enthusiastic encouragement and suggestions during the work. This

acknowledgment will be incomplete if I forget to take the name of a person who has guided me in so many ways to come this far in academic journey, Dr. David L. Monts. I sincerely thank Dr. Monts for being a part of my academic journey and helping me in all possible ways. I am also thankful to the staff of our department for their assistance during various projects. I am especially thankful to Mr. Ben Ardahl for making several custom-instruments for my experiments. I thank Ms. Susan Galloway, Ms. Connie Vaughn, and Ms. Joe McKenzie for their administrative assistance all the time. I also appreciate the support offered by my colleagues Mr. Jehan Seneviratne, Mr. Satam Alotibi, Ms. Jing Wen, and Mr. Peter Anderson.

I acknowledge the financial support provided for my research by the US Army Research Office and the National Science Foundation. I also thank our Department of Physics and Astronomy for proving me a teaching assistant position in various semesters during my doctoral program. I am also thankful to the Bagley College of Engineering and Graduate School for providing me funding to attend workshops and conferences. I am also thankful to the Bagley College of Engineering Writing Center tutors, Ms. Karleigh Kimbrell and Ms. Tori Bruno, for the careful proofreading of this dissertation.

I am indebted to my family and friends for their love, support, and encouragement during this long journey. Above all, I owe all my academic accomplishments and successes to my parents, Mr. Padam Lal Subedi and Mrs. Sushila Subedi. The sacrifices made by them have taken me this far in my life. I am greatly thankful to all my relatives and friends for being part of my life. In this cherished movement, I could not forget better half of my life, my wife, Sabita; and my lovely son, Shuvam for providing

me incentive, support, and inspiration during all the time of my work. Without their support, I could not imagine any success of the work.

Finally, I thank God for blessing me with the strength, courage, and determination, without which I would have never reached to this journey of my life.

TABLE OF CONTENTS

LIST OF TABLES

LIST OF FIGURES

CHAPTER I

INTRODUCTION

Aerosols are small particles ranging in size from about one nanometer to tens of microns and suspended in the air with a lifetime of at least minutes. These particles are ubiquitous in nature and greatly influence properties of the system in which they reside. However, the lack of understanding about the physical properties and chemical composition of these particles greatly limits our ability to understand, predict, and control their applications and impacts in the system [1, 2]. The recent progress in technology makes it possible to characterize these particles and study their properties in controlled environments, but the contact-free characterization of such particles is still challenging. Typically, "characterization" refers to the determination of a particle's shape, size, and in some cases, it material compositions. Often, this must be done in a contact-free manner as the collection of samples for microscope-based characterization may distort the true morphology (e.g., considers liquid or frozen particles). Therefore, the contact-free characterization of these particles is an important objective in many scientific and engineering applications.

There are various laboratory-based techniques available in the scientific community for imaging and characterization of micron-sized particles. These particles' characterization techniques can be classified into two categories: microscopy and spectroscopy. The microscopy-based techniques, such as light microscopy, X-ray

diffraction, transmission electron microscopy (TEM), scanning electron microscopy (SEM), atomic force microscopy (AFM), scanning probe microscopy (SPM), etc., are widely available for the analysis of particles' physical structures such as shape, size, and surface roughness. On the other hand, the spectroscopy-based techniques available for composition analysis are mass spectrometry (MS), X-ray spectroscopy (XRS), electron spectroscopy (ES), secondary ion mass spectroscopy (SIMS), atomic absorption spectroscopy (AAS), X-ray fluorescence (XRF), laser spectroscopy [3, 4]. Even though there are many well-established techniques in the scientific community, they are all laboratory-based and need a collection of samples, and rapid particle on-the-fly characterization is not possible. Ideally, the scientific community would prefer to characterize these particles directly and is continuously looking for a high-speed, contact-free, and non-invasive new instrumentation technique for optical imaging, extinction cross-section measurement, and characterization of a variety of micron-sized particles. This motivates the uses of the light-scattering approach due to its inherent contact-free nature.

The newly developed digital holography (DH) technique can be one of the best particle imaging and characterization techniques (details about the technique will be explained in Chapter II and III). With the recent availability of high-resolution image acquisition (charge-coupled device (CCD) camera or Complementary metal-oxide-semiconductor (CMOS) camera) devices and advanced computer technology, the field of holography has evolved greatly over the past two decades from using photographic plates as a recording media to employing very sensitive CCD cameras to record holograms and numerical reconstruction techniques to display computationally processed images. This

advancement in the electronic imaging devices - larger arrays, smaller pixels, faster processing, and bigger storage data sets - makes digital holography more feasible and sensitive to a wide range of new capabilities [5, 6]. The increasing processing speed followed by electronic acquisition and numerical reconstruction of the image replaces the lengthy and tedious photochemical procedures of conventional holography and opens a new door to broader applications. Digital holography not only allows contact-free tracking of a variety of particles, but it also enables potentially near real-time image reconstruction and rapid particle on-the-fly characterization, which are either difficult or impossible to implement using the traditional film-based technique [7]. However, DH technique is free from these drawbacks and offers real-time *in situ* characterization of the atmospheric aerosols, ambient pollens, and many biological samples. This emerging technique avoids many of the drawbacks of the conventional holography and offers some possibilities not given by conventional optical microscopy. In particular, the characterization of small aerosol particles is possible with such techniques and has important applications, including the determination of atmospheric aerosol compositions for climate modeling, the detection of biological weapons agents for defense applications, and the *in vitro* and *in vivo* studies of various living species in life sciences and biomedical applications [8-12].

The major advantage of DH is that chemical procession of the hologram is suppressed, thus adding more flexibility and speed to the holographic process. The recent advances in the computer performance and digital sensor array have made digital holography an option for many applications. Unlike the conventional technique, digital holography offers a means of measuring both optical amplitude and phase data in the

recording medium. The optical amplitude describes the brightness, and the phase data contains the size and shape information of the object [18]. This makes a hologram capable of holding complete optical information on the particle profile and typically delivers three-dimensional surface or optical thickness images during the reconstruction. The progress in recording devices and processing schemes have made DH capable of assessing many optical wave characteristics such as phase, amplitude, and polarization state, making DH a very powerful method for different promising applications [7, 11, 19]. On the other hand, digital holographic microscopy (DHM) has been widely applied as a quantitative phase imaging tool to analyze topographies of living cells on both macroscopic and microscopic scales. In this dissertation, DH technique in imaging, and, in some cases, in investigating surface texture of microparticles, is emphasized.

This work explores several techniques in digital holography to image 10-300 μm sized particles and provide information useful for their characterization. Different experimental configurations to record both forward- and backward-scattering holograms are established. Images of these particles are then rendered from the holograms using Fresnel-Kirchhoff diffraction theory, presented in Chapter III. The forward- and backward-scattered light holograms are obtained simultaneously so that a side-by-side comparison of the two images is possible. This imaging modality will be helpful to establish a new method for tomographic imaging and topographic surface outlining in micrometer scale and, eventually, execute three-dimensional image of the particle.

1.1 Research motivation

As previously mentioned, the contact-free characterization of small particles is a persistent objective in applied electromagnetic scattering applications. Optical

microscopes have been used as a central instrument for centuries to see objects that are orders of the magnitude smaller than what our naked eyes can see. Unfortunately, these conventional imaging devices only resolve the objects within a certain limit and face serious drawbacks when the size of the particle is in the micron range. In that case, imaging from this conventional technique becomes quite complex, bulky, and highly expensive, in addition to having a limited depth-of-field due to the need for larger numerical aperture and bigger lens-based optical magnification [11-13].

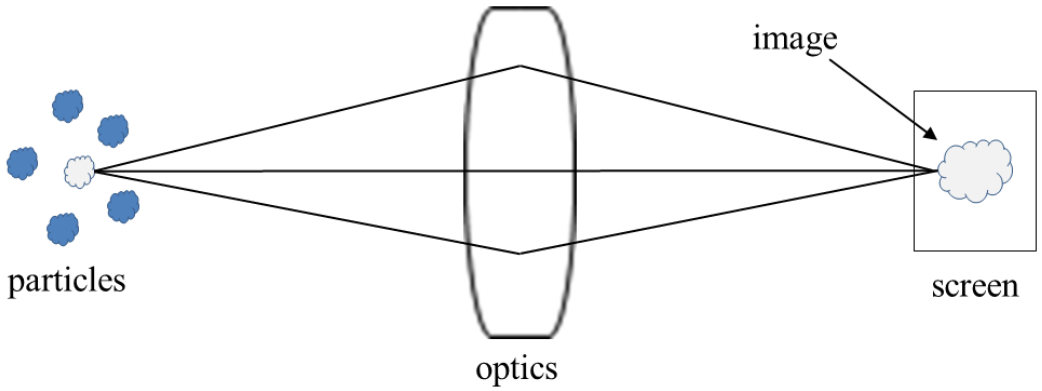

Figure 1.1 Schematic diagram of conventional optical microscopy.

However, current research trends require more accurate data, precise measurement, the inclusion of a wide range of samples, and real-time imaging techniques. All these are possible only with high numerical-aperture (NA) optics in the small focal volume. This typically requires collection and immobilization of particle samples, and thus, such imaging is not a practical technique for particle characterization in many applications requiring high sample throughput or images of the particle in their undisturbed form. However, with the available resources, traditional microscopy cannot

extend that far, and there is an ongoing search for alternative methods that can fulfill these requirements. Therefore, DH can be an alternative technique that incepts the useful properties of conventional imaging technique and provides some unique features of its own.

Since DH is largely free from these limitations and capable of providing a real-time image, it can be the best substitute for numerous imagery applications. In DH method, computation is used to replace bulky components of traditional imaging devices to reduce the size, cost, and complexity, in addition to broadening the imaging field-of-view. This technique can be assembled in a compact, cost-effective, and lightweight manner.

Unlike the conventional technique, in the holographic design, there are no optical elements between the particle and sensor in order to reach a desired field-of-depth and magnification. Therefore, there are no surfaces on which ambient dust can collect and become sources of stray light, nor are there any lens-based spherical aberrations, distortion, or multiple reflections. The absence of these optical elements in the holographic design is especially advantageous when one wishes to investigate particles that are roughly the same size as ambient dust [14]. This is because of the absence of optical elements will help to eliminate a large degree of noise that can result from ambient dust that collects on the optical surface. Moreover, this gives a working distance for the apparatus of several centimeters, which is substantially greater than the single- to sub-millimeter working distance of the microscope objective in conventional microscopy. Additionally, with the holographic technique, a single-shot hologram provides different perspectives of single or multiple particles [20]. Unlike the conventional microscopic

technique, where the images at different focus-depths convey a sense of a particle's 3D structure, in DH this focusing can be done computationally by varying the reconstruction distance [21-23].

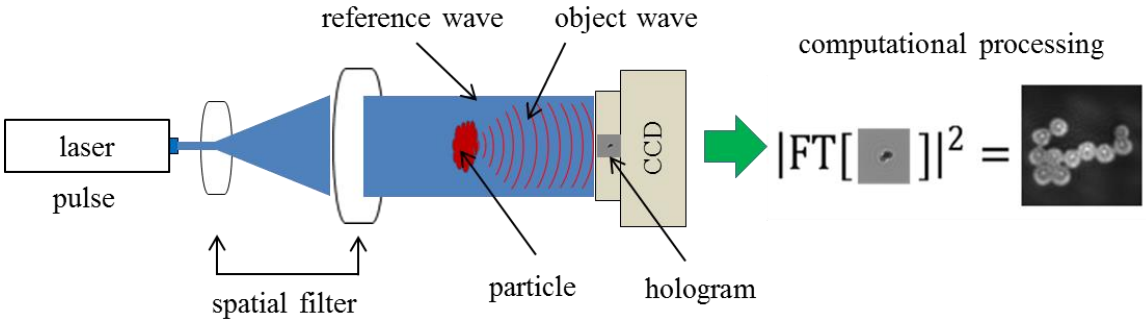

Figure 1.2 Schematic diagram of digital holographic microscopy.

A detail about the procedure in the digital holographic microscopy is provided in the later chapters.

One motivation for this work is to study the feasibility of different DH alignments and layout the foundation for a high-speed, contact-free, and non-invasive new instrumentation technique for optical imaging, extinction cross-section measurement, and, eventually, characterization of a variety of micron-sized particles. The performance of DH heavily relies on the experimental setup, sensitivity of the sensor, wavelength of the illuminating source, and the hologram processing method. In this work, I study the feasibility of different experimental layouts and their capability to image single and multiple particles from holograms derived from scattered light from different directions.

1.2 Research objective

This work explores the feasibility of imaging of single and multiple microparticles and investigating their surface structures through digital holography using

both forward- and backward-scattered light rather than the more commonly and solely used forward-scattered light. Furthermore, this work also demonstrates the feasibility of the experimental alignments of DH, which shows the capability of analyzing two different samples simultaneously. The most commonly used traditional digital holographic technique uses a particle's forward scattering light to form a hologram, whereas this work uses both forward- and backward-scattered light simultaneously so that a side-by-side comparison of the two reconstructed images is possible. Besides this, this work also demonstrates the feasibility of imaging two different samples due to both forward- and backward-scattered light holograms simultaneously. In the traditional holographic microscope arrangement (i. e., that using the forward-scattered light), an opaque particle yields only its silhouette after image reconstruction. Thus, the particle surface information is obscured. By using backward-scattered light, however, it may be possible to discern surface textures, or structural features that are sufficiently larger than the diffraction limit [15]. A variety of microparticles, such as environmental dust, pollen, volcanic ash, clay, and biological samples are thoroughly analyzed using different alignments. In this research work, I have mostly focused on the experimental designs and on demonstrating the feasibility and applicability of the design to the various applications. Therefore, this work eventually helps in extending the capability of DH to a wide range of applications including non-invasive imaging of both transparent (suitable on forward-scattering configuration) and opaque (suitable on backward-scattering configuration) samples. Furthermore, this work makes DH equally suitable for the study of a variety of biological samples in many biomedical applications.

The main objective of this work is to lay the foundation for the eventual development of a portable sensor that will characterize man-made and naturally occurring aerosol particles. The future goal of this work is to improve the resolution of the image down to the sub-micron range and extend DH's capability to measure *optical observables*, such as the scattering pattern, total cross sections, and single-scattering albedo, and develop a real-time particle characterization methodology.

1.3 Research contribution

This work has been aimed to contribute to the study of aerosols particles especially in characterizating their physical form and light-scattering behavior. Some selective contributions include, but are not limited to:

1.3.1 Inclusion of wide range of samples

Making DH work for both forward- and backward-scattered light and capable of analyzing multiple samples simultaneously would allow us to investigate a wide variety of samples, including both transparent and opaque samples. Transparent samples, such as living cells, which are soft and have little natural color contrast, are suitable in forward-scatting configuration, and opaque samples, such as highly reflecting particles and thick objects, are suitable in backward-scattering configuration. Therefore, a key advantage of this work is that it can allow a real-time investigation of different samples by recording holograms derived from different light scattering directions that have been very difficult or infeasible to achieve in the past and process the recorded holograms to better compare different views.

1.3.2 Rendering 3-D information

In DH, the recorded hologram contains all information from the object profile needed to reconstruct the image, and it is possible to reconstruct the image at any given focal plane by changing the focal distance parameter in the reconstruction algorithm. This makes it possible to fully characterize the optical characteristics of an object and numerically reconstruct the images of the object at the selected two-dimensional imaging plane within three-dimensional recording volume. This allows a variety of analyses to be performed, which are either difficult or impossible to achieve using any traditional methods.

1.3.3 Digital autofocusing

In the conventional photomicroscope, images have a very narrow depth-of-field, and only particles constrained within a narrow volume are in focus. The focusing is achieved by changing the focal distance until a focused image plane is found; whereas, in DH the focusing is done computationally after the hologram is recorded. It is possible to use any passive autofocus method to digitally select the focal plane. This digital focusing capability of DH opens up the possibility to scan and image object's surfaces extremely fast. This enables DH to use for imaging multiple particles present at different locations and in different depths in the measurement volume [16].

1.3.4 Building foundation for low-cost microscopy system

In traditional microscopy systems, optical aberrations are corrected by combining lenses into a complex and costly microscope objective. Furthermore, the narrow focal depth at high magnification requires high precision mechanics. This tremendously

increases the cost of microscopy systems, but DH systems do not have an image forming lens, and traditional optical aberrations do not apply. In DH, optical aberrations are corrected using appropriately designed reconstruction algorithms. Also, in traditional microscopy systems, only one sample can be examined at a given time after suitably preparing the sample. Since DH is free from all these limitations, it offers a very low-cost digital holographic microscopy system. The result of this work provides the feasibility of different experimental alignments and their capabilities for imaging a variety of microparticles so this work helps to contribute some basic ideas in building future low-cost microscopy system.

1.4 References

1. P. Kulkarni, P. A. Baron, and K. Willeke, *Aerosol Measurement: Principles, Techniques, and Applications*, 3rd ed. (Wiley, 2011).

2. National Research Council (US) Chemical Sciences Roundtable, "*Challenges in Characterizing Small Particles: Exploring Particles from the Nano- to Microscale: A Workshop Summary. Washington (DC): National Academics Press (US); 2012. 2, What Are Small Particles and Why Are They Important?*" Available from: http://www.ncbi.nlm.nih.gov/books/NBK98070/

3. W. D. Callister and D. G. Rethwisch, *Materials Science and Engineering: An Introduction,* 8th ed. USA; John Wiley & Sons, Inc., (2009).

4. Y. Leng, *Materials Characterization: Introduction to Microscopic and Spectroscopic Methods:* John Wiley & Sons (Asia) Pte Ltd., Singapore (2008).

5. M. K. Kim, *Digital Holographic Microscopy: Principles, Techniques, and Applications* (Springer Series in Optical Sciences, 2011).

6. T. Kreis, *Handbook of holographic interferometry: Optical and digital methods* (Wiley-VCH, 2005).

7. U. Schnars and W. Jueptner, *Digital Holography: Digital Hologram Recording, Numerical Reconstruction, and Related Techniques* (Springer, Berlin 2010).

8. D. Gabor, "A new microscopic principle," *Nature* **161**(4098), pp. 777-778 (1948).

9. M. I. Mishchenko, L. D. Travis, and A. A. Lacis, *Scattering, Absorption, and Emission of Light by Small Particles* (Cambridge, 2002).

10. V. Mico, C. Ferreira, Z. Zalevsky, and J. Garcia, "Basic principles and application of digital holography microscopy," (Formatex, 2010).

11. M. K. Kim, "Principles and techniques of digital microscopy," SPIE Rev. **1**(1). 018005 (2010).

12. Z. Gorocs and A. Ozcan, "On-chip biomedical imaging," IEEE Rev Biomed Eng **6**, pp. 29-46 (2013).

13. M. Lee, O. Yaglidere, and A. Ozcan, "Field-portable reflection and transmission microscopy based on lensless holography," *Biomed. Opt. Express* **2**(9), pp. 2721-2730 (2011).

14. M. J. Berg and G. Videen, "Digital holographic imaging of aerosol particles in flight," *J. Quant. Spectrosc. Radiat. Transfer* **112**(11), pp. 1776-1783 (2011).

15. N. R. Subedi, N. B. Fowler, and M. J. Berg, "Backscatter digital holography of microparticles," *Opt. Express* **21**(10), pp. 12611-12616 (2013).

16. W. Xu, M. H. Jericho, I. A. Meinertzhagen, H. J. Kreuzer, "Digital in-line holography of microparticles," *Appl. Optics* **41**(25), pp. 5367-75 (2002).

17. K. B. Aptowicz, R. G. Pinnick, S. C. Hill, Y. L. Pan, and R. K. Change, "Optical scattering patterns from single urban aerosol particles at Adelphi, Maryland, USA: a classification relating to particle morphologies," *J. Geophys. Res.* **111**, D12212 (2006).

18. G. K. Ackermann and J. Eichler, *Holography: A Practical Approach* (Wiley, 2007).

19. T. Colomb, P. Dahlgren, D. Beghuin, E. Cuche, P. Marquet, and C. Depeursinge, "Polarization imaging by use of digital holography," *App. Optics* **41**(1), pp. 27-37 (2002).

20. Y. Frauel, T. J. Naughton, O. Matoba, E. Tajahuerce, and B. Javidi, "Three-dimensional imaging and processing using computational holographic imaging," *Proceedings of the IEEE* **94**(3), pp. 636-653 (2006).

21. P. McElhinney, B. M. Hennelly, and T. J. Naughton, "Extended focused imaging for digital holograms of macroscopic three-dimensional objects," *App. Opt.* **47**(19), pp. D71-D79 (2008).

22. F. Palacios, J. Ricardo, D. Palacios, E. Gonçalves, J. L. Valin, R. De Souza, "3D image reconstruction of transparent microscopic objects using digital holography," *J. Quant. Spectrose. Radiat. Transf.* **248**(1-3), pp. 41-50 (2005).

23. S. Grilli, P. Ferraro, S. De Nicola, A. Finizio, G. Pierattini, and R. Meucci, "Whole optical wavefields reconstruction by digital holograpy," *Optics Express* **9**(6), pp. 294-302 (2001).

CHAPTER II

GENERAL OPTICAL CONCEPT OF HOLOGRAPHY

Holography was first introduced in 1948 by Denis Gabor in an effort to improve the resolution of the electron microscope, where the correction of the electron lens aberration posed increasing technical difficulty. When working with an electron microscope, he realized that the diffracted wave of an object can be recorded and reconstructed with the help of an interference pattern containing the complete amplitude and phase information of the diffracted wave. Instead of attempting to perfect the electron imaging system, Gabor laid down theoretical foundations and anticipated novel and important features of the new imaging methods, such as aberration compensation by replicating the aberrations of the recording optics in the reconstruction optics. Being able to save both amplitude and phase information, he named his discovery after the Greek words **ὅλος** = "holos-" meaning "whole or complete" and **γραφὴ** = "graphē-" meaning "record or to write." Thus, the word holography stands for the complete recording of information on the object profile [1, 2, 3]. The original concept first presented by Gabor is shown in Fig. 2.1. At that time, the lack of light sources of sufficiently high coherence and intensity prevented much progress in optical holography, and the actual potential of the technique was realized only after the invention of the laser in the 1960's. The discovery of laser, a strong coherence source of light, makes holography capable of opening completely new possibilities in science and engineering. With its many

applications, holography is considered to be one of the most fascinating discoveries of the 20th century.

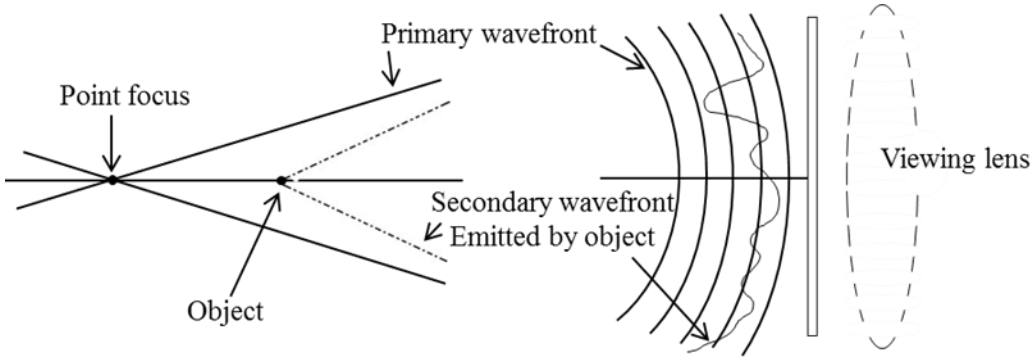

Figure 2.1 The original concept presented by Gabor when he first introduced holography as a new microscopic technique.

The plot is adapted from Gabor's original paper, "A new microscopic principle."

Fundamentally, holography is a two-step process: recording and reconstruction. First, an object is illuminated by a coherent source of light, and then the microscopically fine intensity pattern generated by the superposition of unscattered light with that scattered by a particles is recorded. This pattern constitutes the hologram. Second, an image of the object is reconstructed using numerical reconstruction algorithm on the recorded hologram computationally.

Holography uses the properties interference and diffraction of light, which make it possible to reconstruct the object wave completely. To be able to see these effects, a coherent light source, such as a laser, has to be used. Unlike the photography, holography offers a number of significant advantages, such as the ability to acquire holograms rapidly, availability of complete amplitude and phase information of the optical field, and

versatility of the interferometric and image processing techniques [4]. Depending on the nature of recording and reconstruction process, holography is classified into three types.

1.1 Conventional or analog holography

In conventional holography, the hologram is recorded using photographic film or any other media whose optical transmission or reflection properties change in response to the light intensity impinging on it [4]. To get the final image of the particle, the photographic film should be processed through a chemical development. The subsequent chemical development of the film is time-consuming, cumbersome, and costly. Also, real-time processing of a conventional hologram is not feasible unless one uses photo-refractive and other nonlinear optical materials. This greatly limits the practical utility of the technique.

2.2 Digital holography

In this holography, the interference pattern is recorded on a digital device, either a charge-coupled device (CCD) chip or complementary metal-oxide-semiconductor (CMOS) chip of a digital camera, but the basic principle is same as the conventional holography. This means that an opto-electronic sensor digitizes the hologram and reconstruction of an image is performed numerically in a computer from that digitized hologram. In DH, holograms are numerically reconstructed at selected two-dimensional (2D) image plane within a three-dimentional (3D) recording volume to render the shape, size, surface roughness, and orientation of the object without *a priori* information. Although DH yields a high depth resolution, the range for reconstruction is restricted to the half of the wavelength of the light used during the recording of the hologram. This

restriction occurs due to a 2π phase ambiguity when the phase is calculated [4, 10]. However, it can be improved using several measurements at different wavelengths. Unfortunately, DH also imposes some constraints upon the available recording configurations which are generally more restrictive than those required for analog holography [5].

The unique capability of DH is that some sense of the three-dimensional form of an object's image can be computed from a single recorded hologram [7]. The basic idea is analogous to the "focusing in" on an object in conventional microscopy. In the conventional microscopy, the microscope objective is moved to vary the distance between it and the microscope slide, causing a blurred image of a particle to evolve into a sharp image. For a sufficiently thick and transparent object, different depths within the object can be brought into focus to give a real sense of the particle's three-dimensional structure. This same process can be done in digital holography by computationally varying the distance used in the image reconstruction stage [8]. The resulting sequence of images gives the same impression of focusing-in on the object as one gets from a microscope. However, unlike microscopy where an image must be recorded at each "focus depth," the holography route can obtain a similar image sequence from a single recorded hologram only. The image location and magnification are dependent on, and therefore can be controlled by, the selection of wavelengths, reference directions, and curvatures. Different adaptive optics can be employed for both transparent and reflective objects. The positive lenses are typically used in DH to increase magnification; negative lenses are sometimes employed to reduce the apparent size of objects otherwise too large

to record holographically [4-6]. The three most commonly used digital holography setups are shown in Fig. 2.2 below.

In Fig. 2.2(a) a Gabor type setup (the actual Gabor setup used a photographic plate as a recording medium) is presented. In this setup, the object (particle) is illuminated with a single collimated beam after passing through the spatial filter, and there is no separate reference wave. Since there is no beam splitting into reference and object beams, the method is sometimes called single beam holography. During the illumination, a small portion of the incident light undergoes scattering from the object, and a so-called object wave is created. This wave contains the information about the particle [8]. The remaining portion of the wave, which passes by the particle mostly unscattered is called the reference wave. These two waves interfere with each other across a 2D CCD sensor to produce the digital hologram. This method is more effective for a smaller object so that the reference is not excessively disturbed. The simplicity of the optical setup in Gabor holography makes it useful for many applications, such as a particle or thin fiber image analysis. When the size of the object is in the micron range, the effect of twin images is often negligible because even at a relatively short distance the Fraunhofer condition is satisfied and the twin image may be completely defocused [4].

In Fig. 2.2(b) a Michelson interferometer setup is presented. In this setup, there is a separate reference beam. The incident laser beam is split into the illumination beam and reference beam using a beamsplitter; both the object beam and reference beam get reflected from the object and mirror, respectively. These two reflected beams then interfere with each other across a 2D CCD sensor to produce the digital hologram. This setup is particularly suitable for non-transparent, but reflective samples [4]. This

holographic setup uses comparatively less optical components and is easy to align as compared to Mach-Zehnder interferometric setup presented in Fig. 2.2(c).

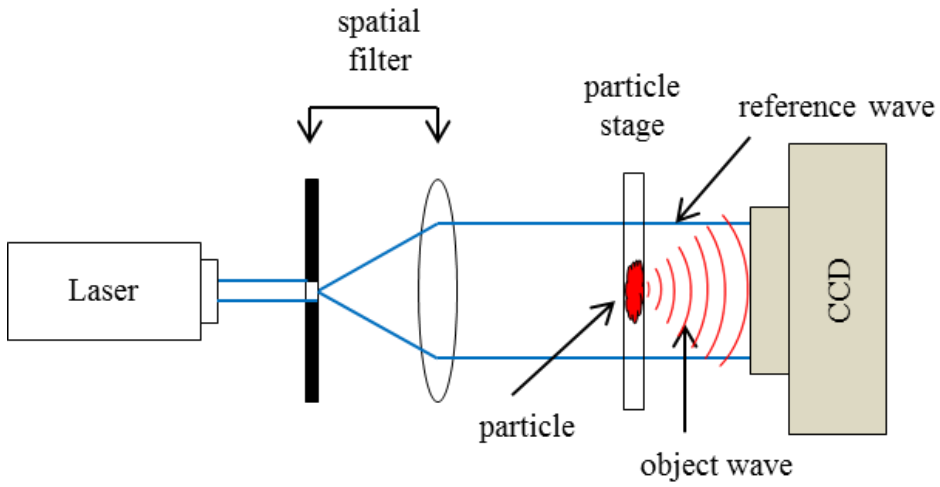

(a) Gabor type setup

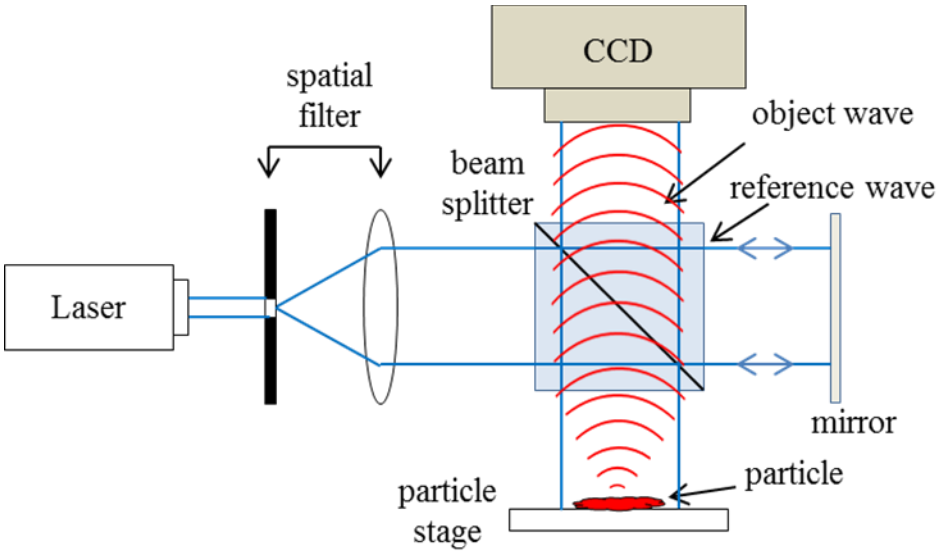

(b) Michelson interferometer setup

Figure 2.2 Digital holography setups.

Plots (a), (b), and (c) show Gabor type setup, Michelson interferometer setup, and Mach-Zehnder interferometer setup, respectively.

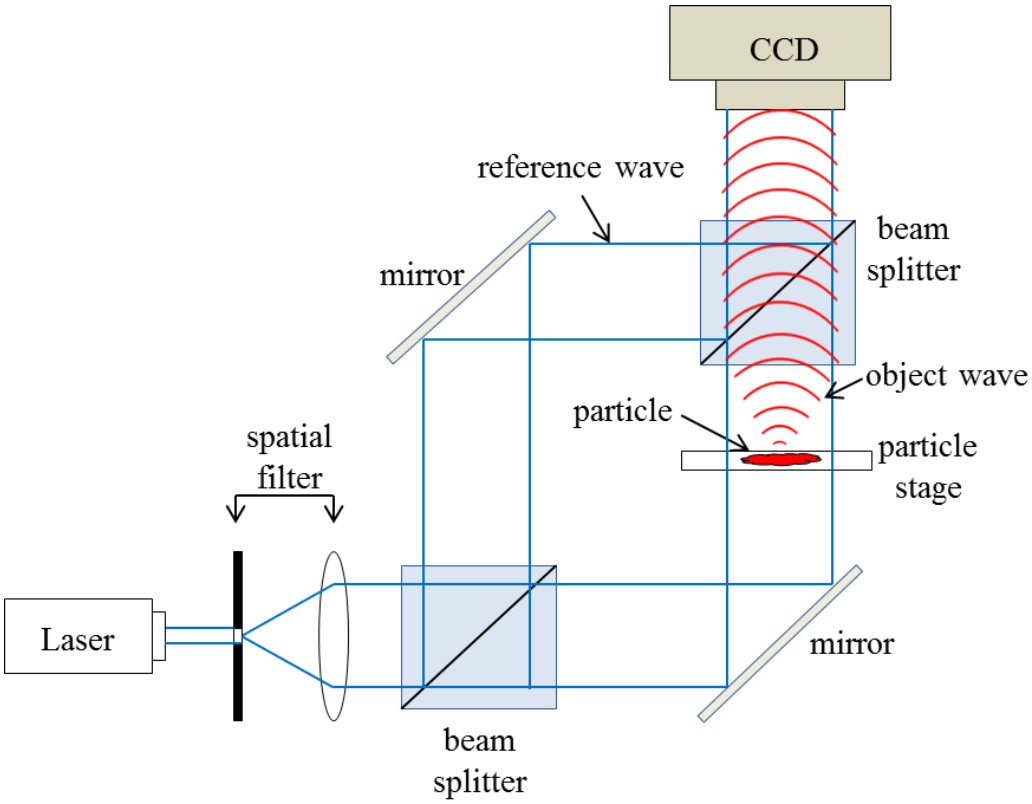

(c) Mach-Zehnder interferometer setup

Figure 2.2 (continued)

In this alignment, the illuminating beam passes through the transparent object after being split into the illumination beam and reference beam from a beam splitter. The reference beam is brought together using a mirror and second beam splitter with the object beam on the recording plane. This setup is particularly suitable for transparent samples [4]. Although the overall setup is more complex and uses more optical components, the additional mirror and beamsplitter make the setup more flexible as the both paths can be adjusted as required. As in analog holography, the path difference between the reference beam and object beam must not be more than the coherence length of the applied light source.

2.3 Applications of digital holography

With the advancement in the technology, DH is expanding its applications and becoming a versatile tool in science and engineering. There are a lot of practical uses of digital holography. Some of the selective applications are:

2.3.1 Biomedical applications

The study of biological processes with cellular and even sub-cellular resolution is of particular interest in the field of life science. A large spectrum of living biological specimens is virtually transparent and produces the change in refractive index or variations in morphology when examined through the optical microscope under bright illumination [25]. Therefore, the analysis of transparent specimens under traditional microscopy is the most tedious job in many biomedical applications, and this greatly limits our ability to understand the process [38-40]. Since DH allows a fast, non-invasive, label-free, and quantitative high-resolution full field measurement of the optical amplitude and phase, this makes DH suitable for many biomedical applications, including the tomographic and topographic study of different biological samples [22, 23]. The DH's ability to quantify the optical path length changes has special importance in biomedical applications, because it enables the measurement either the refractive index or optical thickness variation from the measured optical path length with nanometer precision [24, 25]. Besides this, DH offers many suitable applications in the biomedical field, such as label-free cell counting, red blood cell analysis, time-lapse microscopy of cell division, growth, and migration, and imaging of optic nerve and ophthalmic tissue with micrometer resolution. [25-27, 38-40].

2.3.2 Field-portable lensless microscope

The digital holographic technique provides the total flexibility in imaging of the specimen in both transmission and reflection geometries using in-line and off-axis configurations. Also, the DH configuration can be built in lensless condition using partial coherence light source, such as LED, which can be powered using ordinary batteries [15, 34]. This property of DH dramatically helps to reduce the architecture of the design and cost of operation. Due to this simplicity and ease of operation, it is possible to build a weightless, cost-effective, and completely field-portable lensless holographic microscope based on the principle of DH that can even work in resource-limited environments, such as in farm or desert [35].

2.3.3 Shape and deformation measurements

The micro-scale shape and deformation measurement is very important to ensure reliability and precision of the products in engineering, which is only possible with the precise knowledge of the materials' properties. A simple and robust method to analyze the materials' shape and deformation under a given tension is in great demand. Since DH method provides full three-dimensional deformation information under a given mechanical load, digital holographic interferometry technique is widely used as highly sensitive and contact-free method for shape and deformation measurements [29].

2.3.4 Vibration analysis

The measurement of vibration of different engineering structures is an important objective in industrial works. The main goal of this measurement is the prevention of fatigue failure or the early detection of noise-generating parts or areas of the structure

[30]. For this purpose, a contact-free measurement technique that does not affect the vibration in any way is recommended. The time average holographic interferometry is the most frequently used and experimentally easiest digital holographic method for displaying and evaluating two-dimensional vibration modes [9, 31].

This testing is performed using a pulse laser triggered to a time instant when the modes of vibration have maximum amplitude [32]. Then the comparison between the reconstructed phase with the evaluated phase distribution related to a hologram of the object with no vibration is done. This comparison provides the information of the vibration of the object. Also, the time average method in the digital mode can be performed for the vibration analysis. This testing is performed by recording the successive holograms of the vibrating objects with a single exposure, employing a continuous wave laser with an exposure time longer than the period of the vibration. The interference patterns of the vibration have been recorded using the time average method, which contains the complex structural information of the vibrating object in the form of amplitude and phase. The amplitude of the wavefield reconstructed from such a time average hologram obeys a squared Bessel function. These patterns are then interpreted as contour lines of the vibration modes, and detail information about the vibration is extracted [30].

2.3.5 Particle imaging and scattering measurement

There is a tremendous interest in imaging and characterizing of various micron-sized particles in a contract-free manner. Tabletop microscopy seems an ideal tool for characterizing these particles. However, these particles can easily fragment, aggregate, or even distort upon collection of the sample, all leading to an inaccurate picture of the

particle's true morphology. In some cases, the morphology may even be completely destroyed, as with liquid or frozen particles [33, 36, 37]. Thus, only a contact-free technique will suffice for these situations, and digital holographic technique offers this capability. The scattering pattern formed by a particle due to the scattering of incident light into other directions merely depends on the particle's morphology, composition, and orientation [36]. Therefore, a proper interpretation of this scattering pattern is very important to obtain the desired properties of an unknown particle. However, the problem is that there is not a general unambiguous relationship between a measured pattern and a particle's characteristics, a difficulty that is known as the inverse problem. Recent efforts in DH are aimed to overcome this inverse problem and simultaneously measure the both holographic image and light-scattering pattern of individual particles [33].

2.4 References

1. D. Gabor, "A new microscopic principle," *Nature* **161**(4098), pp 777-778 (1948).

2. D. Gabor, "Microscopy by reconstructed wave-fronts," *Proceedings of the Royal Society of London, Series A*, **197**, pp. 454-487 (1949).

3. D. Gabor, "Microscopy by reconstructed wave fronts: II," *Proceedings of the Physical Society, Section B*, **64**(6), pp. 449 (1951).

4. M. K. Kim, *Digital Holographic Microscopy: Principles, Techniques, and Applications* (Springer Series in Optical Sciences, 2011).

5. U. Schnars and W. Jueptner, *Digital Holography: Digital Hologram Recording, Numerical Reconstruction, and Related Techniques* (Springer, Berlin 2010).

6. V. Mico, C. Ferreira, Z. Zalevsky, and J. Garcia, "Basic principles and application of digital holography microscopy," (Formatex, 2010). Retrieved from http://www.formatex.info/microscopy4/1411-1418.pdf

7. S. Grilli, P. Ferraro, S. De Nicola, A. Finizio, G. Pierattini, and R. Meucci, "Whole optical wavefields reconstruction by digital holograpy," *Optics Express* **9**(6), pp. 294-302 (2001).

8. W. Xu, M. H. Jericho, I. A. Meinertzhagen, and H. J. Kreuzer, "Digital in-line holography of microspheres." *Appl. Opt*. **41**, pp. 5367–5375 (2002).

9. G. K. Ackermann and J. Eichler, *Holography: A Practical Approach* (Wiley, 2007).

10. T. Kreis, *Handbook of Holographic Interferometry* (Wiley, 2005).

11. S. Murata and N. Yasuda, "Potential of digital holography in particle measurement, *Opt. Laser Technol.* **32**(7-8), pp. 567-574 (2000).

12. J. W. Goodman and R. W. Lawrence, "Digital image formation from electronically detected hologram," *Appl. Phys. Lett.* **11**, pp. 77-79 (1976).

13. U. Schnars and W. Jueptner, "Digital recording and numerical reconstruction of holograms," *Meas. Science. Technol.* **13**, R85-R101 (2002).

14. W. Xu, M. H. Jericho, I. A. Meinertzhagen, and H. J. Kreuzer, "Digital in-line holography for biological applications," *Proc. Natl. Acad. Sci.* **98,** pp. 11301-05 (2001).

15. M. Lee, O. Yaglidere, and A. Ozcan, "Field-portable reflection and transmission microscopy based on lensless holography," *Biomed. Opt. Exp.* **2**(9), pp. 2721-2730 (2011).

16. G. Indebetouw and P. Klysubun, "Optical sectioning with low coherence spatio-temporal holography," *Opt. Commun.* **172**(1-6), pp. 25-29 (1999).

17. T. Zhang and I. Yamaguchi, "Three-dimensional microscopy with phase-shifting digital holography," *Opt. Lett.* **23**(15), pp. 1221-1223 (1998).

18. L. Xu, J. M. Miao, and A. Asundi, "properties of digital holography based on in-line configuration," *Opt. Eng.* ***39***(12) pp. 3214-3219 (2000).

19. N. Verrier and M. Atlan, "Off-axis digital hologram reconstruction: some practical consideration," *Appl. Opt.* **50**, H136-H146 (2001).

20. E. N. Leith and J. Upatnieks, "Reconstructed wavefronts and communication theory," *J. Opt. Soc. Am.* **52**, pp. 1123-1130 (1962).

21. E. Cuche, P. Marquet, and C. Depeursinge, "Spatial filtering for zero-order and twin-image elimination in digital off-axis holography," *Appl. Opt.* **39**(23), pp. 4070-4075 (2000).

22. Yamaguchi and T. Zhang, "Phase-shifting digital holography," *Opt. Lett.* **22**(16), 1268-1270 (1997).

23. D. Carl, A, Höink, G. Bally, and C. Denz, "Digital holographic microscope for the analysis of living cells," *DGaO-Proceedings* (2004).

24. J. Mann, L Yu, C. Lo, and M. K. Kim, "High-resolution quantitative phase-contrast microscopy by digital holography," *Opt. Express* **13**(22), pp. 8693-8698 (2005).

25. Rappaz, P. Marquet, E. Cuche, Y. Emery, C. Depeursinge, and P. J. Magistretti, "Measurement of the integral refractive index and dynamic cell morphometry of living cells with digital holographic microscopy," *Opt. Express* **13**(23), pp. 9361-9373 (2005).

26. B. Rappaz, E. Cano, T. Colomb, J. Kuhn, V. Simanis, P. J. Magistretti, and P. Marque, "Noninvasive characterization of the fission yeast cell cycle by monitoring dry mass with digital holographic microscopy," *J. of Biomed. Opt*. **14**(3), 034049 (2009).

27. T. Reya, S. J. Morrison, M. F. Clarke, and I. L. Weissman, "Stem cells, cancer, and cancer stem cells," *Nature* **414**(6859), pp. 105-111 (2001).

28. J. Mann, L. Yu, and M. K. Kim, "Movies of cellular and sub-cellular motion by digital holographic microscopy," *Biomed. Eng. Online* 5 (21), pp. 1-10 (2006).

29. S. Seebacher, W. Osten, and W. P. O. Jueptner, "Measuring shape and deformation of small objects using digital holography," *Proceeding of SPIE – The international Society for Optical Engineering* 3479, pp. 104-105 (1998).

30. Chen, G. M. Brown, M. M. Marchi, and M. Dale, "Recent advances in brake noise and vibration engineering using laser metrology," *Opt. Eng.* **24**(5), 1359-1369 (2003).

31. R. L. Powell and K. A. Stetson, "Interferometric analysis by wavefront reconstruction, *J. Opt. Soc. Am.* A **55**(12), pp. 1593-1598 (1965).

32. Pedrini, P. Fröning, H. Fessler, and H. J. Tiziani, "In-line digital holographic interferometry," *Opt. Comm.* **37**(26), pp. 6262-6269 (1998).

33. M. J. Berg and S. Holler, "Simultaneous holographic imaging and light-scattering pattern measurement of individual microparticles," *Opt. Lett.* **41**(14), pp. 3363-3366 (2016).

34. S. Seo, T. W. Su, D. K. Tseng, A. Erlinger, A. Ozcan, "Lensfree holographic imaging for on-chip cytometry and diagnostics," *Lab Chip* **9**, pp. 777–787 (2009).

35. O. Mudanyali, D. Tseng, C. Oh, S. O. Isikman I. Sencan, W. Bishara, C. Oztoprak, S. Seo, B. Khademhosseinia, and A. Ozcan, "Compact, light-weight and cost-effective microscope based on lensless incoherent holography for telemedicine applications," *Lab Chip* **10**(11), pp. 1417–142 (2010).

36. C. F. Bohren and D. R. Huffman, *Absorption and scattering of light by small particles* (Wiley-VCH, 2006).

37. K. B. Aptowicz, R. G. Pinnick, S. C. Hill, Y. L. Pan, and R. K. Chang, "Optical scattering patterns from single urban aerosol particles at Adelphi, Maryland, USA: A classification relating to particle morphologies," *J. Geophys. Res.* **111** (D12), D12212 (2006).

38. B. Kemper, P. Langehanenberg, and B. von Bally, "Digital holographic microscopy. A new method for surface analysis and marker-free dynamic cell imaging," *Biophotonics* **2**, pp. 41-44 (2007).

39. B. Kemper and G. von Bally, "Digital holographic microscopy for live cell applications and technical inspection," *Applied Optics* **47**(4), pp. A52-A61 (2008).

40. B. Kemper, P. Langehanenberg, A.Vollmer, S. Ketelhut, and G. von Bally, "Label-free 3D migration monitoring of living cells," *Imaging and Microscopy* **11**(4), pp. 26-28 (2009).

CHAPTER III

THEORY OF OPERATION IN DIGITAL HOLOGRAPHY

Interference and diffraction, which are due to the wave nature of light, are the two basic phenomena behind the principle of holography. Therefore, it is essential to introduce them in the description of holographic processes. Sommerfield first introduced the term "diffraction" as a deviation of light rays from their rectilinear paths as a result of passing through a narrow aperture or across an edge, which cannot be interpreted as reflection or refraction. After Thomas Young introduced the phenomenon of interference, Fresnel made assumptions about the amplitude and phase of Huygens's secondary waves and gave a broader explanation about the diffraction of wave.

In this chapter, a brief discussion about the interference, scalar diffraction theory, and Fresnel approximation are presented, which are all used to describe the propagation of the optical field from an input plane to the output plane [1-4]. Afterwards, the process of recording of a hologram, reconstruction of an image, and resolution of the reconstructed image will be presented.

3.1 Fundamental of interference

Interference is a phenomenon in which two waves superpose to form a resultant wave of greater, equal, or lower amplitude than the individual incident wave. In other words, interference usually refers to an interaction of waves that are correlated or

coherent with each other either because they incident from the two virtual sources derived from a real source or because they have same or nearly same frequency.

For the purpose of interference, these two waves can be thought of as a reference wave $\boldsymbol{A_R}$ and object wave $\boldsymbol{A_O}$ given by,

$$\boldsymbol{A_R}(x,y) = |\boldsymbol{A_R}(x,y)|e^{-k\psi(x,y)} = A_R(x,y)e^{-k\psi(x,y)} \tag{3.1}$$

$$\boldsymbol{A_0}(x,y) = |\boldsymbol{A_0}(x,y)|e^{-k\emptyset(x,y)} = A_0(x,y)e^{-k\emptyset(x,y)} \tag{3.2}$$

where $|A_0|$ and $|A_R|$ are the field magnitudes with phases $\emptyset$ and ψ, respectively [1, 2]. Then the resulting interference intensity at any point on the recording plane is given by,

$$\begin{aligned} I &= |\boldsymbol{A_R} + \boldsymbol{A_O}|^2 \\ &= |\boldsymbol{A_R}|^2 + |\boldsymbol{A_O}|^2 + \boldsymbol{A_R}.\boldsymbol{A_O^*} + \boldsymbol{A_R^*}.\boldsymbol{A_O} \\ &= {A_R}^2 + {A_O}^2 + A_R A_O\{e^{-k(\psi-\emptyset)} + e^{k(\psi-\emptyset)}\} \\ &= {A_R}^2 + {A_O}^2 + 2A_R A_O cos(\psi - \emptyset) \end{aligned} \tag{3.3}$$

where the * notation denotes the complex conjugate. The Eq. (3.3) represents the actual intensity distribution of the pattern of interference in the recording plane including information regarding the phase of the object wave relative to the reference wave. The first two terms of this equation depend only on the intensities of the two waves while the third depends on their relative phases [2-4]. Thus, the information about both amplitude and phase of the object wave has been recorded. This recording of the pattern of interference between two wavefronts is considered as a hologram. In a typical holographic setup, the reference beam exhibits either planar or spherically diverging wavefronts. During the process of the reconstruction, the interference pattern of the

object beam with a well-characterized reference beam allows recovery of both intensity and phase of the object's scattered wavefront [5-7].

In the Eq. (3.3), if the light sources are emitting completely independently, then the average of $cos(\psi - \emptyset)$ vanishes since the phases vary statistically. This results in,

$$I = {A_R}^2 + {A_O}^2 = I_R + I_O \tag{3.4}$$

In this case, the waves are called "incoherent." At that time, intensities of both waves add up and interference does not occur.

However, if the waves are "coherent," then the average of $cos(\psi - \emptyset)$ does not vanish but varies between ±1. If the waves oscillate in the same phase (+), i.e., *in-phase,* this results in the maximum intensity point on the space, which is given by,

$$I_{max} = {A_R}^2 + {A_O}^2 + 2A_R A_O \tag{3.5}$$

This condition is known as the condition of constructive interference. Here, the intensities of the reference wave and object wave add up and result in the "maximum intensity" point on the recording plane. The whole phenomena of interference are summarized in the Fig. 3.1.

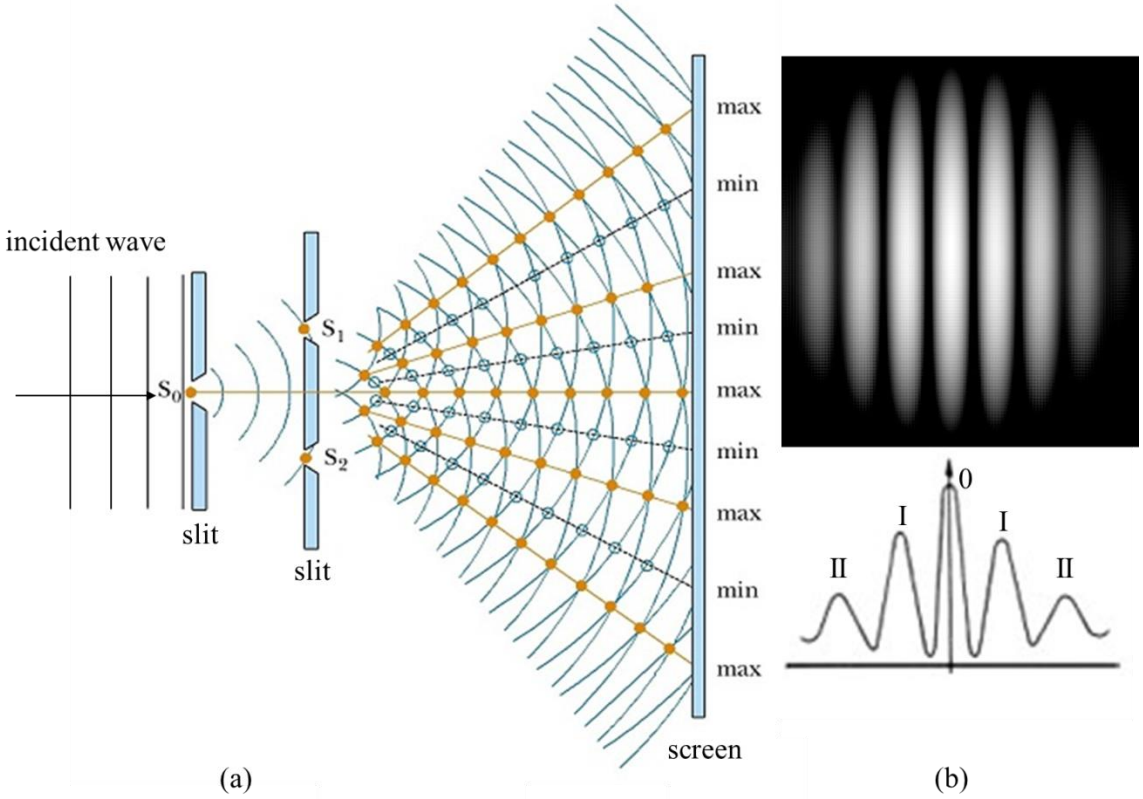

Figure 3.1 Phenomena of interference.

Plot (a) shows the Young's double slits experiment explaining the process of the constructive and destructive process and (b) shows the variation of the intensity on the recording media due to the interference.

Plot (a) is adapted from Kshitij Education India website (http://www.kshitij-iitjee.com/Young's-double-slit-experiment) and a part of the plot (b) is adapted from Wikimedia Commons's web page contributed by Timm Weitkamp (https://commons.wikimedia.org/wiki/File:Double_slit_x-ray_simulation_0600mm_log-grayscale.jpg), respectively.

Likewise, if the waves oscillate in the opposite phase (-), i.e., *out-phase,* this results in the minimum intensity point on the space, which is given by,

$$I_{min} = {A_R}^2 + {A_O}^2 - 2A_R A_O \tag{3.6}$$

This condition is known as the condition of destructive interference. Here, the intensities of the reference wave and object wave cancel up and result in the "minimum

intensity" point on the recording plane. Therefore, the last term in the Eq (3.3) (i.e., $2A_R A_O cos(\psi - \emptyset)$) is known as the "interference term." This is the basic foundation of the holography.

3.2 Optical method for hologram recording and reconstruction

The basic difference between analog and digital holography lies in the ability of recording and reconstruction of the field. The most incredible stage in the process of holography is the optically recording information of a three-dimensional object, i.e., the object wave on a two-dimensional photographic plate. This section briefly describes the conventional way of impinging the object information on the photographic plate and reconstruction of the image.

If $\boldsymbol{A_R}$ and $\boldsymbol{A_O}$ are the complex amplitudes of the reference wave and the object wave, respectively. Then the resulting interference intensity at any point on the recording plane is given by,

$$I = |\boldsymbol{A_R} + \boldsymbol{A_O}|^2 = |\boldsymbol{A_R}|^2 + |\boldsymbol{A_O}|^2 + \boldsymbol{A_R}.\boldsymbol{A_O^*} + \boldsymbol{A_R^*}.\boldsymbol{A_O} \tag{3.7}$$

When considering the conventional method of holography, the intensity pattern given in Eq. (3.7) is typically recorded on photographic film, which is developed to render a hologram transparency $h(x, y)$ and is proportional to the recorded intensity given by,

$$h(x, y) = \beta.\tau.I(x, y) \tag{3.8}$$

where β is the film sensitivity and τ is the exposure time [1, 5, 6].

In the conventional method, the hologram is generally reconstructed by illuminating the transparency with a replica of the reference wave, $\boldsymbol{A_R}$, often called the

"reading beam," such that the complex field emanating directly behind hologram transparency U is given by,

$$\begin{aligned} U &= \boldsymbol{A_R}.\beta\tau\, h(x,y) \\ &= \boldsymbol{A_R}.(|\boldsymbol{A_R}+\boldsymbol{A_O}|^2) \\ &= \boldsymbol{A_R}.(|\boldsymbol{A_R}|^2+|\boldsymbol{A_O}|^2+\boldsymbol{A_R}.\boldsymbol{A_O^*}+\boldsymbol{A_R^*}.\boldsymbol{A_O}) \\ &= \boldsymbol{A_R}|\boldsymbol{A_R}|^2+\boldsymbol{A_R}|\boldsymbol{A_O}|^2+\boldsymbol{A_R}\boldsymbol{A_R}\boldsymbol{A_O^*}+\boldsymbol{A_R}\boldsymbol{A_R^*}\boldsymbol{A_O} \\ &= \boldsymbol{A_R}(|\boldsymbol{A_R}|^2+|\boldsymbol{A_O}|^2)+A_R^2\boldsymbol{A_O^*}+|\boldsymbol{A_R}|^2\boldsymbol{A_O} \end{aligned} \tag{3.9}$$

where $\beta\tau$ term is a constant and physically represents the image brightness, which has been suppressed. In the Eq. (3.9), the first term represents the noninterfering intensity pattern of the reference and object fields separately. These terms are referred to as the "undiffracted" or "zero-order" terms and are generally of no interest. If the reference fields have no spatial structure, then the last two terms are proportional to the complex object field and its conjugate, and they are called first-order twin-image terms. The second term essentially describes the conjugate complex object wave, $\boldsymbol{A_O^*}$, and represents the real image of the object due to the presence of the complex conjugate of the object field [5-14]. Likewise, in the third term the object wave, $\boldsymbol{A_O}$, itself is reconstructed with the amplitude of the reference wave $|\boldsymbol{A_R}|^2$ being constant over the whole hologram and forms a virtual image of the object. The conventional holographic process is shown in Fig. 3.2.

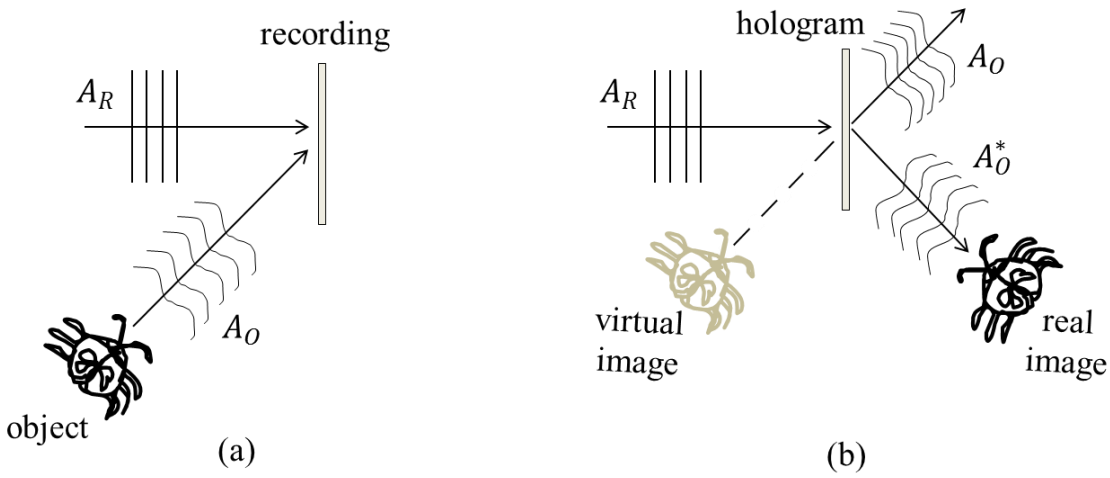

Figure 3.2 Conventional holography process.

Plot (a) shows the recording of the hologram and plot (b) shows the hologram reconstruction with the reference wave.

The concept of the plot is adapted from [4].

The main problem with this method lies not with the presence of twin images, but rather with their nature of inseparability. At the reconstruction plane of the real image, the third term gives to a distorted, i.e., out of focus, reconstruction of the virtual image. In a similar way, at the reconstruction plane of the virtual image, the second term gives to a distorted, i.e., out of focus, reconstruction of the real image [5, 6]. However, in the digital reconstruction of the hologram recorded via CCD is simplified by the fact that the reconstruction wave is numerically simulated; the zero-order terms may be numerically suppressed, generally by subtracting the reference wave from the recorded hologram.

3.3 Fresnel Approximation

In the holographic method, the light field that is recorded in the hologram is optically reconstructed by diffraction of the reference wave. This dissertation is mainly focused on numerical reconstruction rather than an optical reconstruction. Therefore, a

quantitative theory of diffraction is the eminent prerequisite in order to arrive at accurate and consistent results in a description of the reconstructed wave field [2, 5, 8]. In-depth discussions can be found in the literature such as [5, 8]; here we only consider a practical approach to the scalar diffraction theory and take the Fresnel-Kirchhoff diffraction formula as our starting point.

For this, let us consider the geometry of Fig. 3.3 where diffraction aperture lies in the $(\xi,\ \eta,\ z = 0)$-plane and propagates along the positive z-direction. Then the complex diffracted field amplitude at any point P_0 on the $(x,\ y,\ z)$-plane, $U(P_0)$, which is the Fresnel-Kirchhoff diffraction formula, is given by the equation,

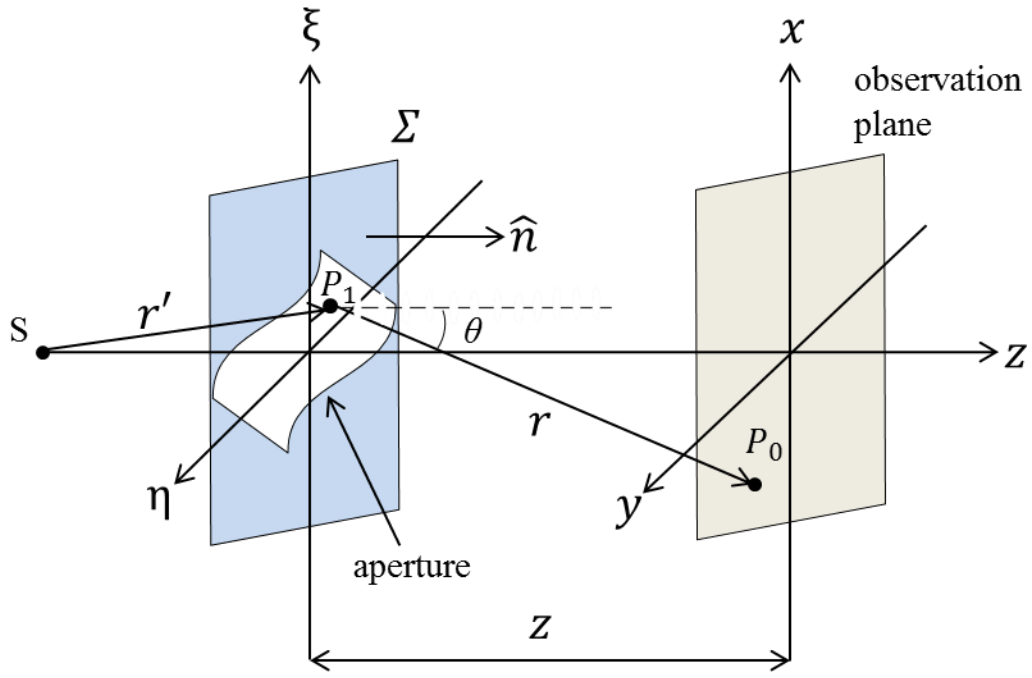

Figure 3.3 Geometry for the Fresnel approximation.

In the diagram, S is the source of light and Σ is the plane of the aperture. At the distance z from this aperture plane is the observation plane.

$$U(P_0) = \frac{1}{i\lambda}\iint_{\Sigma} U(P_1)\frac{e^{ikr}}{r}F(\theta)dA \tag{3.10}$$

where, $F(\theta) = cos\theta = \frac{z}{r}$ is the obliquity factor, θ is the angle between the unit vectors $\hat{\boldsymbol{n}}$ and $\hat{\boldsymbol{r}}$, $k = 2\pi/\lambda$ is the wave number, λ is the wavelength of the light, $U(P_1)$ is the complex field amplitude at any point P_1 on the aperture, and $dA = d\xi d\eta$ is the elementary surface area on the surface of the aperture, respectively.

Then, the Eq. (3.10) can be rewritten as,

$$U(x, y, z) = \frac{z}{i\lambda}\iint_{\Sigma} U(\xi, \eta)\frac{e^{ikr}}{r^2}d\xi d\eta \tag{3.11}$$

Since the oblique distance r is given by,

$$r = \sqrt{(x-\xi)^2 + (y-\eta)^2 + z^2} \tag{3.12}$$

Let, $\rho^2 = (x-\xi)^2 + (y-\eta)^2$, then,

$$\begin{aligned} r &= \sqrt{\rho^2 + z^2} \\ &= z\sqrt{1 + \frac{\rho^2}{z^2}} \end{aligned} \tag{3.13}$$

Let us consider that the distance z between the diffracting aperture and the observation plane is large compared to the lateral distances of the points in the x-, y-, ξ-, and η- directions, i.e., $z \gg \rho$. Then r in the denominator in Eq. (3.11) can be replaced by z, but this replacement is not feasible in the exponential term because r in the exponent is multiplied by $k = 2\pi/\lambda$ with λ in the sub-micrometer range while r in the meter range. Thus, a small variation of r would lead to significant phase errors. Therefore, more

precise approximation for r in the exponent is needed, which is known as the Fresnel approximation. With this approximation Eq. (3.11) becomes,

$$U(x,y,z) = \frac{1}{i\lambda z}\iint_{\Sigma} U(\xi,\eta)e^{ikr}\,d\xi\,d\eta \tag{3.14}$$

For our assumption $z \gg \rho$, the Taylor series expansion in Eq. (3.13), we get,

$$\begin{aligned} r &= z\sqrt{1+\frac{\rho^2}{z^2}} \\ &= z\left[1+\frac{\rho^2}{2z^2}-\frac{1}{8}\left(\frac{\rho^2}{z^2}\right)^2+\cdots\right] \\ &= z+\frac{\rho^2}{2z}-\frac{1}{8}\frac{\rho^4}{z^3}+\cdots \end{aligned} \tag{3.15}$$

Since we have assumed $z \gg \rho$ $(i.e., \rho \gg \lambda$ or $z \gg \lambda)$, the higher order of $\frac{\rho}{z}$ becomes very small, which can be neglected so the Eq. (3.15) becomes,

$$\begin{aligned} r &\approx z+\frac{\rho^2}{2z} \\ &\approx z+\frac{(x-\xi)^2+(y-\eta)^2}{2z} \end{aligned} \tag{3.16}$$

This equation is known as the Fresnel approximation, and the inequality stated above is a condition for the validity of the approximation. Using this result in Eq. (3.14), we get,

$$U(x,y,z) = \frac{1}{i\lambda z}\iint_{\Sigma} U(\xi,\eta)e^{ik\left[z+\frac{(x-\xi)^2+(y-\eta)^2}{2z}\right]}d\xi d\eta$$

$$= \frac{e^{ikz}}{i\lambda z}\iint_{\Sigma} U(\xi,\eta)e^{\frac{ik}{2z}[(x-\xi)^2+(y-\eta)^2]}d\xi d\eta \tag{3.17}$$

The Eq. (3.17) is the well-known Fresnel-Kirchhoff diffraction integral. This result is nothing, but simply a Fourier transform of the diffracted field $U(\xi,\eta)$. This equation can be used to model the propagation of light in a wide range of configurations, either analytically or numerically. Due to its capability to quantitatively analyze the diffracted field, it is aggressively used in the numerical reconstruction of the diffracted field and the reconstruction of the image in digital holographic technique [1-19].

3.4 Recording of digital hologram

In digital holography, digital recording of object's hologram is the very first and most important step. For this purpose, optoelectronic sensor, i.e., CCD or CMOS camera is used. To acquire the hologram of an object digitally, a coherent light is used to illuminate the object. During this illumination, one part of the incident light undergoes scattering from the object and a so-called object wave is created. This wave contains information about the particle, such as its shape, size, and surface roughness [20]. The other part of the light, which passes the particle, remains unscattered and is called the reference wave. The object wave interferes with the reference wave and generates the microscopically fine interference pattern across the sensor. The digitally recorded interference pattern on the sensor-array is known as object's hologram, which is used to

numerically reconstruct the image to render the shape, size, and surface roughness information on the particle profile.

During this process, we consider a single spherical particle in vacuum illuminated by a collimated linearly polarized beam traveling in vacuum along the z-axis with wavelength λ. In this case, both the reference and scattered wave amplitudes can be represented as:

$$A^{ref}(\boldsymbol{r}) = \frac{exp(ikr)}{r} A_o^{ref}(\hat{\boldsymbol{r}}),$$

$$A^{sca}(\boldsymbol{r}) = \frac{exp(ikr)}{r} A_o^{sca}(\hat{\boldsymbol{r}}), \tag{3.18}$$

respectively, where **r** is the position vector, k=2π/λ is the wave number, and A_o^{ref} and A_o^{sca} are the amplitudes of the reference and scattered waves at the sensor's surface [20-22]. The intensity at the sensor when no particle is present is given by,

$$I^{ref}(\boldsymbol{r}) = \frac{c\varepsilon_o}{r^2} |A_o^{ref}(\hat{\boldsymbol{r}})|^2 \tag{3.19}$$

where c and ε_o are the speed of light and electric permittivity in vacuum, respectively.

Likewise, the intensity at the sensor when the particle is present is

$$I^{holo}(\boldsymbol{r}) = \frac{c\varepsilon_o}{r^2} |A_o^{ref}(\hat{\boldsymbol{r}}) + A_o^{sca}(\hat{\boldsymbol{r}})|^2 \tag{3.20}$$

Subtracting Eq. (3.19) from Eq. (3.20) gives the so-called contrast hologram,

$$I^{con}(\mathbf{r}) = \frac{c\varepsilon_o}{r^2} \left[\left\{ \left[A_o^{ref}(\hat{\mathbf{r}})\right]^* A_o^{sca}(\hat{\mathbf{r}}) + [A_o^{sca}(\hat{\mathbf{r}})]^* A_o^{ref}(\hat{\mathbf{r}}) \right\} + |A_o^{sca}(\hat{\mathbf{r}})|^2 \right] \tag{3.21}$$

where the asterisk denotes complex conjugate [24].

The first two terms in Eq. (3.21) are due to the interference between the reference and scattered waves, whereas the last term is due to the scattered wave only. In principle, an image of the particle can be reconstructed from this pattern. In this work, the particles block only a small fraction of the illuminating light, and consequently, the intensity of the reference wave dominates the intensity of the scattered wave. Thus, the last term in Eq. (3.21) can be neglected, leaving,

$$I^{con}(\mathbf{r}) = \frac{c\varepsilon_o}{r^2}\left[\left\{\left[A_o^{ref}(\hat{\mathbf{r}})\right]^* A_o^{sca}(\hat{\mathbf{r}}) + [A_o^{sca}(\hat{\mathbf{r}})]^* A_o^{ref}(\hat{\mathbf{r}})\right\}\right] \tag{3.22}$$

By subtracting the reference intensity leading to Eq. (3.21), imperfections in the incident beam profile are greatly suppressed [25]. The key characteristic of I^{con} is its linear dependence on the amplitude of the particle's scattered wave. This means that the phase of the wave over the sensor is encoded in the measurement. The Eq. (3.22) can then be used with the reconstruction algorithm described in section 3.5 to render unambiguously an image of the particle [24].

3.5 Reconstruction of image

Although various reconstruction methods available in literature can be utilized for the image reconstruction, including reconstruction by convolution, angular spectrum, and back-projection via the Radon transform, these are not the central to this work. This work primarily relies on the well-known Fresnel-Kirchhoff diffraction integral presented in Eq. (3.17) for the image reconstruction. Once the digital hologram is recorded using a sensor, a contrast hologram is obtained by subtracting the particle-free background from the particle's raw hologram as described in section 3.4. This step is crucial to remove

imperfections in the illumination-beam profile, improving the subsequent object image during the reconstruction.

The contrast hologram is imagined as a transmission diffraction grating illuminated at normal incidence by the same incident plane wave (i.e., a reconstruction wave) as described in [6, 21, 24, 25]. The diffraction process is then modeled computationally using the Fresnel-Kirchhoff approximation theory, and the model is used to describe the light diffracted by this grating in a parallel plane separated by a distance z from the grating [21, 24].

If z corresponds to the distance d between the particle and sensor during the hologram measurement, the resulting diffraction pattern in the reconstruction plane ($z = d$) yields a silhouette-like image of the object. However, the distance d is not known accurately *a priori* such that an image in-focus is reconstructed in a single application of the reconstruction operation. Therefore, an interactive process is used to produce the focused image.

Let the position of a pixel in the hologram be $\boldsymbol{r'} = \xi\hat{\boldsymbol{x}} + \eta\hat{\boldsymbol{y}} + l\hat{\boldsymbol{z}}$, and a point in the image plane be $\boldsymbol{r} = x\hat{\boldsymbol{x}} + y\hat{\boldsymbol{y}} + z\hat{\boldsymbol{z}}$. Then the diffracted wave amplitude K in the image plane using Eq. (3.17) is given by,

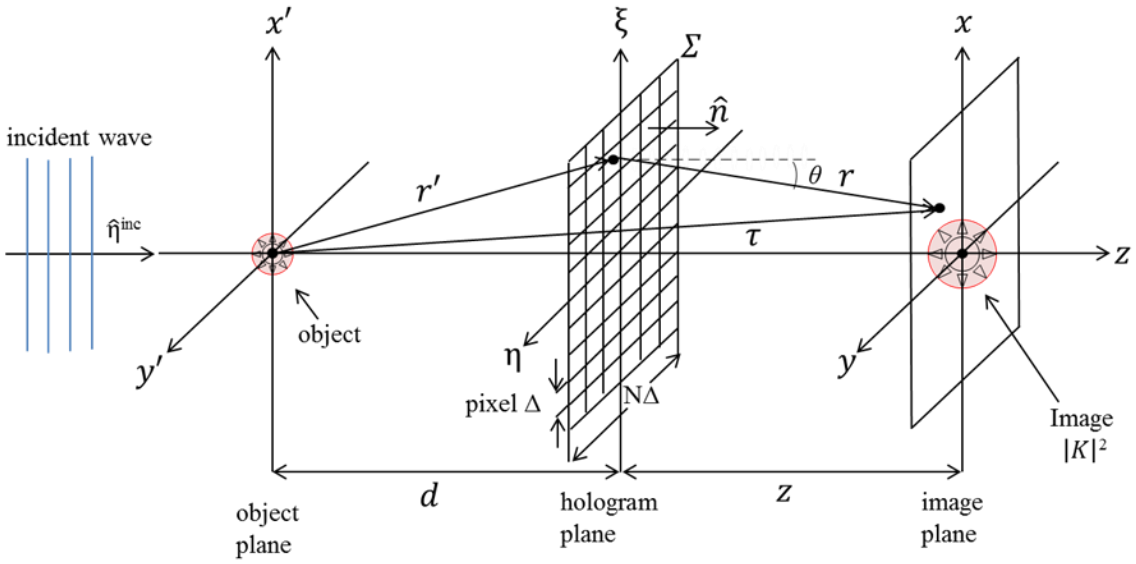

Figure 3.4 Image formation in digital holography.

See text for detail explanation.

$$K(x,y) = \alpha \iint_{\Sigma} I^{con}(\xi,\eta)\exp\left\{\frac{ik}{2z}[(x-\xi)^2+(y-\eta)^2\right\}d\xi\, d\eta \tag{3.23}$$

where $\alpha = \frac{e^{ikz}}{i\lambda z}$ is a constant, $U(x,y) = K(x,y)$ is the diffracted wave amplitude in the image plane, $U(\xi,\eta) = I^{con}(\xi,\eta)$ is the contrast hologram, i.e., wave amplitude in the hologram plane.

The Eq. (3.23) is just a Fourier transform of the diffracted field $I^{con}(\xi,\eta)$. By evaluating this integral in the image plane, the absolute square of the resulting wave amplitude, $|K|^2$, forms the image of the object.

$$|K|^2 = \left|\mathrm{FT}[\,I^{con}(\xi,\eta)]\right|^2 = \text{Image} \tag{3.24}$$

3.6 Resolution limit of the reconstructed image

The ability of digital holographic imaging system to resolve detail in an image is known as the resolution of the image. Even though DH has been established as an important imaging modality with a wide range of applications, it comes with some serious resolution limits, which greatly limit our capability of imaging various micron-sized particles and analyzing their properties. Some parameters that significantly affect the resolution of the reconstructed image are pixel size, pixel number, wavelength of the coherence light used, and reconstruction distance.

In this dissertation, the numerical reconstruction of the image relies on the Fresnel-Kirchhoff diffraction integral based on Fresnel approximation. This numerical diffraction method has pixel resolution, *δr,* proportional to the propagation distance *z* given by the relation:

$$\delta r = \frac{\lambda z_i}{N\Delta} \tag{3.25}$$

where λ is the wavelength of the light, z_i $(= d)$ is the distance between the hologram and sensor, N is the number of pixels in the sensor array, and Δ is pixel size.

The Eq. (3.25) gives the resolution limit for our reconstructed image. Together with the minimum reconstruction distance, $z_i = \frac{\xi^2}{N\lambda}$, where ξ is the linear dimension (either height or width, but the smaller one in the case of a rectangular shaped sensor) of the hologram, the above equation has significant constraint on the size and resolution of the reconstructed image [4]. The Eq. (3.25) clearly shows that the resolution of the reconstructed image is heavily based on the sensor size, and the sensor comes with a finite pixel size that sets a limit to the achievable resolution [26-29]. However, the

resolution can be improved by using a sensor with greater dynamic range, by forming the hologram with shorter wavelength light, and by employing a positive lens to magnify the hologram during recording stage.

3.7 References

1. G. K. Ackermann and J. Eichler, *Holography: A Practical Approach* (Wiley, 2007).

2. T. Kreis, *Handbook of Holographic Interferometry* (Wiley, 2005).

3. C. M. Vest, *Holographic Interferometry* (John Wiley and Sons, 1979).

4. M. K. Kim, *Digital Holographic Microscopy: Principles, Techniques, and Applications* (Springer, 2011).

5. J. W. Goodman, *Introduction to Fourier Optics, 3rd ed.* (Roberts & Company, Englewood, 2004).

6. M. Born and E. Wolf, *Principles of Optics* (Cambridge University Press, Cambridge, 1999).

7. U. Schnars and W. Jueptner, *Digital Holography: Digital Hologram Recording, Numerical Reconstruction, and Related Techniques* (Springer, Berlin 2010).

8. L. A. Williams, *Digital holography for three dimensional tomographic and topographic measurements*, Dissertation, University of Dayton, Dayton, Ohio (2014).

9. W. S. Haddad, D. Cullen, J. C. Solem, J. W. Longworth, A. McPherson, K. Boyer, and C. K. Rhodes, "Fourier-transform holographic microscope," *Appl. Opt.* **31**, pp. 4973-4978 (1992).

10. D. Gabor, *Nobel Lecture,* (1971). Retrieved from http://nobelprize.org/nobel_prizes/physics/laureates/1971/gabor-lecture.pdf

11. D. Gabor, "A New Microscope Principle," *Nature* **161**, pp. 177-178 (1948).

12. D. Gabor, "Microscopy by Reconstructed wavefronts," *Proc. Roy. Soc.* **A197**(1051), pp. 454-487 (1949).

13. E. N. Leith, J. Upatnieks, and K. A. Haines, "Microscopy by Wavefront Reconstruction," *J. Opt. Soc. Am.* **55**(8), pp. 981-986 (1965).

14. J. W. Goodman and R. W. Lawrence, "Digital image formation from electronically detected holograms," *Appl. Phys. Lett.* **11**, pp. 77-79 (1967).

15. U. Schnars and W. Jueptner, "Direct recording of holograms by a CCD target and numerical reconstruction," *Appl. Opt.* **33**, pp. 179–181 (1994).

16. U. Schnars and W. Jueptner, "Digital recording and numerical reconstruction of holograms *Meas. Sci. Technol.* **13**, pp. R85-R101 (2002).

17. G. Pedrini and H. J. Tiziani, “Quantitative evaluation of two-dimensional dynamic deformations using digital holography,” *Opt. Laser Technol*. **29,** pp. 249–256 (1997).

18. P. Picart, J. Leval, D. Mounier, and S. Gougeon, “Some opportunities for vibration analysis with time averaging in digital Fresnel holography,” *Appl. Opt*. **44**, pp. 337–343 (2005).

19. P. Ferraro, S. De Nicola, A. Finizio, G. Coppola, S. Grilli, C. Magro, and G. Pierattini, “Compensation of the inherent wave front curvature in digital holographic coherent microscopy for quantitative phase-contrast imaging,” *Appl. Opt.* **42,** pp. 1938-1946 (2003).

20. P. Kulkarni, P. A. Baron, and K. Willeke, *Aerosol Measurement: Principles, Techniques, and Applications*, 3rd ed. (Wiley, 2011).

21. M. J. Berg and N. R. Subedi, “Holographic interferometry for aerosol particle characterization,” *J. Quant. Spectrosc. Radiat Transf*. **150**, pp. 36-41 (2015).

22. M. J. Berg, N. R. Subedi, P. A. Anderson, and N. B. Fowler, “Using holography to measure extinction,” *Opt. Lett.* **39**, pp. 3993-3996 (2014).

23. N. R. Subedi, N. B. Fowler, and M. J. Berg, “Backscatter digital holography of microparticles,” *Opt. Express.* **21**(10), pp. 12611-12616 (2013).

24. M.J. Berg and G. Videen, “Digital holographic imaging of aerosol particles in flight,” *J. Quant. Spectrosc. Radiat. Transf*. **112**, pp. 1776–1783 (2011).

25. W. Xu, M. H. Jericho, I. A. Meinertzhagen, and H. J. Kreuzer, “Digital in-line holography of microspheres.” *Appl. Opt*. **41**, pp. 5367–5375 (2002).

26. T. Latychevskaia and H. W. Fink, “Resolution enhancement in digital holography by self-extrapolation of holograms,” *Opt. Express* **21**(6), pp. 7726-7733 (2013).

27. Y. Hao and A. Asundi, “Resolution analysis of a digital holography system.” *Appl. Opt*. **50**(2), pp. 183-193 (2011).

28. D. P. Kelly, B. M. Hennelly, N. Pandey, T. J. Naughton, and W. T. Rhodes, “Resolution limits in practical digital holographic systems,” *Opt. Engineering* **48**(9), pp. 095801-0958013 (2009).

29. K. Khare, P. T. S. Samsheer Ali, and J. Joseph, “Single shot high resolution digital holography,” *Opt. Express* **21**(3), pp. 2581-2591 (2013).

CHAPTER IV

EXPERIMENTAL DESIGNS

In this chapter, different experimental designs that are built to study the imaging modality of DH will be discussed. All the constructed designs are based on the principle of in-line digital holography configuration, i.e., the reference light and particle's scattered wave are incident on the recording plane with no angle difference between them [1-10]. The main objective of this chapter is to explore the feasibility of various imaging modality in DH to image micron-sized particles and lay the foundation for the advancement of aerosol-particle characterization technology and future instrument-development. Different designs are set to form holograms with both forward- and backward-scattered light of various particle samples.

The experimental designs are presented in the Fig. 4.1-4.11 below. The optical source used in this work is a Q-Switched Neodymium-doped yttrium lithium fluoride ultraviolet laser (Nd: YFL UV laser) (Photonics Industries, DC50-351), frequency triple to 351 nm wavelength. The sensors are (Finger Lakes Instrumentation, ML8300 of array size 3448 x 2574 pixels and PointGrey Research Inc., Model # CMLN-13S2M of array size 1296 x 964 pixels) CCD cameras.

4.1 Forward-scattering configuration

In this configuration, the particle, optical components, and sensor are arranged in a line. As such, the configuration uses forward-scattered light to form the hologram,

which minimizes the number of optical components required to construct the design. Because of its simplicity and ease of operation, this configuration is appropriate for the eventual development of a field-portable instrument. However, the in-line forward scattering configuration is not suitable to image dense or cluster objects such as tissue slides since the reference beam gets distorted causing severe aberrations in the reconstruction of such images [5].

Following the description above, two different alignments are considered in the forward-scattering configuration. In the first configuration, at a distance of 19 cm from the laser, a fused silica lens (L1) of focal length 5 cm is used. At the focal point of L1, a pinhole (PH) of diameter 25 μm is placed, which produces the circular diffraction pattern. At a distance of 24 cm from the pin-hole, an iris selects only the central diffraction peak and removes the stray light from the laser beam. Another fused silica lens (L2) with focal length 30 cm then collimates the central diffraction peak from the iris. The optical components from L1 to L2 collectively form a spatial filter, and the sole purpose of this step is to produce a clean beam profile. Next to L2, another lens, L3, is used, which focuses the beam to a waist. The wavefront then diverges like spherical wave after the beam waist. This diverging-like beam is utilized to illuminate the particle. Then a sensor, which is a FLI CCD camera, is used to record the hologram of the particle.

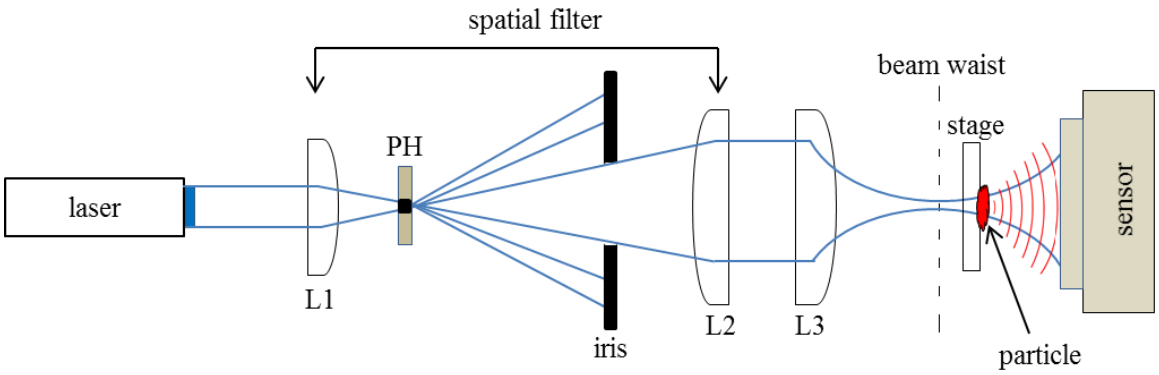

Figure 4.1 Forward-scattering configuration in which particle in a stage is illuminated by diverging-spherical beam profile.

Please note that there is no specific significance for using two color light in the figure. The blue color is for particle illuminating light and the red color is for the particle's forward-scattered light, respectively.

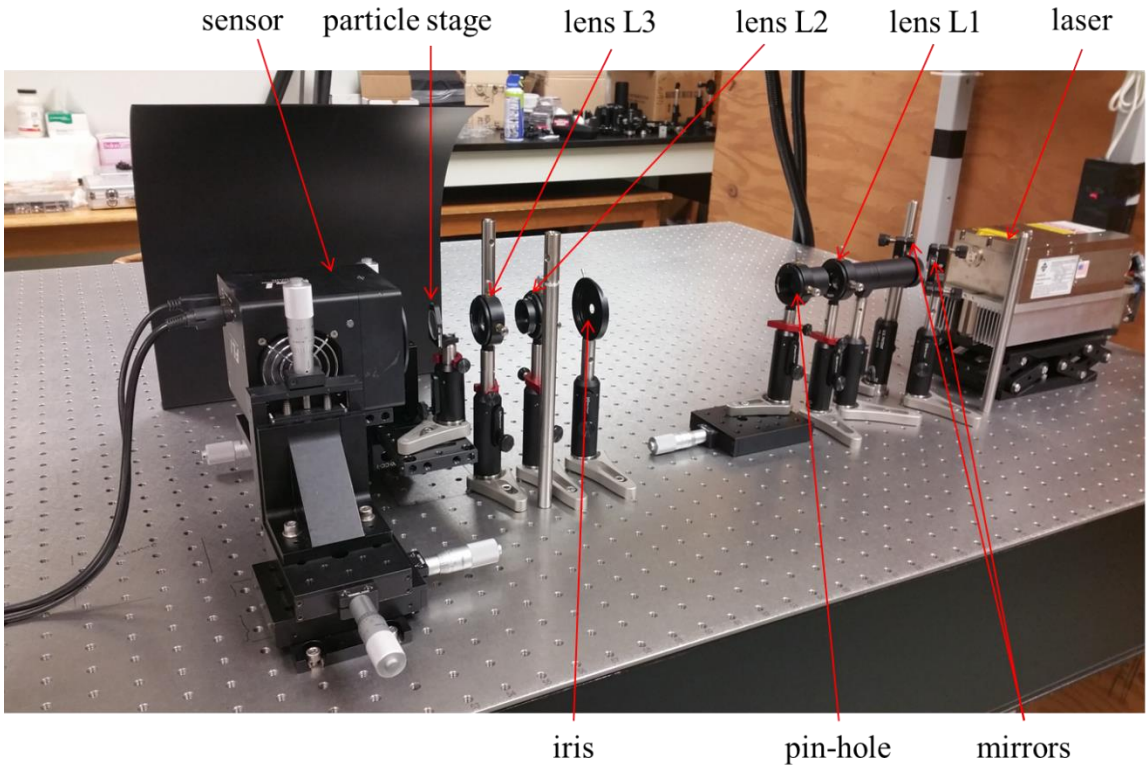

Figure 4.2 Experimental setup for the forward-scattering configuration.

A particle stage of 2.54 cm diameter is then inserted just after the beam waist on xyz- translation stage in between L3 and sensor such that it is at a distance of 4 cm from the L3 and 6.5 cm from the sensor. Later, this stage will hold a particle under investigation. Then, the intensity of the light passing through the stage without a particle is recorded, which provides an estimate for the amount of light incident on the sensor array with the bare glass in order to avoid over-saturation of the sensor through judicious adjustment of the laser intensity. Next, a particle is placed on the particle stage and the hologram is recorded due to the particle's forward scattered light.

The intensities of the beam in the particle-free condition, which is essentially a measurement of the intensity of unscattered light and with the particle on the stage, or a measurement of particle's scattering interference with the unscattered light, are measured. These intensities are reference (I^{ref}) and raw hologram (I^{holo}), respectively. Now, by subtracting reference from the raw hologram, only the particle's scattering wave information is obtained, which is known as the contrast hologram (I^{con}).

At the time of this measurement, it can be determined whether that the intensity of the beam from pulse to pulse is not the same. This can be a problem while subtracting the reference from the raw hologram. This inequality causes either over-subtraction or under-subtraction and comprises a degree of noise and greatly limits the resolution of the image. To eliminate this problem, an averaging method is used. For this case, five different frames of both the reference and raw hologram are recorded and then the average is taken separately. Afterwards, the average of reference frames is subtracted from the average of raw holograms to get the contrast hologram. This is done in Mathematica. After this,

following the procedure explained in section 3.5, an image of the particle is rendered from this contrast hologram.

In the second configuration, L3 is removed from Fig. 4.1 above. In this new configuration, particle stage is at 3 cm and sensor is at 12 cm from L2, respectively. This experimental setup is shown in Fig. 4.3. The same procedure is followed to reconstruct the image of the particle as described above.

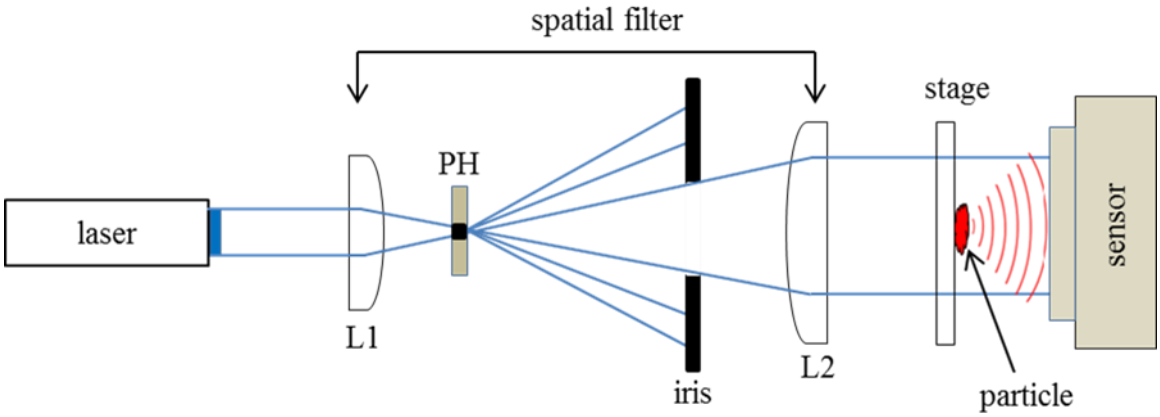

Figure 4.3 Forward-scattering configuration in which particle in a stage is illuminated by collimated beam profile.

In the diagram, blue light is the particle illuminating light and the red light is the particle's forward-scattered light, respectively.

4.2 Backward-scattering configuration

In this configuration, the particle, optical components, and sensor are not arranged in a line. This design is comparatively complex since it uses more optical components and is more sensitive to the alignment of the optics than the one discussed in section 4.1. However, it offers more flexibility to set reference and object paths independently.

To enable this design, a pellicle beamsplitter (BS) of diameter 5.08 cm with a reflection-to-transmission ratio 45:55 is used to split a beam as shown in Fig. 4.4. The

arrangement is initially established by constructing a Michelson interferometer so that proper alignment of the BS can be achieved.

Similar to section 4.1 above, two different alignments are considered in order to record the particle's backward-scattering hologram. In the first configuration, mirror M1 is fixed and mirror M2 is on a one-axis translation stage. The position of M2 is then adjusted until an interference maximum is seen on the sensor, which is a FLI CCD camera at a distance of 5.5 cm from the BS.

Following this alignment setup, M2 is removed and replaced by a beam dump (BD). A particle stage on a xyz-translation stage is then placed in front of this BD. Then another BD is placed in front M1, and the intensity of the backward-scattered light from the particle-free stage is recorded, which provides an estimate for the amount of light scattered by the bare glass. Next, a particle is kept on the stage and the BD in front of M1 is removed. Then the particle's backward-scatted hologram is recorded. By subtracting the particle-free and particle intensity patterns at the sensor, the contrast backward-scattered hologram is obtained. In this configuration, the portion of the light transmitted from BS is used to illuminate the particle under investigation.

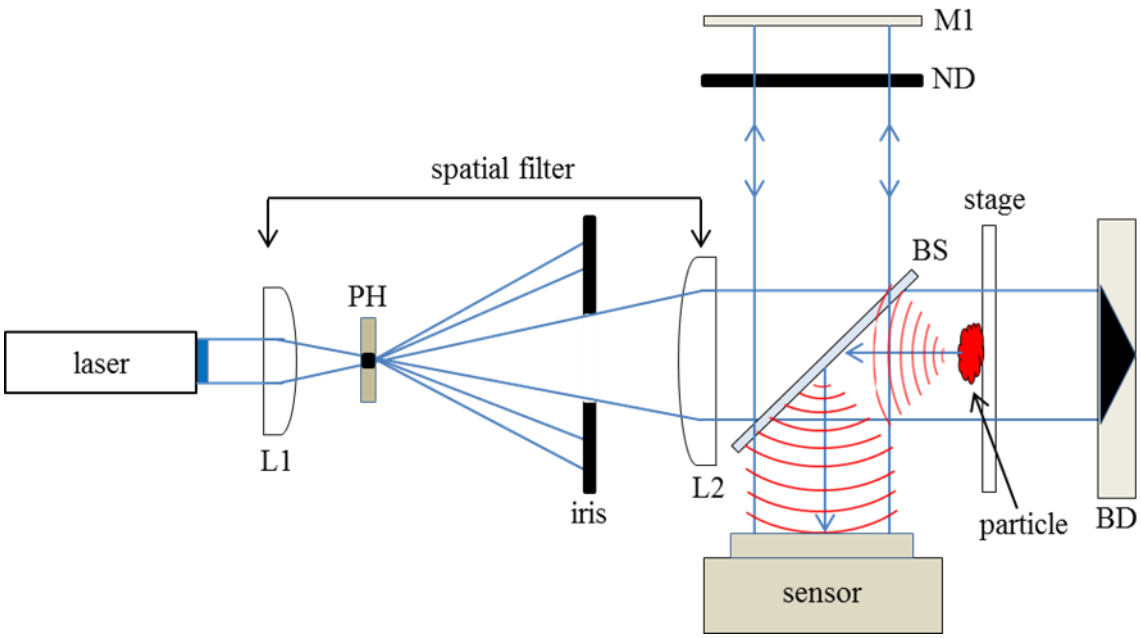

Figure 4.4 Backward-scattering configuration in which particle in a stage is illuminated by the light transmitted through the BS.

In the diagram, blue light is the particle illuminating light and red is the particle's backward-scattered light, respectively.

In the next configuration, the procedure above of keeping M2 fixed and M1 on a translation stage is repeated until an interference maximum is seen on the sensor. This configuration is different than the one described above in the sense that there is a particle illuminated by the collimated beam transmitted through BS, but here the particle is illuminated by the portion of the collimated beam reflected from the BS. The experimental configuration for this case is shown in Fig. 4.5.

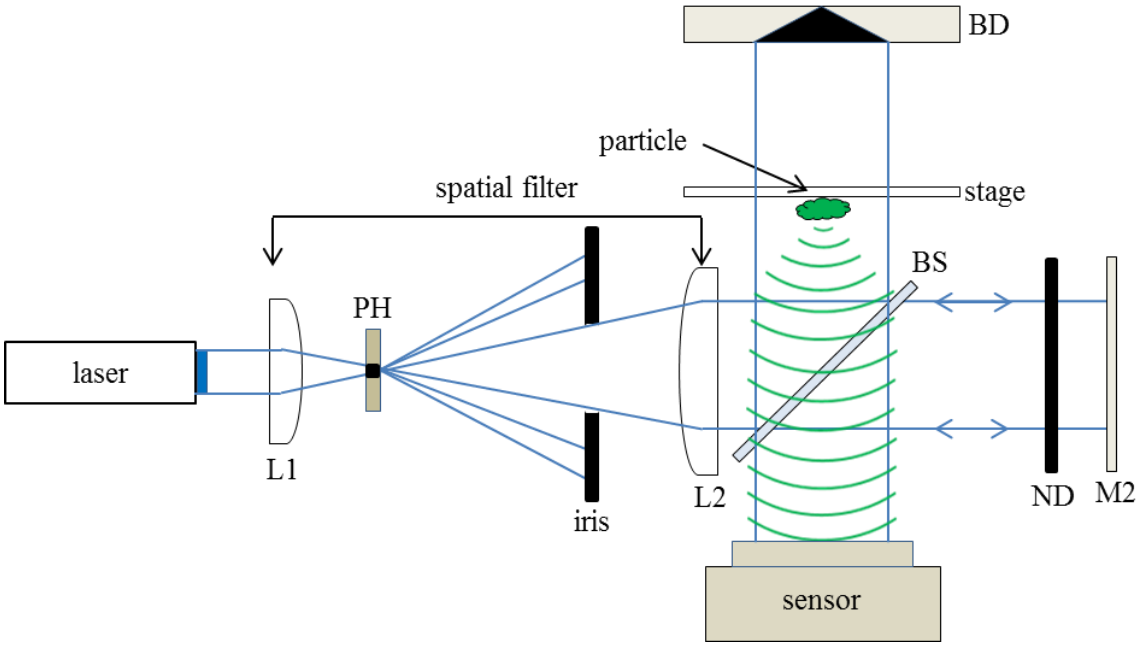

Figure 4.5 Backward-scattering configuration in which particle in a stage is illuminated by the light reflected from the BS.

In the diagram, blue light is the particle illuminating light and green is the particle's backward-scattered light, respectively.

In both configurations, a neutral density filter (ND=0.3) is kept in front of the fixed mirror to make the intensity of the reference wave nearly equal to the intensity of the particle's backward-scattered light.

4.3 Simultaneous configuration

In this section, two different configurations, which are enabled to record a particle's forward- and backward-scattered holograms simultaneously, are constructed. Since forward- and backward-scattered holograms are obtained simultaneously, a side-by-side comparison of the two images is possible. The information obtained from this comparison could be useful for the characterization of a variety of microparticles.

In the first configuration, after following the same procedure described in sections 4.2, M2 is replaced by an additional sensor, which is a PointGrey CCD camera and labeled as "sensor-2" in the figure. This configuration is shown in the Fig. 4.6 below. In this configuration, the back reflection from the sensor-2 overlaps with the particle's backward-scattered wave and produces noise in the backward-scattering hologram, i.e., on sensor-1. This noise deteriorates the resolution of the reconstructed image.

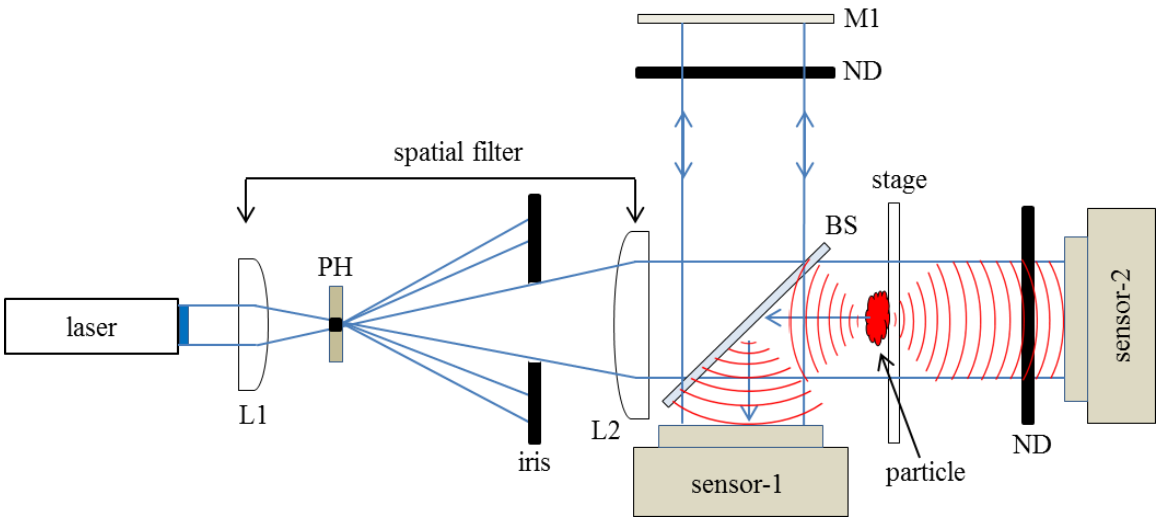

Figure 4.6 A digital holographic configuration in which a particle's forward- and backward-scattered holograms are recorded simultaneously.

In the diagram, red light is the particle's forward- and backward-scattered light.

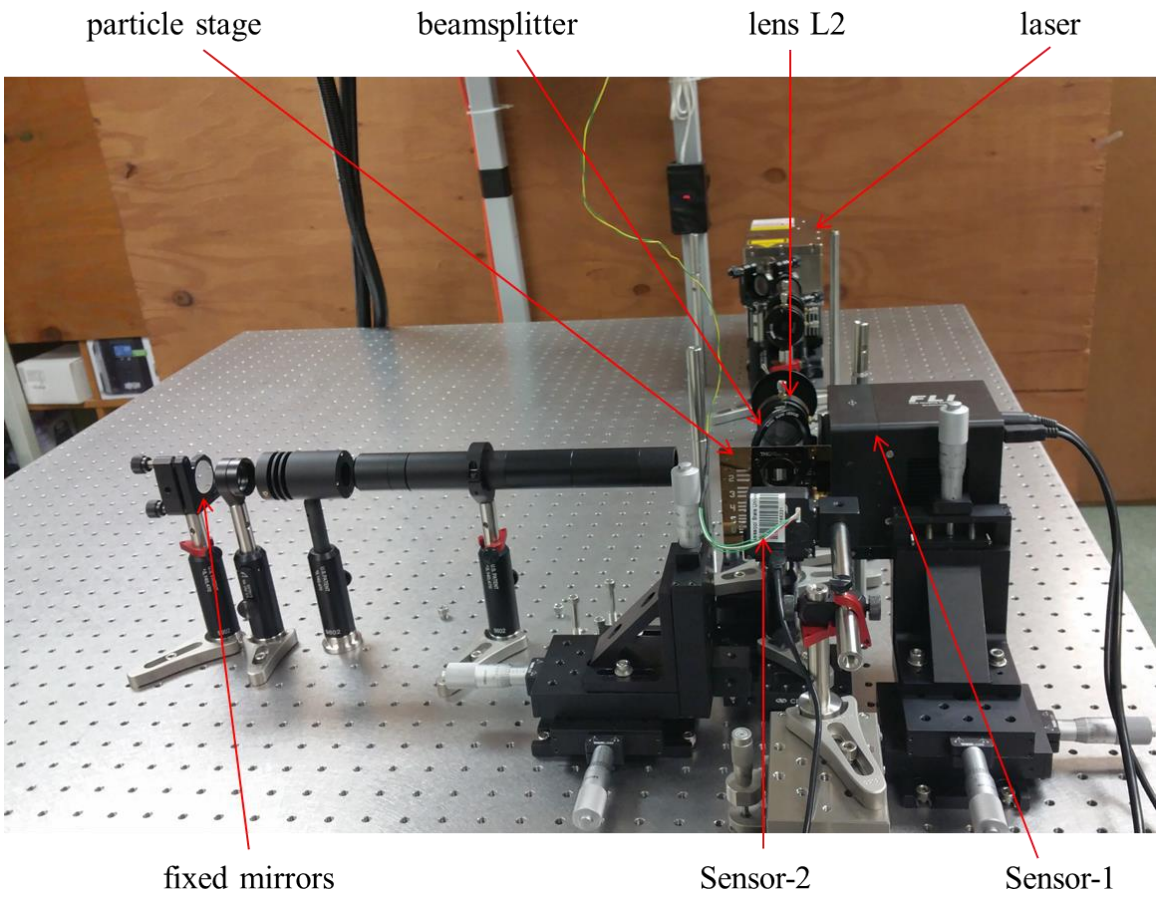

Figure 4.7 Experimental setup for the simultaneous configuration.

In the next arrangement, the same procedure is followed as above, but M1 is replaced by sensor-2 as shown in the Fig. 4.8. In this arrangement, multiple reflections of light between the two sensor arrays also cause background noise in the holograms and hence, impact the reconstructed image quality.

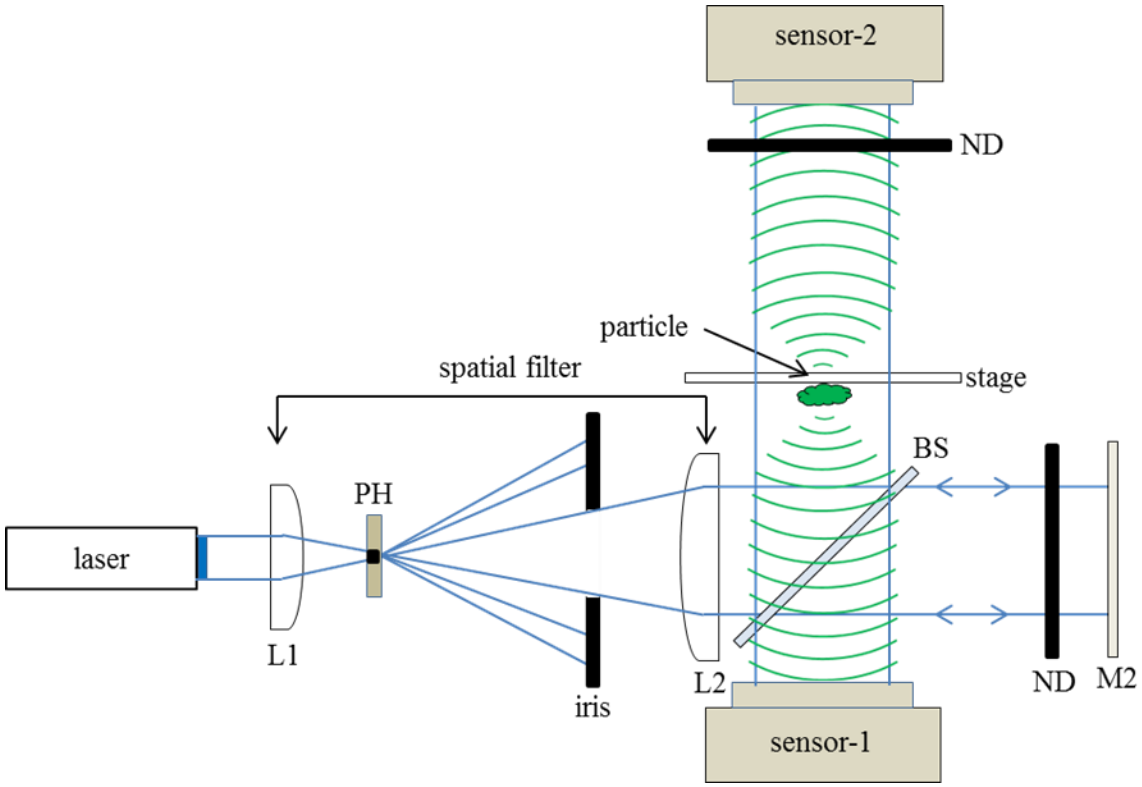

Figure 4.8 A digital holographic configuration in which a particle's forward- and backward-scattered holograms are recorded simultaneously.

In the diagram, green light is the particle's forward- and backward-scattered light.

In these configurations, because of the dynamic range of the two sensors is not equal, another neutral density filter (ND=0.3) is placed in front of sensor-2 to avoid saturation.

4.4 Multiple-sample study

After successful investigation of a particle in forward- and backward-scattering configurations, the concept is extended to examine multiple samples at a time. Multiple samples are examined in both forward- and backward-scattering modes, respectively.

4.4.1 Forward-scattering configuration

First, a configuration is designed to record forward-scattered holograms of two different samples simultaneously. In this configuration, after achieving the Michelson interferometer alignment with the constructive interference pattern on the sensor array when no particle is present, M2 is replaced by sensor-1 and M1 is replaced by sensor-2, respectively. These two sensors are at a distance of 11 cm from the BS. Then the particle stages in the xyz-translation stage are placed in front of the sensors. To avoid saturation on sensor-2, a neutral density filter (ND=0.3) is placed in front of it.

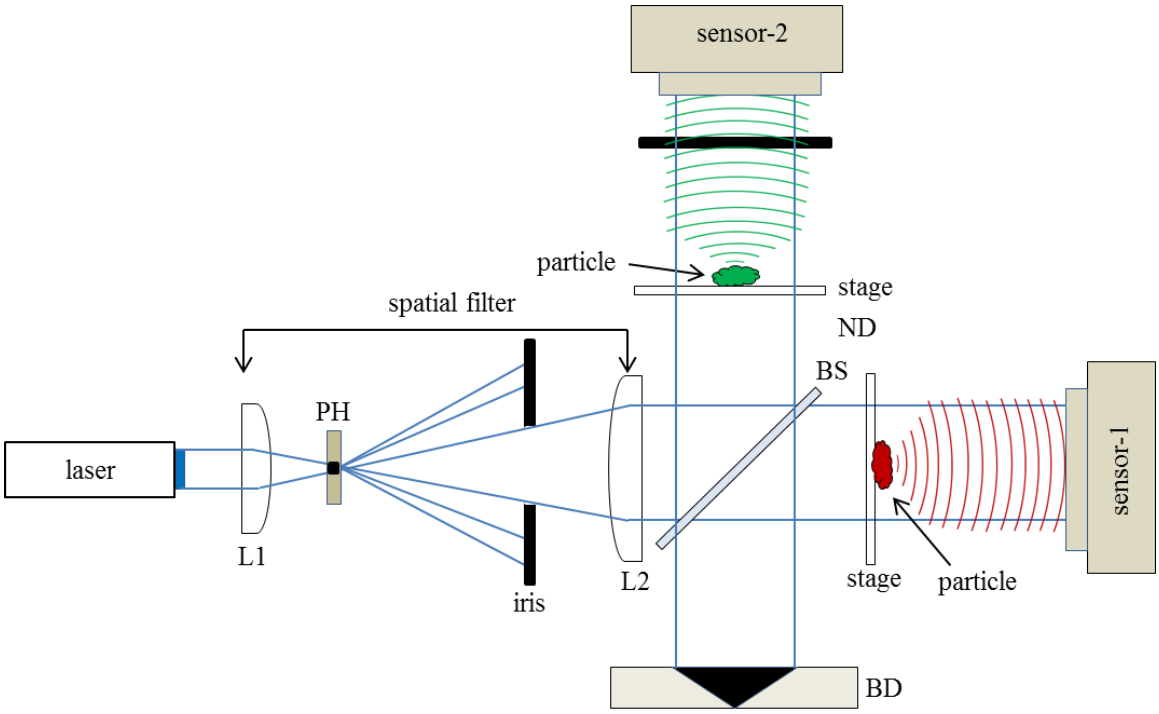

Figure 4.9 A digital holographic configuration in which two different samples are examined by recording particles' forward-scattered holograms simultaneously.

In the diagram, red and green light are the particles' forward-scattered light from the respective samples.

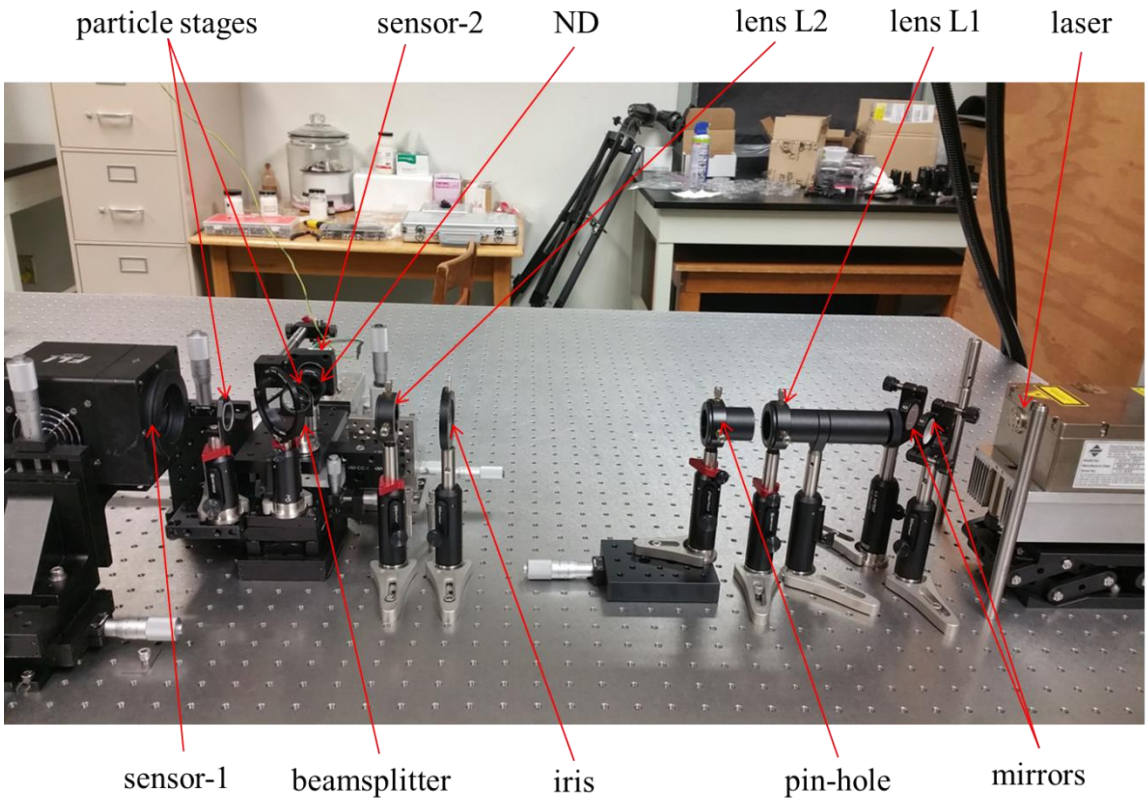

Figure 4.10 Experimental setup for the multiple samples examination.

4.4.2 Backward-scattering configuration

Second, the configuration presented in the Fig. 4.9 is modified to record backward-scattered holograms of two different samples in a single sensor. This configuration is achieved by replacing sensor-1 and sensor-2 by two BDs, and BD by a sensor (FLI Camera) in the Fig. 4.9. This configuration is presented in Fig. 4.11 below.

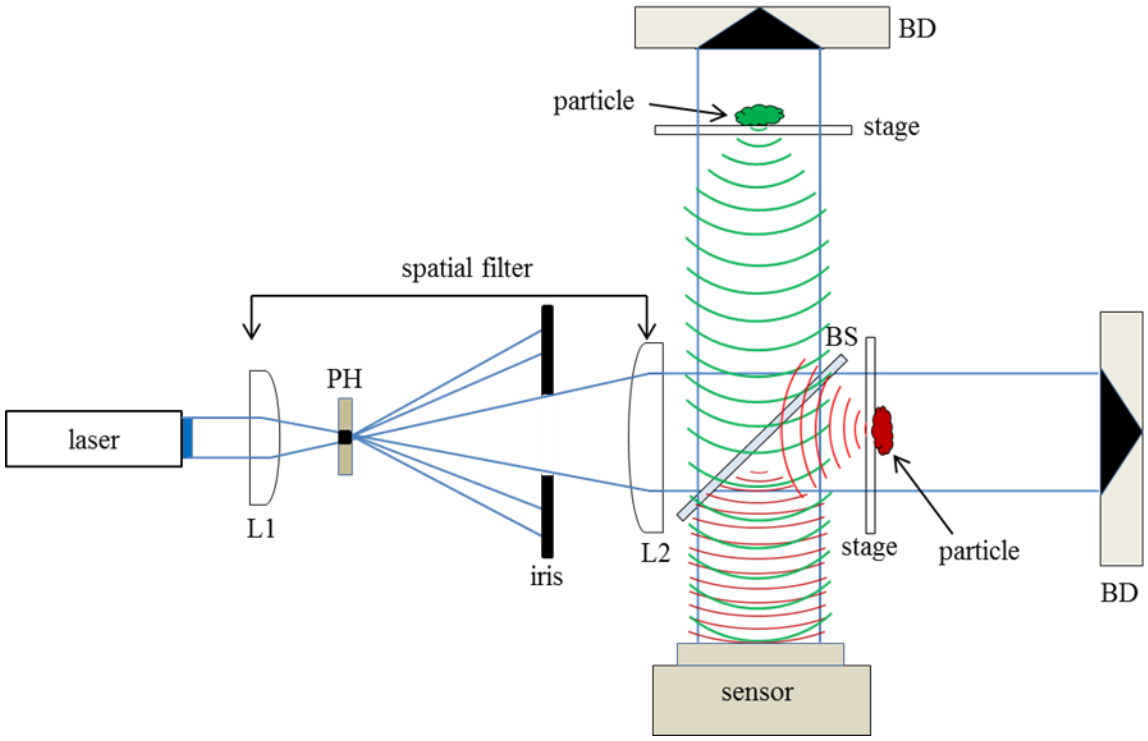

Figure 4.11 A digital holographic configuration in which two different samples are examined by recording particles' backward-scattered holograms simultaneously.

In the diagram, red and green light are the backward-scattered light from the respective samples.

In this configuration, a single wavelength is used to illuminate both samples simultaneously. Therefore, if both samples are at the equal distance from the sensor, it is hard to separate their images during the reconstruction procedure because they coincide with each other. To eliminate this problem, particle samples, which are under investigation, are placed at different distances from the sensor. In this work, one sample is placed at 6.5 cm and another sample is at 11 cm from the sensor during the recording of the holograms. In this case, the respective images of the samples focus at different reconstruction distances. Thus, the focusing on one image will not disturb by the other,

i.e., when one is in focus, other will be out of focus and disappear from the field-of-view and vice-versa.

4.5 References

1. Javidi and E. Tajahuerce, “Three-dimensional object recognition by use of digital holography,” *Opt. Lett*. **25**(9), pp. 610–612 (2000).

2. J. Garcia-Sucerquia, W. Xu, S. K. Jericho, P. Klages, M. H. Jericho, and H. J. Kreuzer, “Digital in-line holographic microscopy,” *Appl. Opt*. **45**, pp. 836–850 (2006).

3. M. K. Kim, *Digital Holographic Microscopy: Principles, Techniques, and Applications* (Springer, 2011).

4. G. K. Ackermann and J. Eichler, *Holography: A Practical Approach* (Wiley, 2007).

5. T. Kreis, *Handbook of Holographic Interferometry* (Wiley, 2005).

6. N. R. Subedi, N. B. Fowler, and M. J. Berg, “Backscatter digital holography of microparticles,” *Opt Express,* **21** (10), pp. 12611–12616 (2013).

7. M.J. Berg and G. Videen, “Digital holographic imaging of aerosol particles in flight,” *J Quant Spectrosc Radiat Transf*. **112**, pp. 1776–1783 (2011).

8. W. Xu, M. H. Jericho, I. A. Meinertzhagen, and H. J. Kreuzer, “Digital in-line holography of microspheres.” *Appl. Opt*. **41**, pp. 5367–5375 (2002).

9. M. Lee, O. Yaglidere, and A. Ozcan, “Field-portable reflection and transmission microscopy based on lensless holography,” *Biomed. Opt. Exp.* **2**(9), 2721-2730 (2011).

10. V. Mico, C. Ferreira, Z. Zalevsky, and J. Garcia, “Basic principles and application of digital holography microscopy,” *Formatex* (2010).

CHAPTER V

RESULTS AND DISCUSSION

In this chapter, various experimental results based on the in-line digital holographic principle using Fresnel-Kirchhoff diffraction integral presented in Eq. 3.23 will be discussed. To reconstruct the image of a variety of particles available in the laboratory, the recorded digital holograms of these particles in different configurations presented in Fig. 4.1-4.11 are used. To make the results consistent, the parameters that influence the process of recording of holograms are kept fixed and all the holograms are recorded exactly in the identical condition for the given configuration.

This work readily describes a proof-of-principle experiment where the digital holograms of single and multiple microparticles are measured simultaneously using forward- and backward-scattered light. Following reconstruction of the particle image, the pattern can then be unambiguously and quantitatively associated with the shape, size, and orientation of the particle produced. The computationally reconstructed images from the digitally recorded holograms compare well in quality and accuracy to the corresponding microscope images.

5.1 Validation and calibration

After following the recording procedure explained in Sec 3.4, the contrast hologram of the sample is obtained. The result is presented in Fig. 5.1 below. This step is

crucial to remove imperfections in the illumination-beam profile and improve the resolution of the subsequent particle-image.

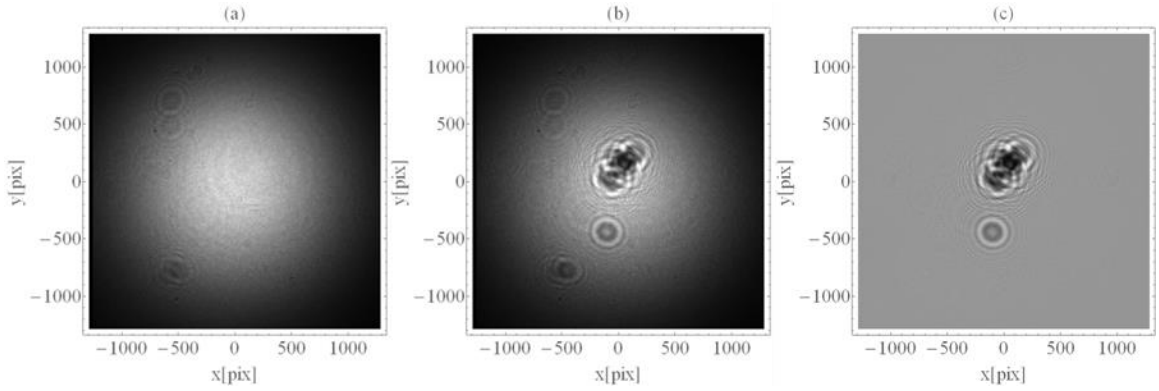

Figure 5.1 Plots (a), (b), and (c) show background, raw hologram, and contrast hologram of the ragweed pollen cluster, respectively.

The contrast hologram in the plot (c) is the result of the subtraction of plot (a) from the plot (b).

The reconstruction procedure explained in Sec 3.5 is then applied to that contrast hologram to render the image of the particle. The contrast hologram, I^{con}, in the plot (c) above is fed into the Fresnel-Kirchhoff diffraction integral presented in Eq. 3.23, and then by evaluating integral in the image plane, the absolute square of the resulting wave amplitude, *K,* forms the image of the particle. This image of the particle is presented in Fig. 5.2 below.

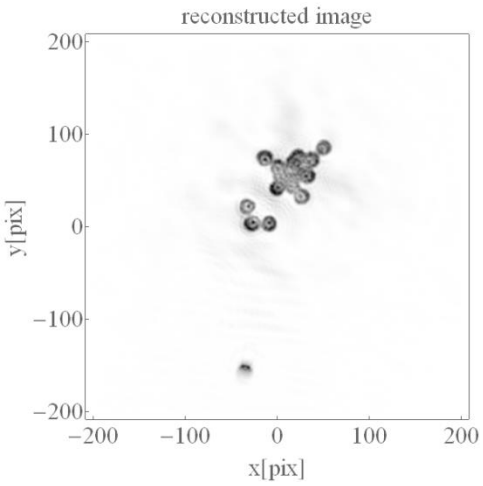

Figure 5.2 Plot shows the reconstructed image of the ragweed pollen cluster using contrast hologram presented in Fig. 5.1 (c).

To test the apparatus and validate the result, a comparison is made between the holographic and conventional optical microscope images of the same particle. This is done by placing a ragweed pollen cluster on a particle stage. For this purpose, the pollen cluster is first put on a clean stage and then imaged with the conventional optical microscope. Afterwards, the stage with the same pollen cluster is transferred to the holographic measurement position, and a hologram is recorded, on which the image reconstruction procedure is followed. The almost similar procedure is followed on 50 μm traceable borosilicate glass spheres. At this time, the borosilicate glass spheres are sprinkled in a clean particle stage and image of the particle is taken using a smartphone (Samsung galaxy, Note 4, 12 Megapixel camera). Afterwards, the stage with the same spheres is transferred to the holographic measurement to record a hologram. The holographic reconstructed image is compared with the smartphone image. In both cases, immediately after recording the raw holograms, the background intensities are recorded

by blowing the particle samples from the stage, which are then used to get the respective contrast holograms.

Both the examples demonstrating the comparison between the reconstructed holographic and conventional optical microscope images of the same sample are presented in Figs 5.3 and 5.4, respectively.

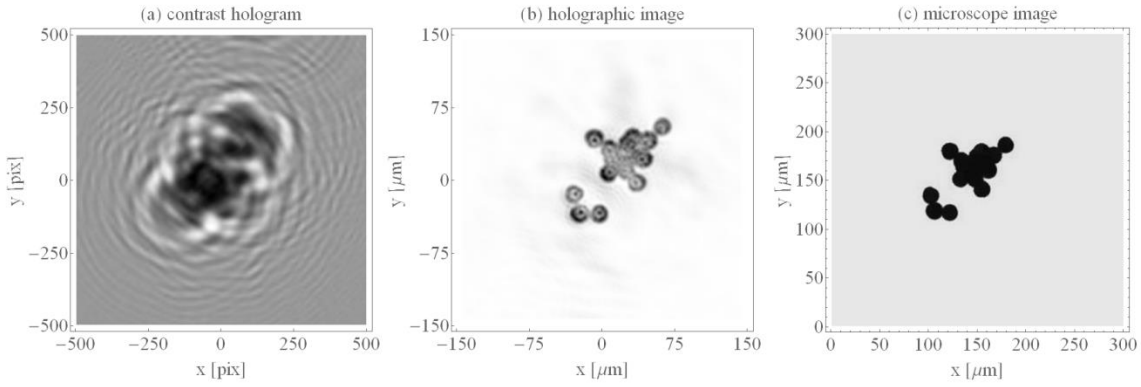

Figure 5.3 Plots (a), (b), and (c) show contrast hologram, reconstructed image, and conventional microscope image of the same ragweed pollen cluster, respectively.

The above contrast hologram shown does not display the full sensor output; it is cropped to show only the portion of the hologram that is considered in validation.

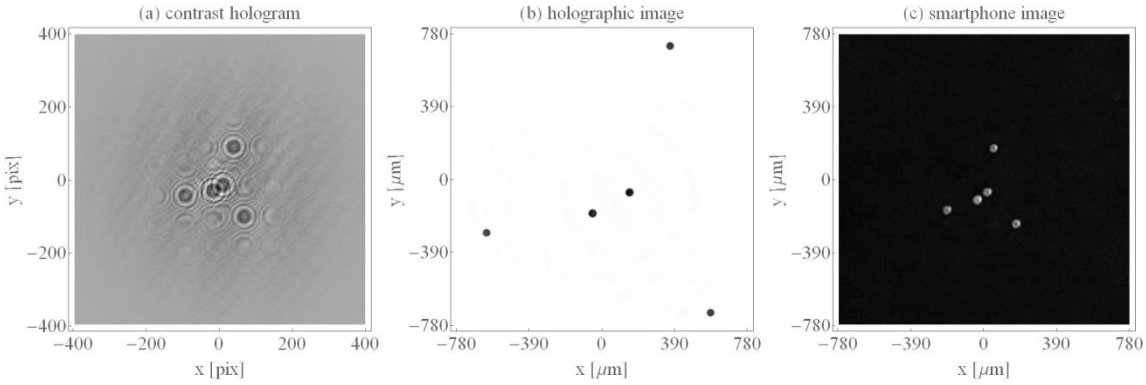

Figure 5.4 Plots (a), (b), and (c) show contrast hologram, reconstructed image, and smartphone image of the same 50 μm borosilicate glass spheres, respectively.

The above contrast hologram shown does not display the full sensor output; it is cropped to show only the portion of the hologram that is considered in validation.

In the Figs. 5.3 and 5.4, plots are not calibrated. The field-of-view in the Fig. 5.4 is significantly larger (or, less magnification) than that in Fig. 5.3 to include all the particles inside the reconstructed image so even the 50 μm glass spheres are appearing smaller than the ragweed pollen, which are approximately 20 μm in size. A comparison between two contrast holograms, i.e., Figs. 5.3 (c) and 5.4 (c), shows that when the particles are clustered, the hologram is more complex. For a large group of particles, the hologram is extremely complex, but there is no well-established general rule to interpret them.

By comparing these two images, it can be seen that the holographic setup successfully produces an accurate image of the ragweed pollen cluster and 50 μm traceable borosilicate glass spheres with sufficient resolution to discern individual particles. In other words, computationally reconstructed images from the digitally

recorded holograms compared well in quality and accuracy to the corresponding microscope images.

While a holographic image at once presents a particle's shape and size, it is necessary to describe these properties quantitatively. Yet, irregularly-shaped particle images vary with particle orientation. Thus, it is necessary to use analysis that is rotationally invariant to quantitatively describe the shape of these particles. However, in this work, only a rough calibration is performed using Thorlabs resolution plate (R1L3S2P-1mm Stage Micrometer) and 1951 U.S. Air Force (USAF) glass slide resolution target (Edmund Optics), and the calibration is then tested in various standard-sized particles, such as National Institute of Standards and Technology (NIST)-traceable borosilicate microspheres (Duke Scientific Corp.) and optical fiber (Newport Corporation, F-SMF-28) of diameter 245 μm. For this purpose, a scale factor is determined relating the microscope-image pixel number to micrometers. Then, by comparing the holographic image of a resolution plate to the microscope image of the same test plate, an additional scale factor is determined relating the hologram pixel number to micrometers. In this way, the holographic images of all subsequent particles are rendered in calibrated micrometer length rather than pixel number. This overall process of relating the pixel number to micrometers is identical with the process explained in [9].

Examples are presented in Fig. 5.5 - 5.7 demonstrating the calibration of the scale from hologram pixel number to micrometers.

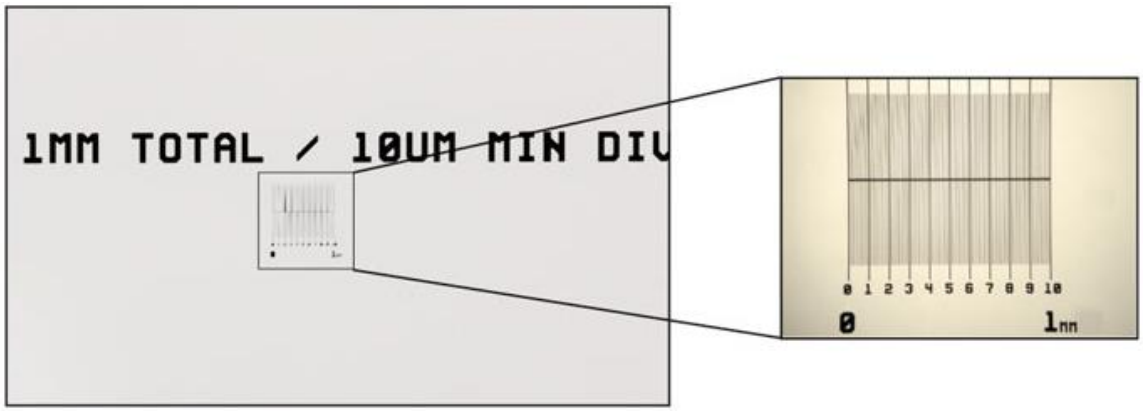

Figure 5.5 Thorlabs resolution plate.

The plot shows the Thorlabs resolution plate picture provided by the manufacturer company to show the product details.

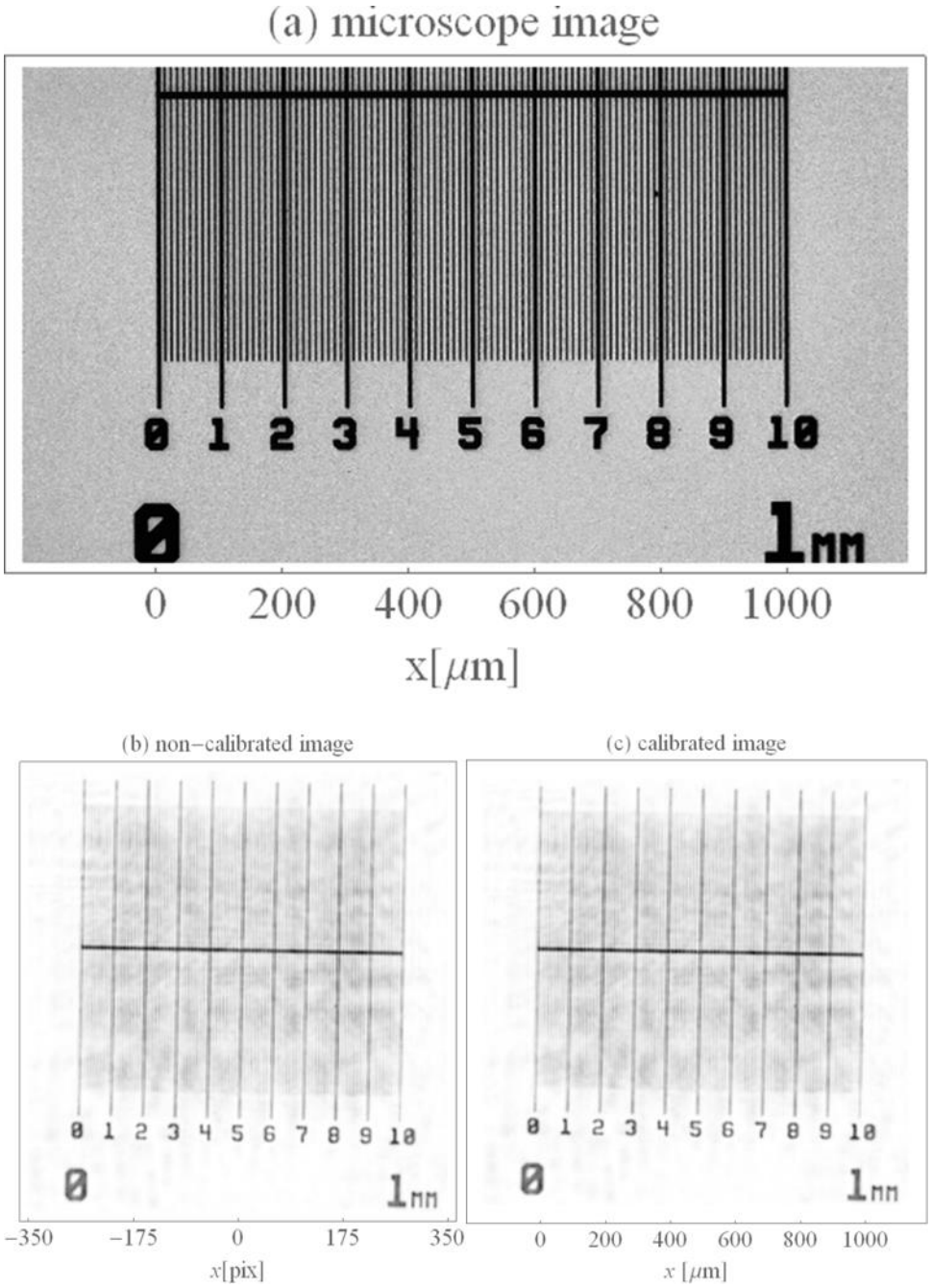

Figure 5.6 Plot (a) shows the microscope image of Thorlabs test plate, and plots (b), and (c) show non-calibrated and calibrated reconstructed images, respectively.

The purpose of showing plots (b) and (c) the same size as the reconstruction output is to make small lines visible.

In this Thorlabs resolution plate, two small lines are 10 μm apart and makes the total distance from 0 to 1 mm equal to 1000 μm. In the above reconstructed images, these lines are clearly distinguishable; however the resolution is poor. This somehow indicates the resolution limit of this work.

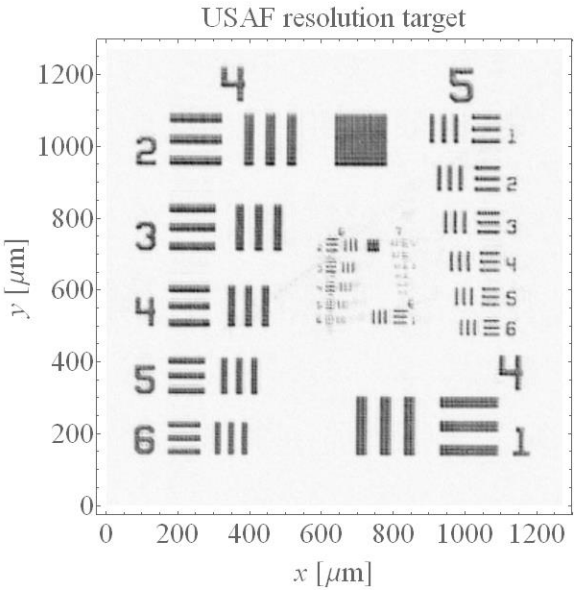

Figure 5.7 Plot shows the calibrated reconstructed image of 1951 U.S. Air Force (USAF) resolution target due to the forward scattering light.

After calibrating the scale on Thorlabs resolution plate (R1L3S2P-1mm Stage Micrometer) and 1951 U.S. Air Force (USAF) glass slide resolution target (Edmund Optics), the calibration is tested in 245 μm optical fiber and 30 μm borosilicate glass spheres, and the result is presented in Fig. 5.8 below.

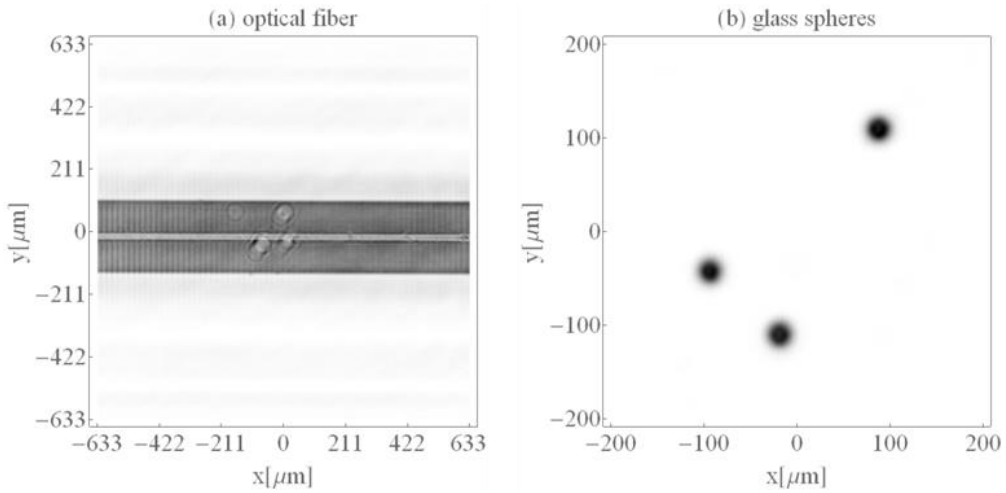

Figure 5.8 Plots show the calibrated reconstructed images of 245 μm optical fiber and 30 μm borosilicate glass spheres due to the forward scattering light, respectively.

Above results show that the calibrated scale is working well for standard particles, such as optical fiber and borosilicate glass spheres. This makes it convenient to use the same calibrated scale factor for a variety of other particles.

5.2 Resolution limit

A rough estimate for the resolution of the holographic image is made using 10 μm diameter traceable borosilicate glass microspheres on a particle stage and positioning the stage in the measurement volume of the laser beam. The result is presented in Fig. 5.9 below.

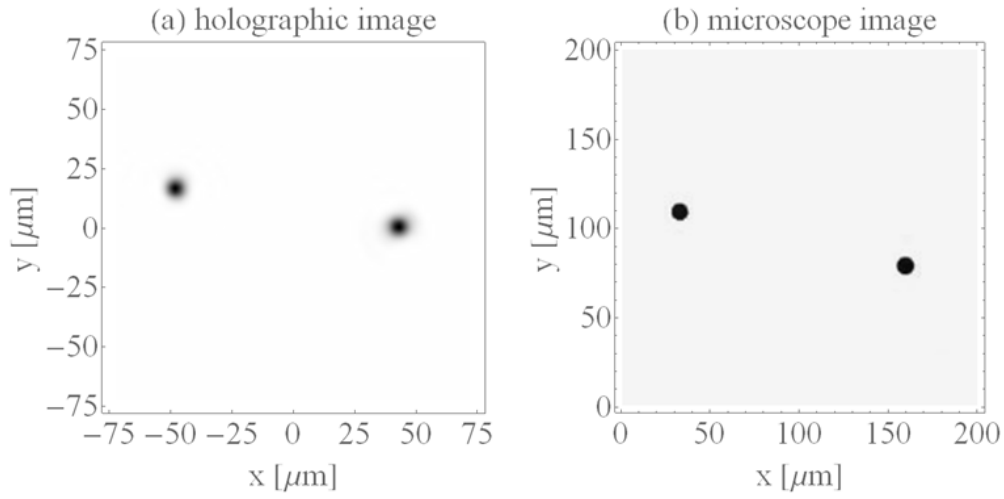

Figure 5.9 Estimation of the resolution limit of the experimental configurations.

Plot (a) shows the holographic image of the 10 μm diameter borosilicate glass microspheres and (b) shows the conventional optical microscope image of the same microspheres.

The image resolution in this work is ~10 μm. This resolution is sufficient for most of the micron-sized particles to clearly discern the size and shape of a single particle, but this does not resolve the smaller features, such as surface roughness of many particles like the spikes on the ragweed pollen spores, which are roughly about 1 μm in size. Partly the resolution is determined by the numerical aperture, *NA*, as defined by the solid angle subtended by the sensor at the particle. Thus, increasing the sensor size and decreasing λ will improve the resolution.

In short, the resolution limit is given by the eq. (3.25) as,$\delta r = \frac{\lambda z_i}{N\Delta}$, where λ is the wavelength of the light used to illuminate the particle, z_i is the distance between the object and sensor, N is the number of pixels in the sensor array, and Δ is pixel size.

In our case, $\lambda = 351$ nm, N = 2574 pixels (only lower side of FLI camera is considered), Δ = 5.4 μm, and $z_i \approx 6.5$ cm; therefore the approximate resolution limit of

the reconstructed image is $\delta r \approx 1.6$ μm. However, the sensor pixel-size Δ restricts the fringe-spacing resolved in the hologram, and hence, the subtle details in the images. The effect of Δ can be decreased with increasing polar scattering angle θ. But, due to the physical limitation, the sensor size cannot be arbitrarily increased as its outer portions will not resolve the hologram. Therefore, only optimal resolution is achieved for a given pixel and array size by balancing the different limitations during the recording phase.

However, a single lens can be used to magnify the hologram such that a large-format sensor can resolve it fully without degrading the *NA*. I have planned to implement this step in my future research directions.

5.3 Computationally focusing of image in DH

The holographic imaging technique offers a unique capability of obtaining some sense of the three-dimensional form of an image from a single measurement. The basic concept is analogous to the "focusing in" on a particle in conventional microscopy. In the conventional microscopy, the microscope objective is moved mechanically to vary the distance between it and the microscope slide, causing a blurred image of a particle to evolve into a sharp image and then again blurred once the sharp image is evolved as shown in diagrams (a)-(c) in Fig. 5.10. If the particle is thick and transparent, then different depths within the particle can be brought into focus to provide insight into particle's three-dimensional structure. In DH, the same process can be done by computationally varying the distance $z = d$ used in the image reconstruction stage as described in [1, 2, 9]. The resulting reconstructed image gives the same impression of focusing in on the particle as one gets from conventional microscopy. For this, in the

microscopy, an image must be recorded at each focus depth; however, in DH similar image sequence is obtained from a single contrast hologram only.

Fig. 5.10 presents an example showing this holographic focusing process. The top row (a)-(c) shows the scanning electron microscope image of a gecko-shaped object and Shell logo at three different focus depths; whereas, the middle row (d)-(f) shows the optical microscope images of 30 μm borosilicate glass sphere at three different focus depths. This clearly shows that for a particular given microscope objective, there is only one in-focus image, i.e., images (b) and (e). Below and above that point only a blurred image is possible as shown in images (a) and (c) and (d) and (f). Then the bottom row shows a holographic image sequence for a NaCl particle that is produced by computationally scanning the reconstruction plane along the z-axis around $z = d$. By comparing these three rows, one can clearly see that there is a strong similarity in the focusing behavior of these imaging techniques.

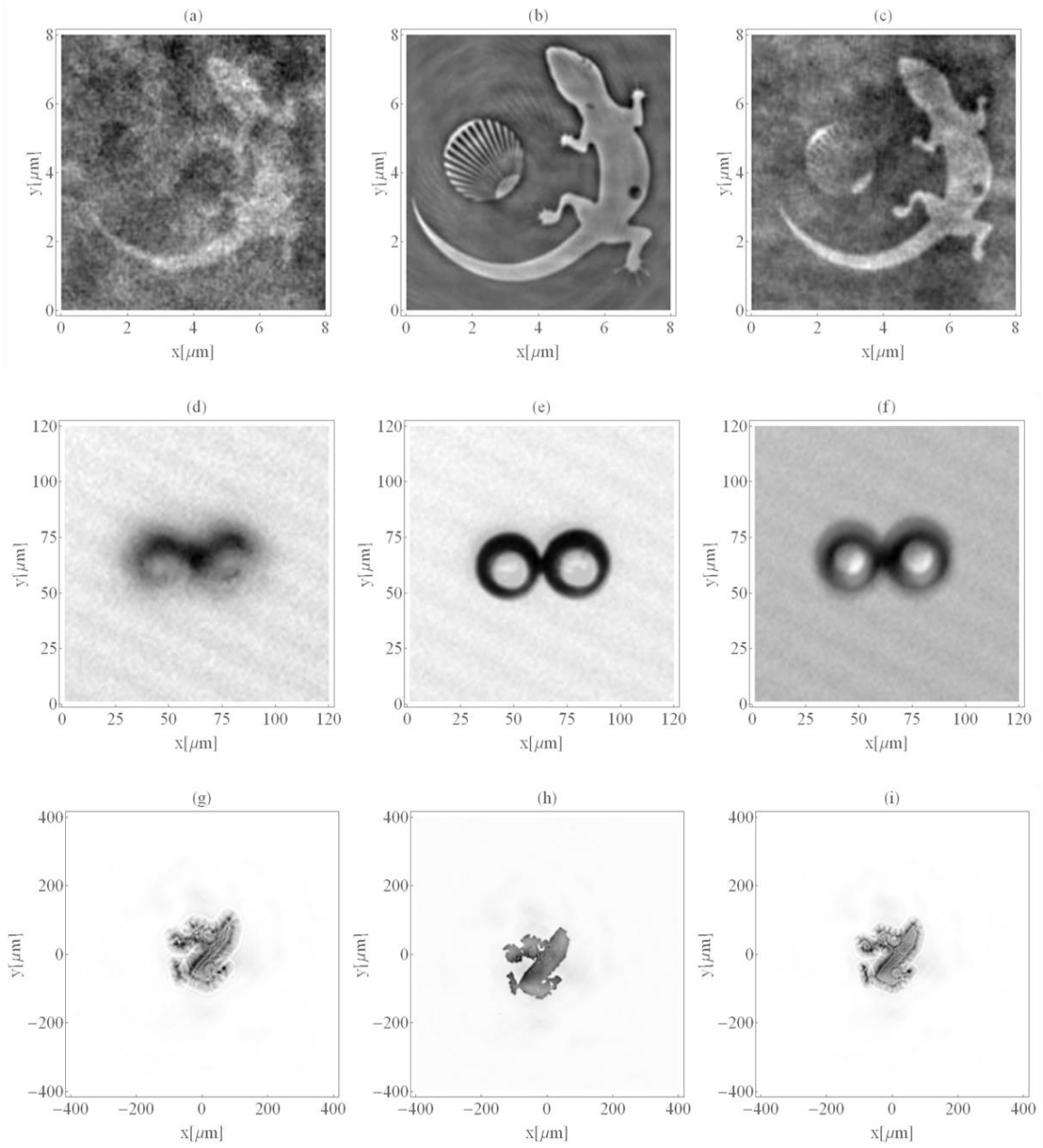

Figure 5.10 Focusing behavior of the holographic image reconstruction process.

The top row shows scanning electron microscope images of a gecko-shaped object and Shell logo at three different focus depths (a) – (c). The middle row shows the optical microscope images of 30 μm borosilicate glass spheres at three different focus depths (d)-(f). The bottom row shows the reconstruction image of NaCl particle when the reconstruction plane is at the three positions for z: $z < d$ for (e), $z = d$ for (f), i.e., in focus, and $z > d$ for (g), respectively.

The idea of the images in the top row is adopted from [2].

After validating the result and finding the resolution limit of the work, different experimental configurations are considered to record the forward- and backward-scattering holograms of a variety of particles. These configurations are as follows:

5.4 Forward-scattering configuration

The forward scattering configuration is the most commonly used configuration in DH. The reason for this is that it is simple to construct and easy to operate. This configuration is best suited for the small and transparent particles.

To record the hologram of a particle due to forward-scattered light, two different configurations as described in Sec. 4.1 are considered, and corresponding images are reconstructed by following the previously outlined image reconstruction procedure presented in Sec. 3.5.

The contrast holograms and reconstructed images of 20 μm borosilicate glass spheres, volcanic ash, and clay using the configuration in Fig. 4.1 (or, Fig. 4.2) are shown below. In this configuration, particles are illuminated by what is approximately a spherical wave originating from the beam waist. The beam continues until reaching the sensor, at which point it expands to fill the entire pixel array. The separation between the particle sample and the sensor is approximately 6.5 cm.

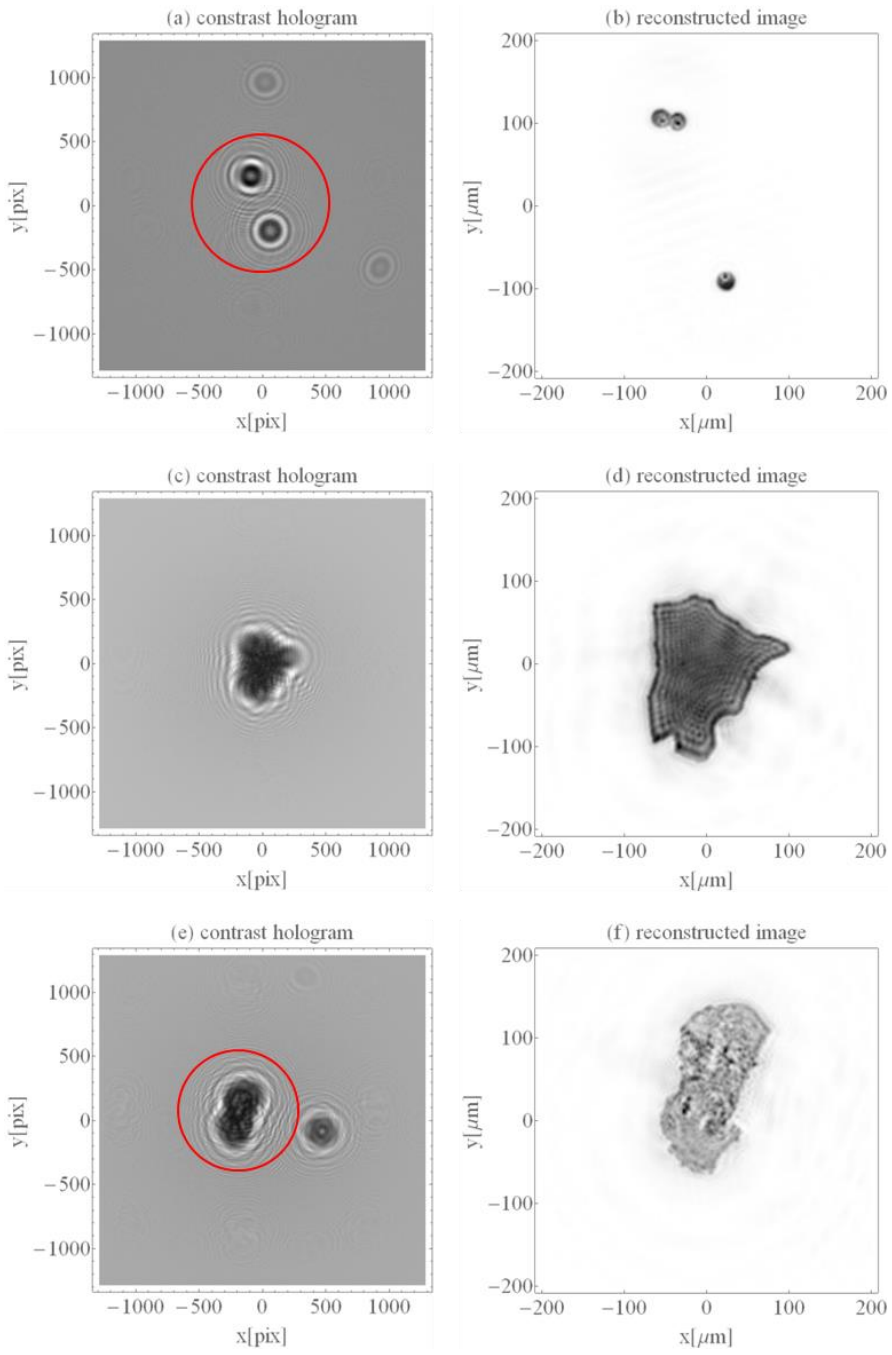

Figure 5.11 Glass spheres, volcanic ash and clay particle.

Images (a) and (b) show the contrast hologram and corresponding reconstructed image for 20 µm borosilicate glass spheres, images (c) and (d) show the same for a single volcanic ash particle, and images (e) and (f) for a clay particle, respectively.

The red circle in the contrast holograms highlight the area of the hologram considered in reconstruction.

Here, due to the spherical nature of the illuminating light, there is a relative amplification of the scattered wave at the sensor, which enhances the interference pattern of the hologram leading to slight magnification on the recording plane. However, it introduces an aberration if a linear type object such as optical fiber is considered. This is in comparison with the results obtained when the same sample is illuminated with the collimated beam.

The contrast holograms and reconstructed images of 30 μm borosilicate glass spheres, NaCl particle, and pecan pollen using the configuration in Fig. 4.3 are shown below.

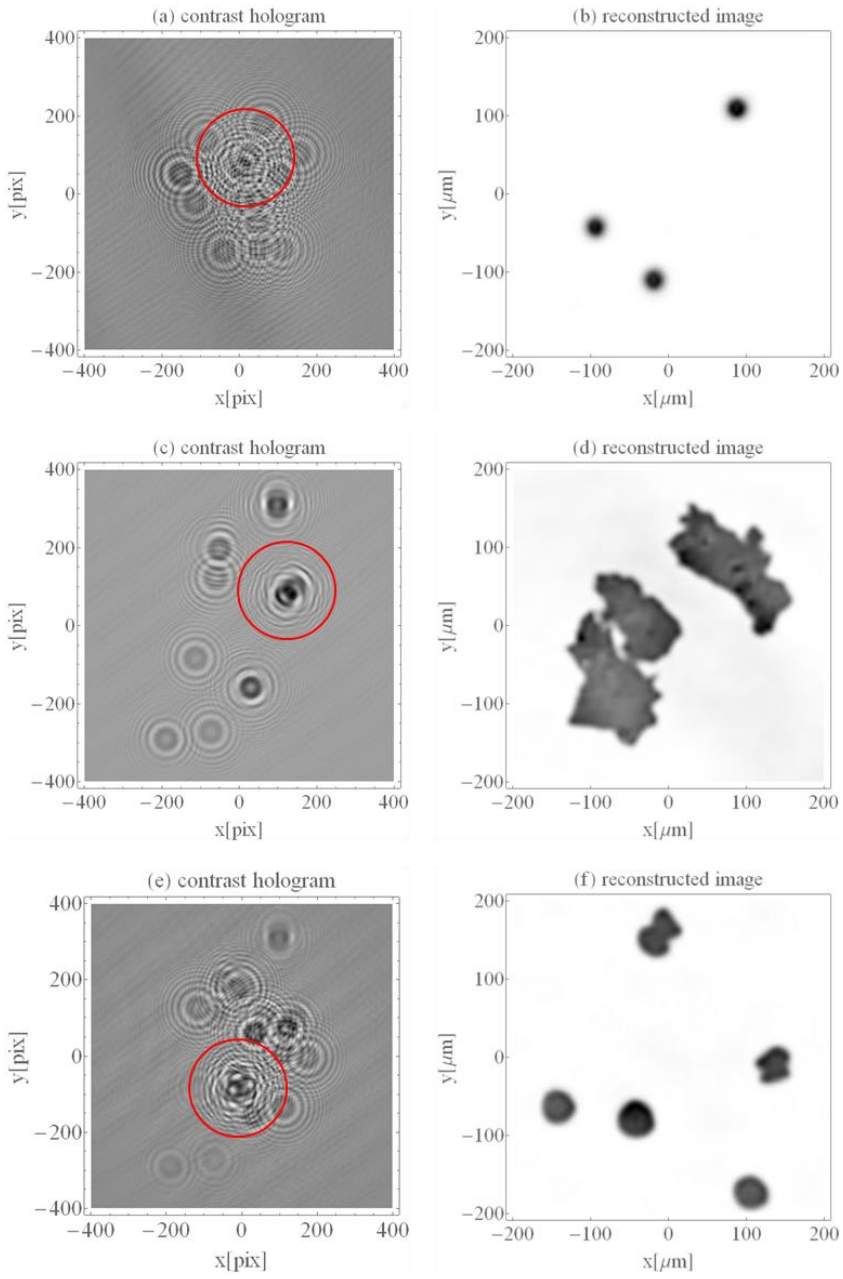

Figure 5.12 Glass spheres, NaCl particle, and pecan pollen.

Images (a) and (b) show the contrast hologram and corresponding reconstructed image for 30 μm borosilicate glass spheres, images (c) and (d) show the same for NaCl particle, and images (e) and (f) for pecan pollen, respectively.

A comparison between two illuminating beam profiles in Figs. 4.1 and 4.3 shows that when a particle is illuminated by diverging beam profile, measurement volume, i.e.,

the volume right after the beam waist, is comparatively smaller than that in the collimated beam profile. This helps to focus into a particular particle on the particle stage and makes the steps of hologram recording much easier because of its magnifying nature. However, this adds some aberrations on the recorded hologram and hence, on the reconstructed image, than that of the case of the collimated beam illumination. To demonstrate this problem, the recorded hologram and corresponding reconstructed image of an optical fiber is presented in Fig. 5.13. It is also noted that the reconstruction distance, z, required to focus the image is highly sensitive to the small variation in the distance between the particle and sensor, d, during recording. To show this effect, a table showing the variation of reconstruction distance with the variation in the recording distance is presented in Table 5.1 below.

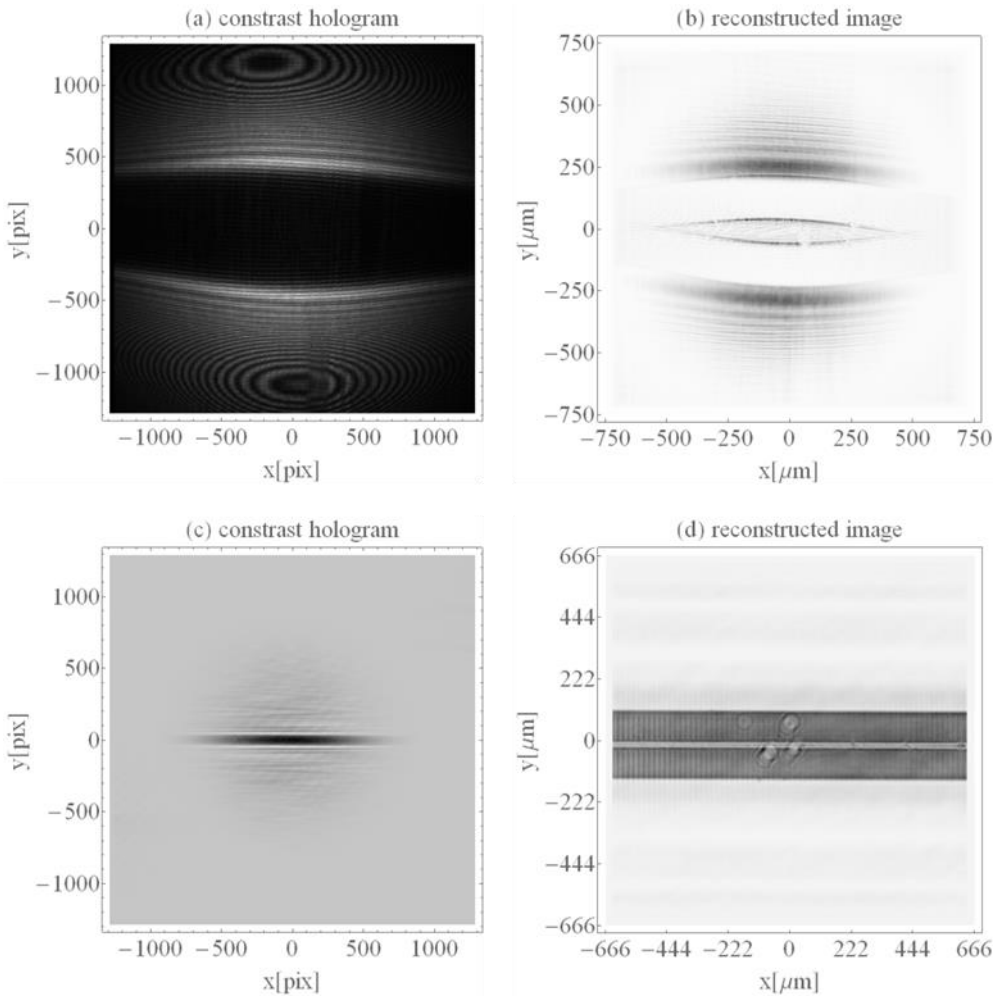

Figure 5.13 In the figure, plots (a) and (b) show the contrast hologram and corresponding reconstructed image of the fiber during the diverging beam illumination, and plots (c) and (d) show the same for collimated beam illumination, respectively.

Table 5.1 Comparison between the recording and reconstruction distances in diverging and collimated beam illumination.

Diverging beam illumination		Collimated beam illumination	
Recording distance (d in cm)	Reconstruction distance (z in log scale)	Recording distance (d in cm)	Reconstruction distance (z in log scale)
7.0	0.8000000	7.0	0.0705775
7.5	0.9500000	7.5	0.0720500
9.0	1.3060000	9.0	0.0767550

5.5 Backward-scattering configuration

In DH, using a particle's forward-scattering light to record the hologram is more common and widely used. Despite its simplicity and ease of operation, the forward-scattering geometry is not suitable to image opaque objects since the forward-scattered hologram yields only its silhouette after image reconstruction. Thus, the particle surface characteristics are obscured. Therefore, the motivations of this configuration relates to imaging opaque particles to discern surface textures, or structural features, that are sufficiently larger than the diffraction limit. While the resolution of the imaging technique can be improved, various results in this configuration demonstrate that backward-scattered light holographic imaging may be useful for studies of opaque micrometer-sized particles that must be examined in a contact-free manner, including liquid or frozen aerosol particles.

Similar to the forward-scattering configuration, two different configurations as described in Sec. 4.2 are considered to record the backward-scattered holograms of the

particles and corresponding images are rendered computationally following the same image reconstruction procedure.

In Fig. 5.14 below, the contrast holograms and their respective reconstructed images using the configuration in Fig. 4.4 are presented.

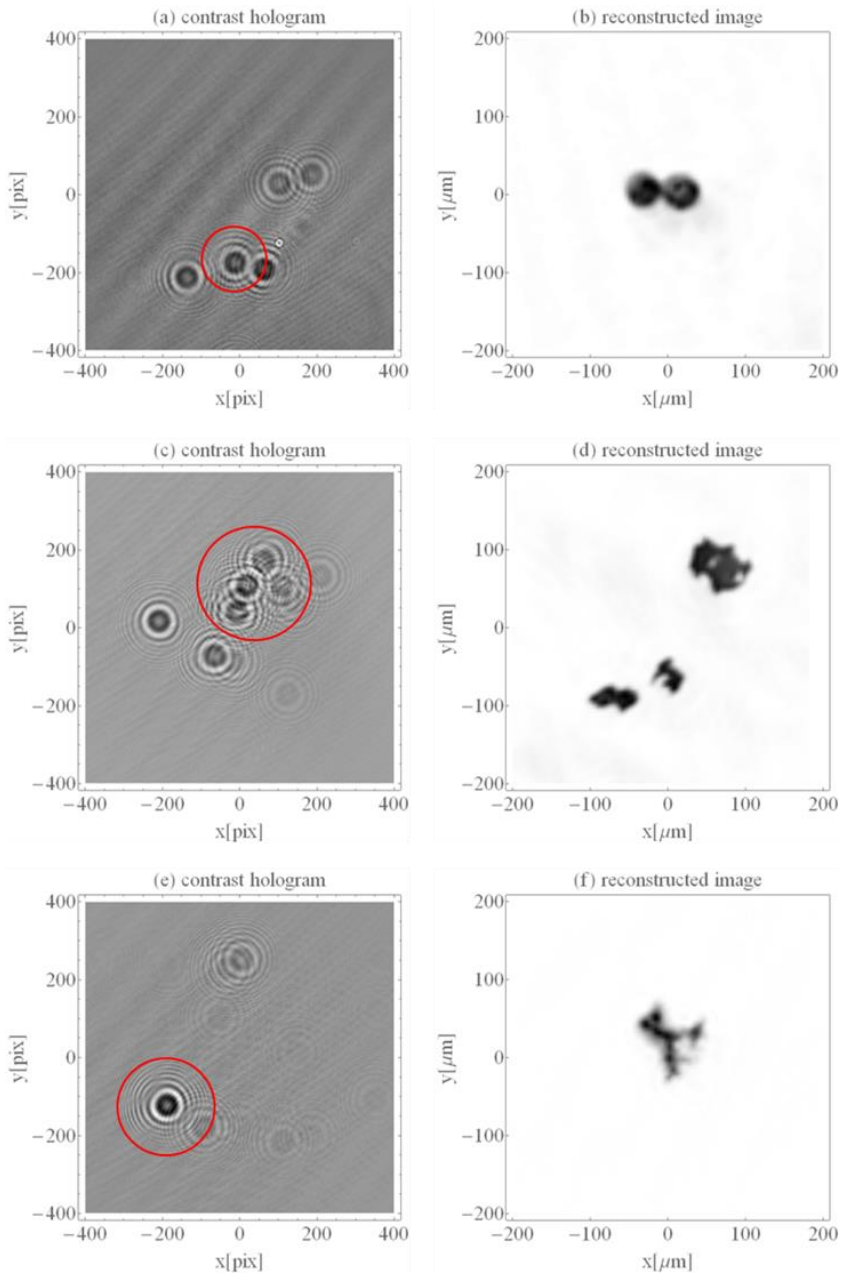

Figure 5.14 Glass spheres, iron powder, and aspergillus flavus spores.

Images (a) and (b) show the contrast hologram and corresponding reconstructed image for 50 μm borosilicate glass spheres, images (c) and (d) show the same for iron powder, and images (e) and (f) for aspergillus flavus spores, respectively.

Likewise, in Fig. 5.15 below, the contrast holograms and their respective reconstructed images using the configuration in Fig. 4.5 are presented.

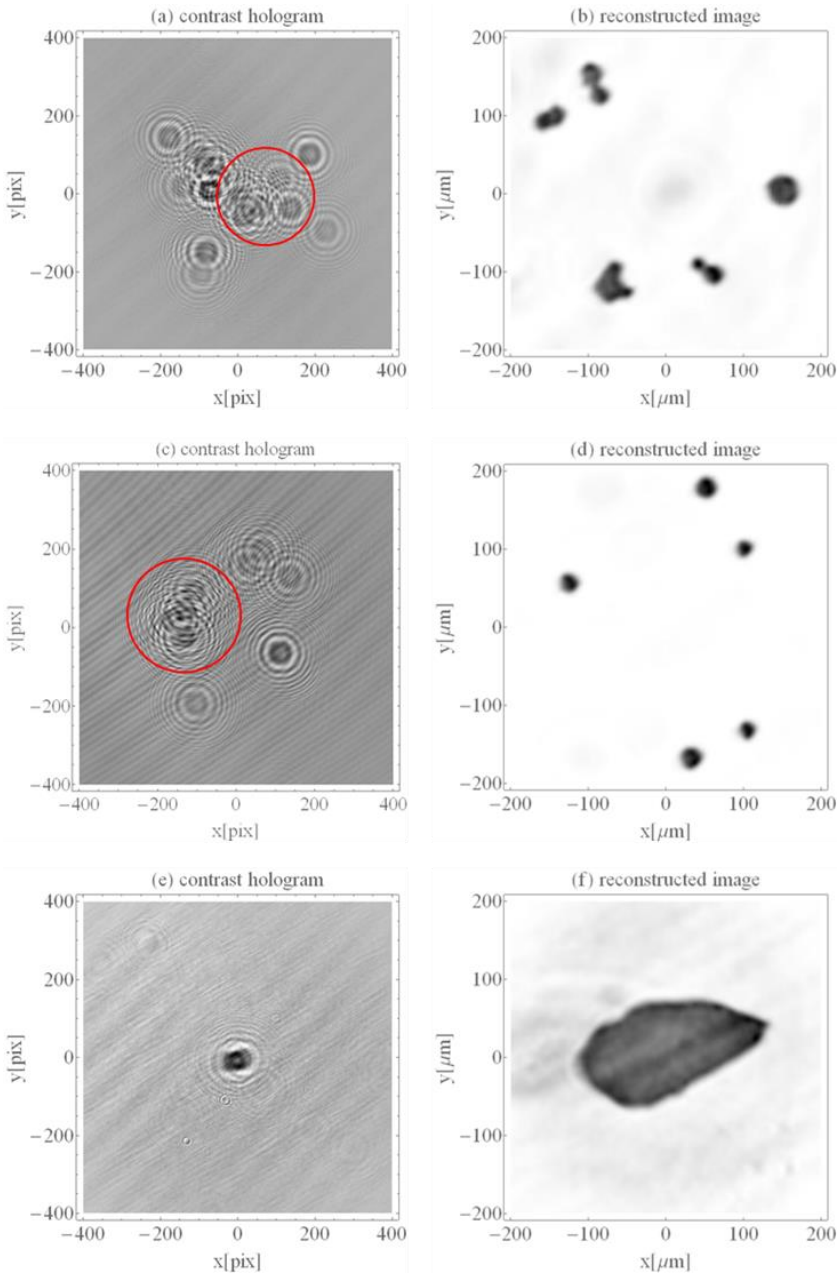

Figure 5.15 Ash, lycopodium powder, and Mississippi road dust.

Images (a) and (b) show the contrast hologram and corresponding reconstructed image for ash particles, images (c) and (d) show the same for lycopodium powder, and images (e) and (f) for Mississippi road dust, respectively.

A close look between the Figs. 5.14 and 5.15 shows that the reconstructed images presented in Fig. 5.15 have some background noise. This noise is either from the twin

images or from the multiple reflections between the sensor array and particle stage. Since the sensor array and particle stage are facing each other, there is a higher chance of multiple reflection between them and ultimately, result in a background noise in the reconstructed images.

5.6 Simultaneous configuration

To record the holograms of a particle due to both forward- and backward-scattering light, two different configurations, as shown in Figs. 4.5 and 4.6, are considered. Since the forward-scattering configuration is suitable mostly for transparent and small particles, the backward-scattering configuration, together with forward-scattering, adds the extra capability to the digital holographic imaging technique, and both transparent and opaque particles can be considered without any limitation. One motivation for this configuration is to develop an imaging modality, which can record both forward- and backward-scattering holograms of a particle simultaneously and allow a side-by-side comparison between the reconstructed images. This information could be useful for the characterization of various micron-sized particles and lay the foundation for the future instrument-development.

The reconstructed images due to both forward- and backward-scattered holograms using the configuration in Fig. 4.6 (or, Fig. 4.7) are presented in the Fig. 5.16 below.

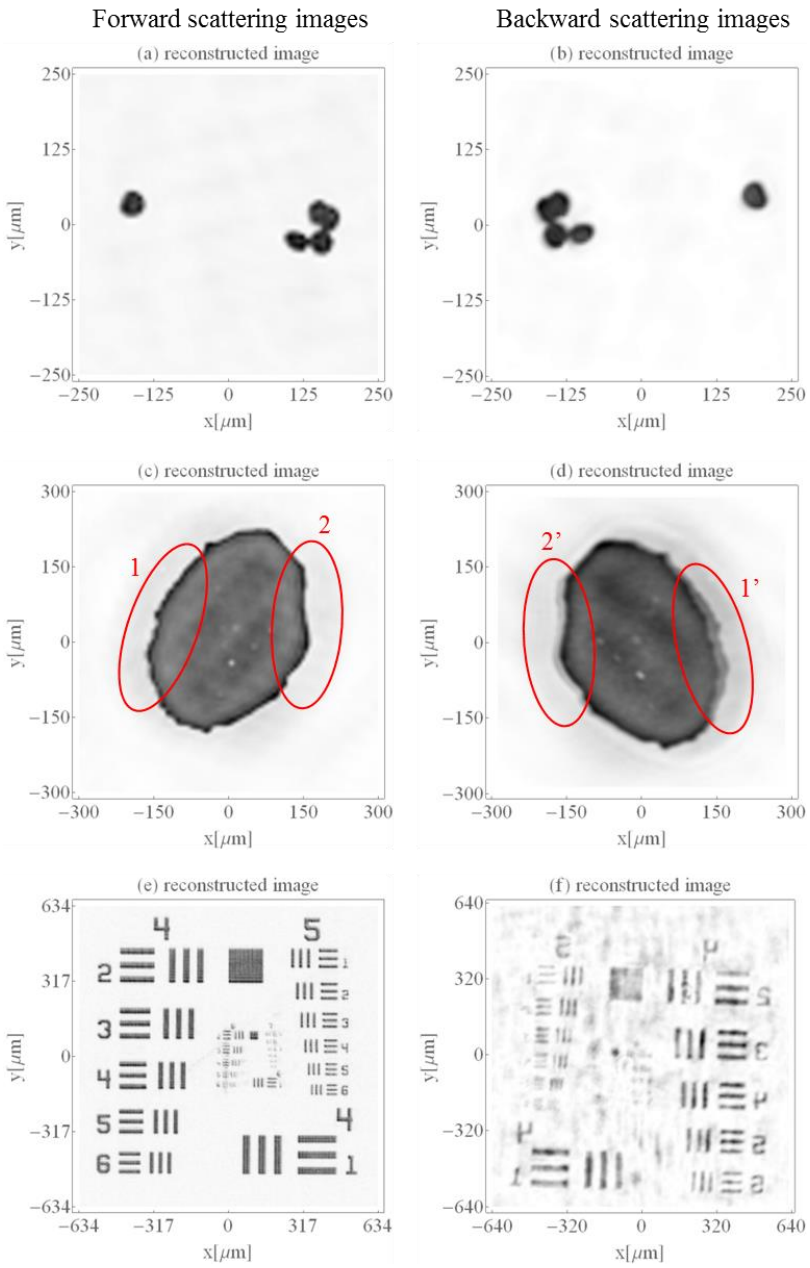

Figure 5.16 Pecan pollen, Mississippi road dust, and USAF resolution target.

Images (a) and (b) show the reconstructed images for pecan pollen due to the forward- and backward-scattered holograms, images (c) and (d) show the same for Mississippi road dust, and images (e) and (f) for the USAF resolution target, respectively.
The red highlights in the images are to show up the explicit differences in a side-by-side comparison of two reconstructed images. To see significant differences, highlight 1 should be compared with 1' and 2 with 2', respectively.

A comparison between the forward- and backward-scattering images (e) and (f) in Fig. 5.16 shows that the backward-scattered image resolution is very poor as compared to the forward-scattered image. The reason for this is the high absorption coefficient of the resolution plate and very low backward-scattering. During the measurement it is found that for other samples, the sensor gets saturated at diode current, I_s=1.98 Amps, but at the time of this resolution plate the sensor only saturated at diode current of 3.25 Amps. This is a good indication that the method of backward-scattering imaging does not work well for highly absorbing particles and is best suited for reflecting particle.

Similarly, the reconstructed images due to both forward- and backward-scattered holograms using the configuration in Fig. 4.8 are presented in the Fig. 5.17 below.

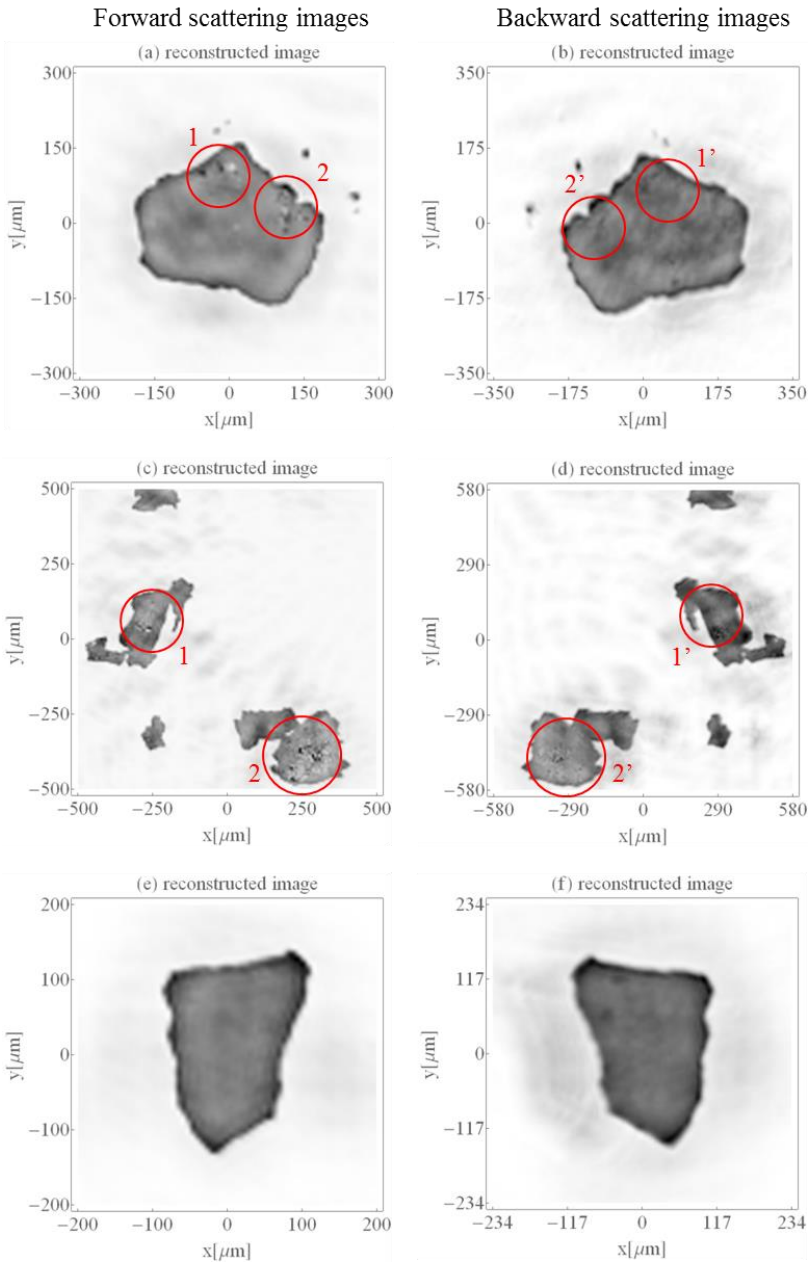

Figure 5.17 Clay, NaCl particle, and volcanic ash.

Images (a) and (b) show the reconstructed images for clay due to the forward- and backward- scattering holograms, images (c) and (d) show the same for NaCl particle, and images (e) and (f) for volcanic ash, respectively.

A close examination of the reconstructed images presented in Figs. 5.16 and 5.17 shows that the forward- and backward-scattering images hold different information on

the particle's surface textures and edge roughness. For example, images (c) and (d) in Fig. 5.16 show a significant difference in the ability to resolve detail about the "edge" of the particle images, whereas images (a) and (b), and (c) and (d) in Fig. 5.17 show noteworthy variation on the surface roughness. These differences show up in a side-by-side comparison of two images, explicitly in the highlighted regions 1 and 1', and 2 and 2'. This clearly suggests that the two image perspectives reveal aspects of the particle structure not available from forward-scattering alone. Therefore, this modality could be supportive to insight more on the particles' profile and hence, in characterizing their morphology and light-scattering behavior.

The poor resolution of the holographic image due to the backward-scattered light does not make the comparison process appealing. However, there should be a clear distinction between the images. To demonstrate the importance of backward imaging, a comparison between two images of the conventional optical microscope using the configurations shown in the Figs. 5.18 and 5.19 is made. These images are presented in Fig. 5.20 below.

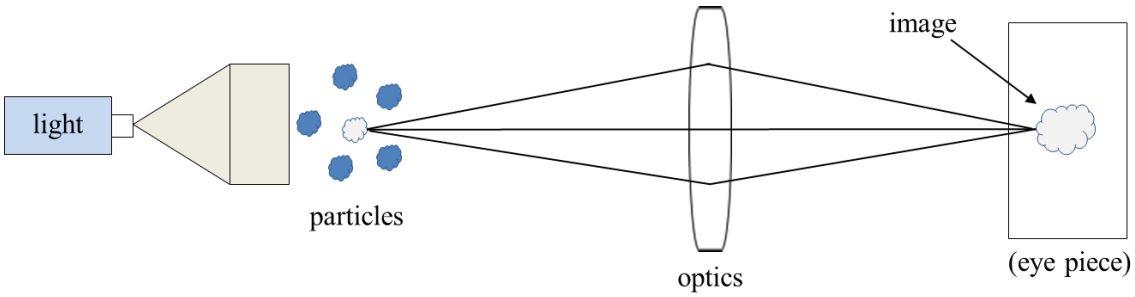

Figure 5.18 Imaging of an object in conventional optical microscope by illuminating through downward.

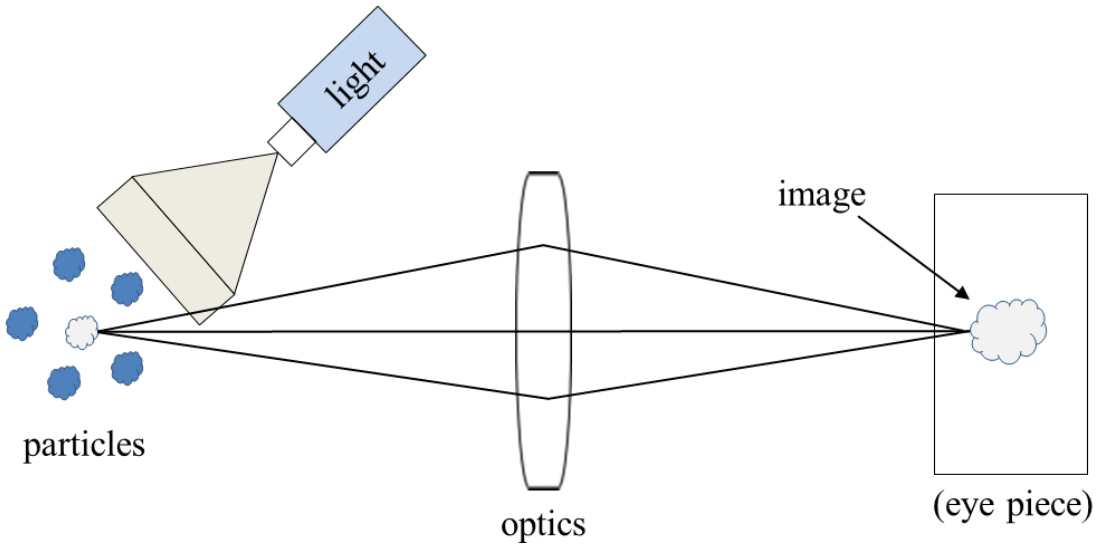

Figure 5.19 Imaging of an object in conventional optical microscope by illuminating from upward.

In these two configurations, the configuration presented in Fig. 5.18 is analog to the forward-scattering imaging, and the configuration presented in Fig. 5.19 is analog to the backward-scattering imaging in holographic system, respectively. By comparing the images of the same sample (opaque sample) in these two configurations, one can easily conclude that two imaging modalities reveal the different particle structures, which is not available from one side image alone. In the traditional configurations, the particles' forward-scattered light is usually used to form the image, thus opaque particles yield only a silhouette-image and the particle surface characteristics are obscured. We find the same is true here, yet some detail can be seen in the forward- and backward-scattered images that are different. The two images presented in Fig. 5.20 clearly demonstrate this feature and elucidate the importance of dual imaging modality. Since the particle's light scattering behavior is greatly depends on the particle's shape, size, surface texture, and

orientation, it is very important to know the details about the particle's morphology to accurately measure the *optical observables*.

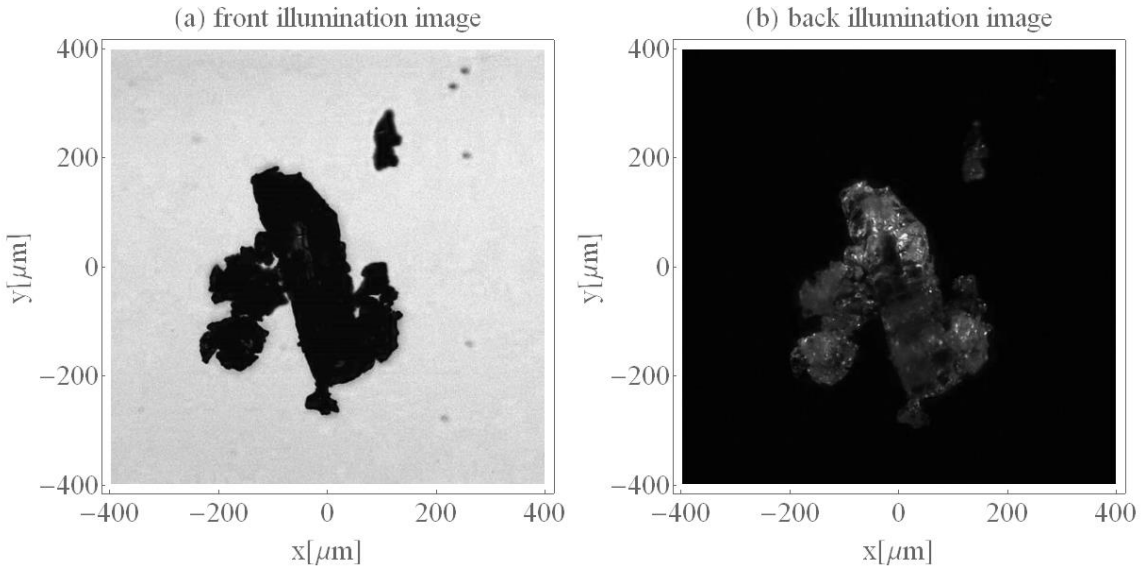

Figure 5.20 Plot (a) shows the image of NaCl particle using setup shown in Fig. 5.18 and plot (b) shows the image of the same particle using setup shown in Fig 5.19, respectively.

However, the resolution of the holographic image due to the backward-scattered hologram is very low as compared to the image due to the forward-scattered hologram. This may be the one reason we could not see the subtle details on the surface texture. To get the details on the surface texture, the resolution of the holographic image should be around 1 μm. The resolution could be improved using a sensor with greater dynamic range, by illuminating the particle with shorter wavelength light, and using a positive lens to magnify the particle's hologram during recording.

5.7 Multiple-sample study

The experimental arrangements presented in Figs. 4.9 - 4.11 are built to analyze multiple samples simultaneously. In Fig. 4.9 (or, Fig. 4.10), forward-scattered holograms of two different samples are recorded using two different sensors, whereas in Fig. 4.11, backward-scattered holograms of two different samples are recorded using a single sensor simultaneously. In the first arrangement, both samples are kept at the equal distance from the sensors, whereas in the later arrangement, these samples are kept at different distances from the sensor to minimize the problem described in Sec. 4.4.2. This means that the two reconstructed images are in focus at different reconstruction distances.

The reconstructed images of the two different samples due to the forward-scattered light using the arrangement in Fig. 4.9 are presented in the Fig. 5.21 below.

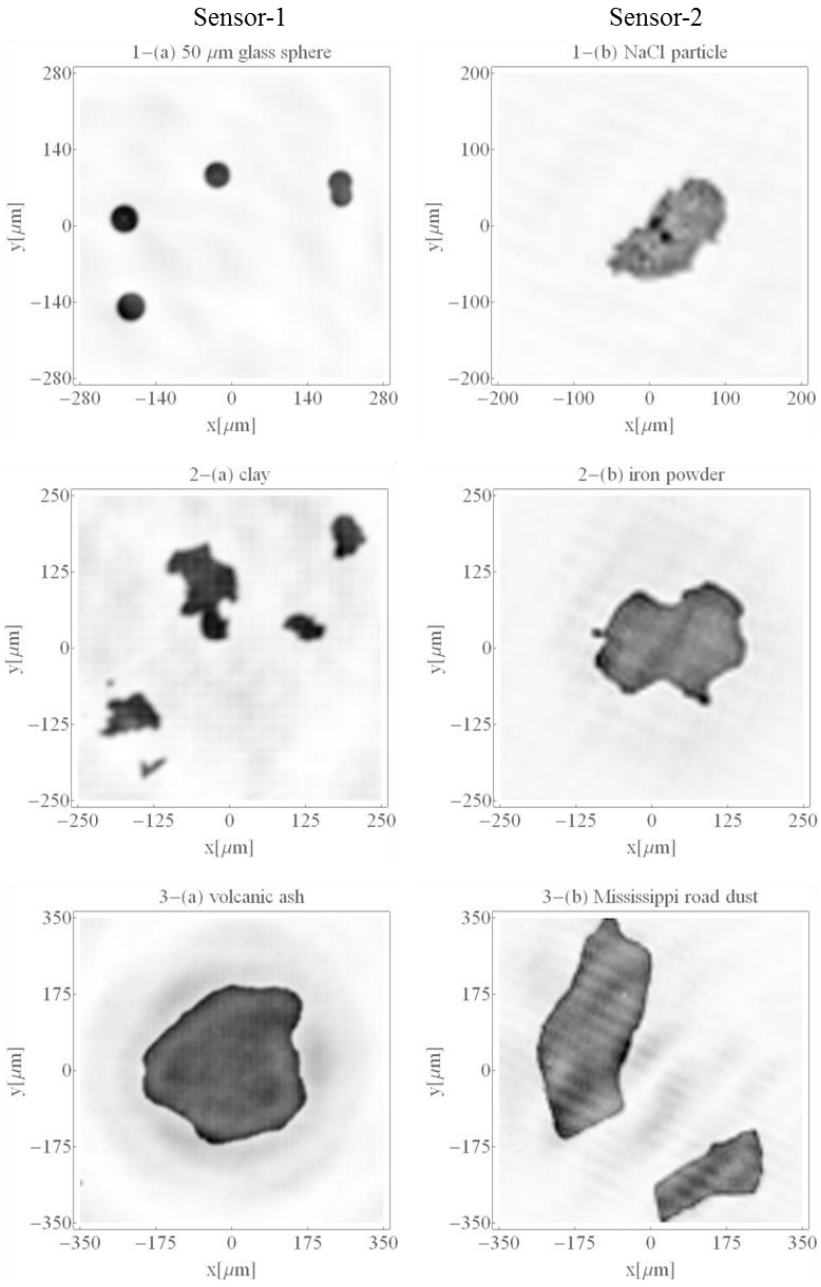

Figure 5.21 Forward-scattering reconstructed images of multiple samples.

Plots 1-(a) and 1-(b) show the reconstructed images for 50 μm glass spheres and NaCl particle due to the forward-scattered light, and images 2-(c) and 2-(d) show the same for clay and iron powder, and images 1-(e) and 1-(f) for volcanic ash and Mississippi road dust, respectively.

Likewise, a contrast hologram and corresponding reconstructed images of the two different samples due to the backward-scattered light using the arrangement in Fig. 4.11 are presented in the Fig. 5.22 below.

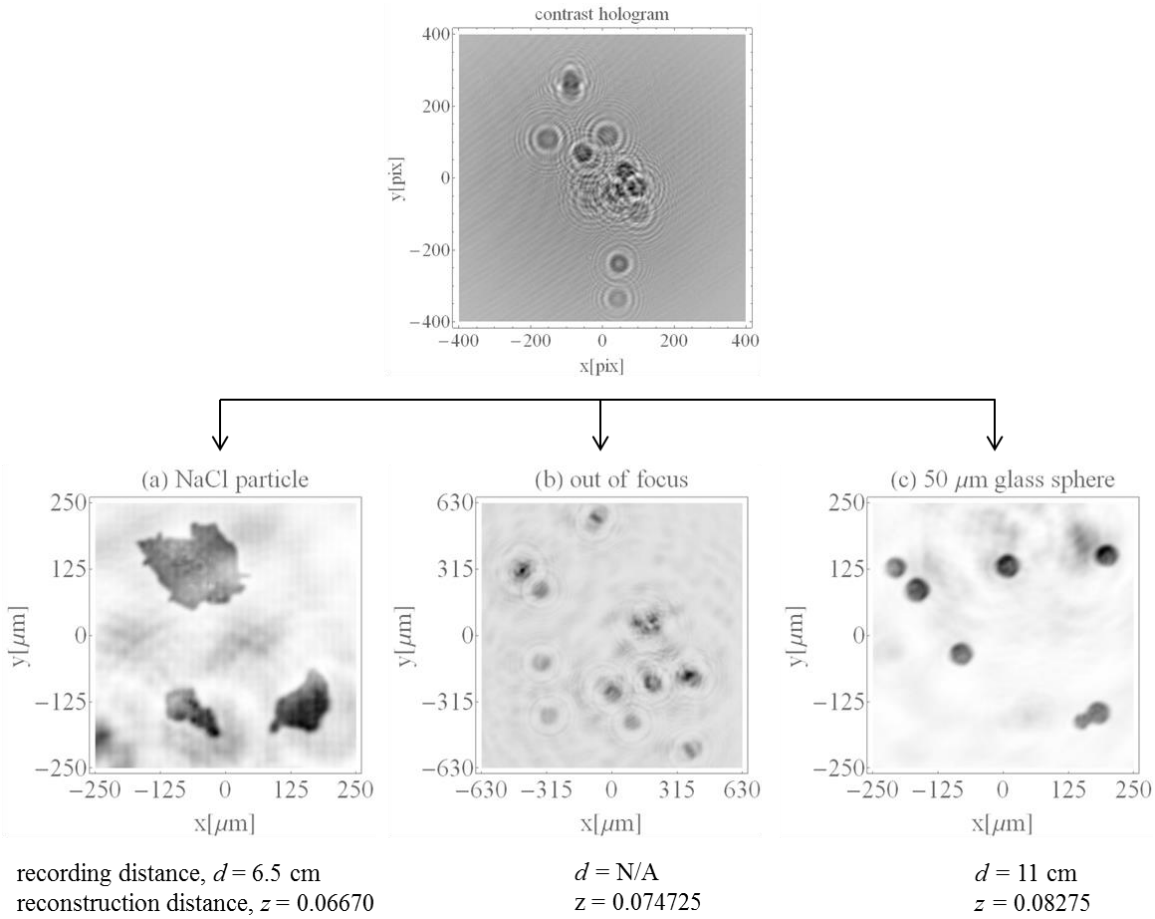

Figure 5.22 Backward-scattering reconstruction images of multiple samples.

Plot at the top is the contrast hologram of two different samples, image (a) shows the reconstructed image for NaCl particle when the reconstruction distance $z = 0.06670$, image (b) shows the out of focus image during scanning the distance, and image (c) shows the reconstructed image for 50 μm glass spheres when the reconstruction distance $z = 0.08275$, respectively.

The results presented in Fig. 5.21 are straightforward since two different samples are kept in two different stages and the corresponding forward-scattered holograms are

recorded by two different sensors, but this step is the basic idea for the next step, i.e. recording of backward-scattered holograms of two different samples simultaneously. The results in Fig. 5.22 clearly show that two different samples can be analyzed at a time using the experimental arrangement presented in Fig. 4.11. The one limitation for this step is either to keep samples at two different recording distances from the sensor or use two different coherence sources to illuminate particles separately. However, this modality is working well in quality and accuracy to the corresponding configurations and might have a greater significance in building a lightweight, cost-effective, and field-portable microscope system, which can analyze multiple microparticles simultaneously.

To my knowledge, in this work I have provided the first successful imaging modality of the multiple samples using forward- and backward-scattering light simultaneously in digital holographic microscopy.

5.8 Imaging of biological samples

Imaging of biological specimens plays a crucial role in the understanding of many physiological processes in biology. Cells are almost invisible in standard light microscopes as they do not absorb light. However, they shift the phase of the light because of the cell refractive index [3]. The digital holographic technique is taking advantage of this property of the cells and able to image them even without staining or labeling. With the capability of real-time imaging and quantitative measurements of different physiological parameters in biological specimens, different cell properties, which previously have been impossible or very difficult to study directly in living cells, such as thickness, volume, and cell refractive index, are now possible without damaging the samples in any way. Therefore, DH utilizes the phase properties of coherent light to

image a sample and extensively in use to measure cell shape, volume, and dry mass without any labeling under a very low-intensity light source [3-5]. The DH is not only limited to the imaging of cells, but also has been successfully applied to study the cell proliferation, cell movement, and cell morphology [6-8]. In this work, DH is restricted to apply only in imaging of some biological samples, i.e., plant cell samples such as mildew, ovule, parenchyma, stoma, bamboo in cross-section, spirogyra moss, etc., available in the laboratory. Despite the low resolution of the reconstructed images, some surface characteristics are clearly visible.

The reconstructed images of selected specimens are presented in Fig. 5.23 below.

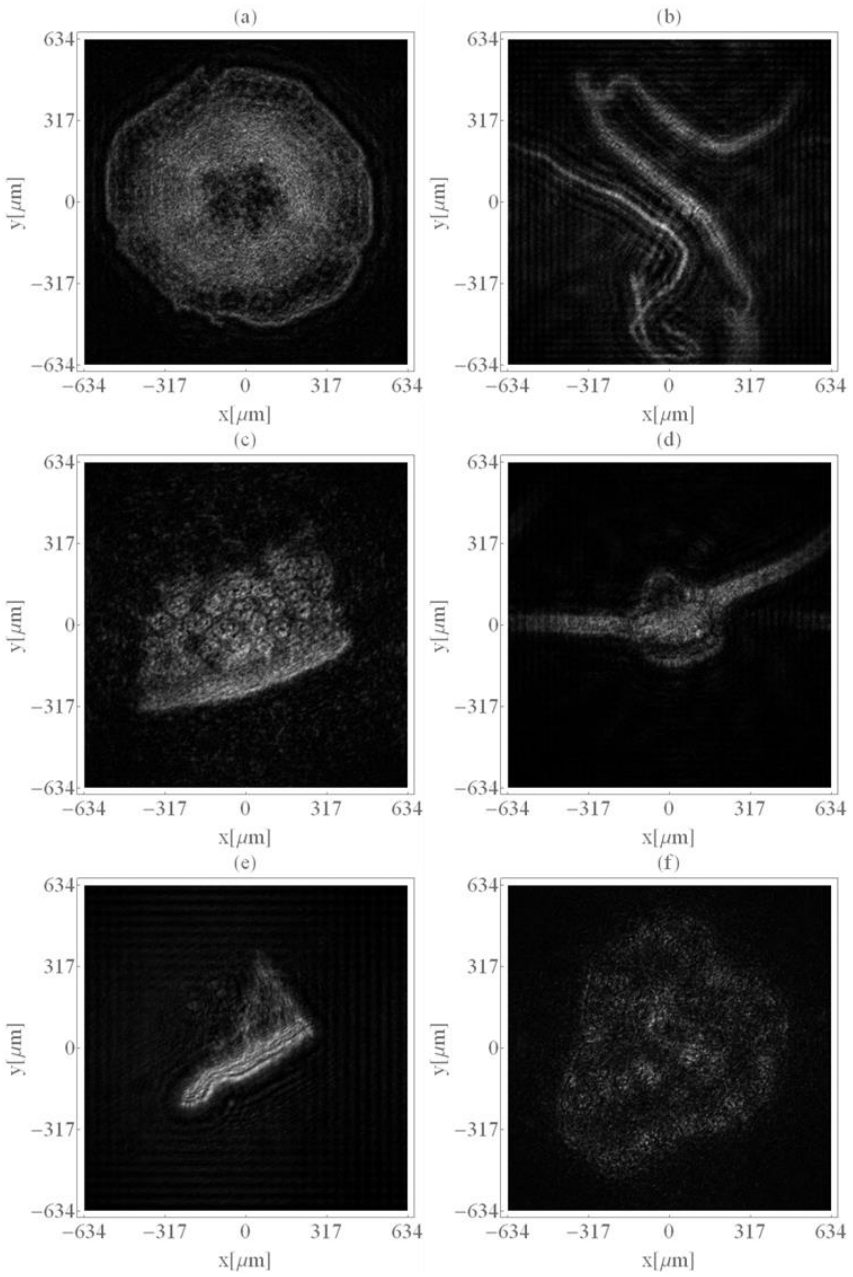

Figure 5.23 Reconstructed image of biological samples.

Image (a) shows the reconstructed image of gymnosperm steam cross-section, images (b), (c), (d), (e), and (f) show the same for spirogyra moss, bamboo cross-section, leaf veins, mildew, and ovule, respectively.

Since there are no optical elements between the sample and sensor in DH, this provides more flexibility in the working distance of several centimeters, which is

significantly greater than the single- to sub-millimeter working distance of the microscope objective in conventional microscopy. This is especially true during the high magnification using large *NA*. The absence of any optical element between the particle and sensor eliminates noise that can result from ambient dust that collects on the optical surface [9]. This makes DH a very versatile technique for many medical and biological applications.

5.9 Conclusion

This work explores the feasibility of imaging single and multiple microparticles with DH using forward- and backward-scattered light rather than the more commonly used forward- scattered light only technique. These images are computationally reconstructed from the digitally recorded holograms and compare well in quality and accuracy to the corresponding microscope images. Even though the resolution of the holographic images is less than that from the microscope, the size and shape of a single particle as small as 10 μm in size are clearly distinguishable. The resolution could be improved using a sensor with greater dynamic range, by illuminating the particle with shorter wavelength light, and using a positive lens to magnify the particle's hologram during recording. Also, replacing the particle stage with a flowing aerosol stream will help to eliminate a large degree of noise that can result from ambient dust that collects on the optical surface. The results of this work may be useful for developing a field-portable microscopy system for real-time characterization of various man-made and environmental dust particles, including liquid or frozen aerosol particles.

5.10 References

1. W. Xu, M. H. Jericho, I. A. Meinertzhagen, and H. J. Kreuzer, "Digital in-line holography of microspheres." *Appl. Opt*. **41**, pp. 5367–5375 (2002).

2. J. Geilhufe, B. Pfau, M. Schneider et al., "Monolithic focused reference beam X-ray holography," *Nat. Commun.* **5,** pp. 3008 (2014).

3. B. Rappaz, P. Marquet, E. Cuche, Y. Emery, C. Depeursinge, and P. J. Magistretti, "Measurement of the integral refractive index and dynamic cell morphometry of living cells with digital holographic microscopy," *Opt. Express* **13**(23), pp. 9361-9373 (2005).

4. B. Rappaz, E. Cano, T. Colomb, J. Kuhn, V. Simanis, P. J. Magistretti, and P. Marque, "Noninvasive characterization of the fission yeast cell cycle by monitoring dry mass with digital holographic microscopy," *J. of Biomed. Opt*. **14**(3), 034049 (2009).

5. T. Reya, S. J. Morrison, M. F. Clarke, and I. L. Weissman, "Stem cells, cancer, and cancer stem cells," *Nature* **414**(6859), pp. 105-111 (2001).

6. B. Kemper, P. Langehanenberg, and B. von Bally, "Digital holographic microscopy. A new method for surface analysis and marker-free dynamic cell imaging," *Biophotonics* **2**, pp. 41-44 (2007).

7. B. Kemper and G. von Bally, "Digital holographic microscopy for live cell applications and technical inspection," *Applied Optics* **47**(4), pp. A52-A61 (2008).

8. B. Kemper, P. Langehanenberg, A.Vollmer, S. Ketelhut, and G. von Bally, "Label-free 3D migration monitoring of living cells," *Imaging and Microscopy* **11**(4), pp. 26-28 (2009).

9. M. J. Berg and G. Videen, "Digital holographic imaging of aerosol particles in flight," *J. Quant. Spectrosc. Radiat. Transfer.* **112**(11), pp. 1776-1783 (2011).

CHAPTER VI

SUMMARY AND RECOMMENDATION FOR FUTURE WORK

In this chapter, a summary of the dissertation work described in Chapter I through Chapter V on the characterization of microparticles through digital holography is given. In addition to this, some recommendations for future research work in the area of digital holography are proposed.

6.1 Research summary

With the recent development of the technology, different accurate particle imaging and characterization techniques are now possible. What is missing, however, are precise contact-free measurements of real particles. The inherent contact-free and rapid nature of DH helps to make DH a sensitive, selective, and robust imaging and characterization technique for many applications. Since a particle's scattering pattern depends on its morphology, composition, and orientation, proper analysis of a measure pattern can be useful for characterization [1, 2, 3]. Unfortunately, no unambiguous relationship between a measured pattern and the particle characteristics is known, which is commonly known as the classical inverse problem in applied light scattering [4, 5]. Despite much work, no such method has demonstrated the ability to confidently characterize arbitrary particles *in situ*. The non-invasive nature of DH can be extended to overcome the inverse problem and in measuring the optical observables, such as the scattering pattern, total cross-sections, and single-scattering albedo [3].

Digital holography is a newly emerging particle characterization paradigm that is mostly free from the drawbacks of conventional holographic technique and can unambiguously describe unknown particle shape, size, and surface texture. One single measurement will automatically feed a novel analysis that can quantify the detailed three-dimensional (3D) morphology of these particles simultaneously with optical observables. More broadly, the outcomes of this work can be used to improve contact-free particle imaging techniques and other novel applications. Particles studied with conventional optical microscopy can distort, aggregate, and fragment upon collection. This is particularly true for liquid or frozen particles. Also, if the size of the particle falls under certain range the microscope-based techniques requires the high Numerical Aperture (NA), which dramatically restricts the depth-of-filed to $z = 2\lambda/(NA)^2 \approx 4\ \mu m$, where z is the particle to microscope objective distance, λ ($\approx 351\ nm$) is the wavelength of the light used, and NA is the numerical aperture. In that case, the position of the particle must be then controlled to within $\sim 4\ \mu m$ for the images to be in-focus. Such precision is highly challenging in practice and often requires a complex and costly microscope objective. Further, conventional optical microscopy systems come with optical aberration and require a complex optical arrangement to remove it. If multiple particles are present in close proximity, it is highly unlikely that each will be in-focus given the small value of z. In such case, the measurement must be repeated if blurred images are obtained. However, in DH technique different prospective of a single particle, separated multiple particles, or a connected cluster is possible by a single shot hologram. This is much like microscopy where some sense of a particle's 3D structure can be garnered from a single measurement. The basic idea is analogous to the "focusing in" on a different particle

focus-depth in conventional microscopy; such focusing is possible in DH computationally by varying reconstruction distance *z* after recording the particle's hologram. The entirely digital nature of DH is a big plus in rendering the image of the particles. Unlike the conventional microscopy technique, in DH the digitally recorded hologram can be used at any time and at any place to image multiple particles present at different locations in the measurement volume.

The main motivation relates this work is to the imaging of single and multiple particles from holograms derived from scattered light from different directions. This work clearly demonstrates the feasibility of different experimental designs in DH, which are capable of imaging a variety of micron-sized particles using both forward- and backward- scattering light simultaneously. Since the images of a particle are rendered from forward- and backward-scattered holograms simultaneously, a side-by-side comparison of the two images is possible. In the traditional in-line holographic configurations, the particles' forward-scattered light is usually used to form the hologram, thus opaque particles yield only a silhouette-image after reconstruction and the particle surface characteristics are obscured. We find the same is true here, yet some detail can be seen in the forward- and backward-scattered holographic images that are different. This suggests that the two image perspectives reveal aspects of the particle structure not available from a forward-scattering based image alone.

The results of this work on backward scattering light holographic imaging may be useful for studying opaque particles that must be examined in a contact-free manner, including liquid or frozen aerosol particles. This different imaging modality in DH could be supportive to insight more on the particles' morphology and crucially important for

the advancement of particle characterization technique and future instrument-development.

6.2 Recommendation of future work

There are numerous works to be done in order to establish DH as a most efficient imaging technique for many applications. Here are the some recommendations for future work:

6.2.1 Resolution enhancement

In this work, the image resolution is found to be ~10 μm. This resolution is only sufficient to distinguish various natural pollens, dust particles, and traceable borosilicate glass spheres, but fails to resolve the smaller features of many particles, such as surface roughness of the particles, spikes on the surface of the ragweed pollen spores, etc., and variation in the images in irregular shaped particles with the particle orientation. Therefore, increasing the resolution of the reconstructed image is the main objective of the future work. There are various factors affecting the resolution of the reconstructed image in DH. In short, the resolution is determined partly by the NA as defined by solid angle subtended by the sensor array at the particle. Thus, increasing the sensor array size and decreasing the distance between the particle and sensor will improve the resolution. However, the sensor pixel-size Δ greatly restricts the fringe-spacing resolved in the hologram, and hence, the fine details images. But this can be improved by increasing polar scattering angle θ. Also, the resolution of the particle images can easily be improved using a sensor with greater dynamic range, by forming hologram with shorter wavelength light, and by employing a positive lens to magnify the hologram [6-10].

Besides this, replacing the particle stage with a flowing aerosol steam helps to eliminate a large degree of stray light and improve the subsequent particle-image resolution. These steps are planned and recommended to implement in the future work to increase the resolution of the image up to the sub-micron range.

6.2.2 Measuring optical observables

The scattering cross section C^{sca}, extinction cross section C^{ext}, absorption cross section C^{abs}, and the single-scattering albedo ϖ are collectively referred to as "optical observables." Our group recently discovered that there is an inherent link between the integral of the particle hologram and these observables. Therefore, an access to the complex scattered wave amplitude K creates the possibility to do more with the digitally recorded hologram than imaging alone [11-20]. A precise measurement of these quantities is very important in the contexts of remote sensing, but there are several technical difficulties underneath the traditional way of measurement. Since they can either be directly measured, or inferred from related measurement, and have historically been used to characterize aerosols. Future work is recommended to precisely measure these observables by recording a perfectly fine single digital hologram.

6.2.3 In field research

These laboratory-based studies will establish the proof-of-principle for the forward- and backward-scattering holographic imaging techniques, which are capable of imaging both transparent and opaque particles. This concept will then be applied to investigate aerosols in the field. To do this, a simplified version of the design in Sec. 4.3 will be constructed where a modulate diode-laser is powered by two batteries and is used

to illuminate a stream of aerosol particles to form holograms on a 2D sensor. Then, a microscope objective will be used to focus the beam onto a 20 μm pinhole. This significantly improves the light's spatial coherence, enhance the hologram contrast, and eventually, quality of the particle image [6, 17, 19]. In this way, a field-portable dual-mode holographic microscope system using inexpensive diode-laser will be built to perform the field research on aerosols from the ambient environment.

6.2.4 In tomographic and topographic study of the biological specimens

Imaging techniques capable for three-dimensional (3D) profiling and sectional imaging of biological specimen are in great demand for many biomedical applications. The presently available conventional optical based microscope provides these features; however, these imaging techniques are quite complex, bulky, and expensive in addition to having a limited field-of-view due to the need of lens-based optical magnification, but the DH modality offers high-throughput lensless imaging in compact, cost effective, and light weight architectures of such specimens. Therefore, the use of digital holographic microscopy (DHM) in such applications is increasing aggressively day-by-day. The non-invasive and label-free nature of digital holographic imaging is best suited for many biological specimens [6, 8, 20-22]. For example, off-axis DH configuration in microscopy has been proven to be a very effective process for achieving high-precision, quantitative, phase-contrast mapping of biological specimens as it allows measurement of optical thickness with nanometer accuracy [21, 22]. Researchers not only in the area of optical imaging, but equally in microbiology, medicine, marine biology, metrology, are realizing the new capabilities of DH. Therefore, a future work is planned to use this forward- and backward- scattering modality of DH to study the surface profile and

sectional imaging of various transparent and absorptive biological specimens for many biomedical applications.

6.2.5 Building holographic optical trapping system

Optical trapping, most commonly known as "optical tweezer," is an increasingly important technique for controlling and probing the structure of matter at length sizes ranging from nanometers to few millimeters. Optical trapping uses forces exerted by intensity gradients in a tightly focused beam of light to trap and move a microscopic particle into a small volume of matter [23, 24]. Its unique ability to trap matter at mesoscopic scales has been particularly successful for studying a variety of biological systems in recent years. The introduction of holographic optical elements into optical trapping setups has multiplied the possibilities of the technique for precisely trapping, moving, and complexly manipulation of micron-sized particles [22-27]. The holographic optical trapping (HOT) is based on the same physical principle as the conventional optical gradient traps [23]. The area of HOT is relatively new but has become an interesting research topic with many potential applications. The basic optical trap is used to manipulate one microscopic object at a time, but HOT system is capable of creating arrays of independent optical traps using diffractive optical elements (DOE) such as a spatial light modulator (SLM) in all three dimensions in a very simple and cost effective way. This opens new era of a very versatile tool in the field of micro-manipulation [28]. Therefore, future work is planned and recommended to implement digital holographic imaging technique to build an integrated holographic optical trapping system.

6.3 References

1. C. F. Bohren and D. R. Huffman, *Absorption and scattering of light by small particles* (Wiley-VCH, 2006).

2. K. B. Aptowicz, R. G. Pinnick, S. C. Hill, Y. L. Pan, and R. K. Chang, "Optical scattering patterns from single urban aerosol particles at Adelphi, Maryland, USA: A classification relating to particle morphologies," *J. Geophys. Res.* **111** (D12), D12212 (2006).

3. M. J. Berg and S. Holler, "Simultaneous holographic imaging and light-scattering pattern measurement of individual microparticles," *Opt. Lett.* **41**(14), pp. 3363-3366 (2016).

4. F. Soulez, L. Denis, C. Fournier, E. Thiébaut, and C. Goepfert, "Inverse-problem approach for particle digital holography: accurate location based on local optimization," *J. Opt. Soc. Am. A* **24**(4), pp. 1164-1171 (2007).

5. B. J. Berne and R. Pecora, *Dynamic Light Scattering: With Applications to Chemistry, Biology, and Physics (*Dover Publication, 2000)

6. M. Lee, O. Yaglidere, and A. Ozcan, "Field-portable reflection and transmission microscopy based on lenseless holography," *Biomed. Opt. Exp.* **2**(9), pp.2721-2730 (2011).

7. V. Mico, C. Ferreira, Z. Zalevsky, and J. Garcia, "Basic principles and application of digital holography microscopy," (Formatex, 2010).

8. M. K. Kim, *Digital Holographic Microscopy: Principles, Techniques, and Applications* (Springer, 2011).

9. M.J. Berg and G. Videen, "Digital holographic imaging of aerosol particles in flight," *J Quant Spectrosc Radiat Transf*, **112**, pp. 1776–1783 (2011).

10. N. R. Subedi, N. B. Fowler, and M. J. Berg, "Backscatter digital holography of microparticles," *Opt Express,* **21** (10), pp. 12611–12616 (2013).

11. H. C. van de Hulst. *Light Scattering by Small Particles* (Dover, 1957).

12. F. Borhen and D. R. Huffman, *Absorption and Scattering of Light by Small Particles* (John Wiley & Sons, 1983).

13. M. J. Berg, N. R. Subedi, P. A. Anderson, and N. B. Fowler, "Using holography to measure extinction," *Opt. Lett.* **39**, pp. 3993-3996 (2014).

14. M. I. Mishchenko, L. D. Travis, A. A. Lacis. *Scattering, Absorption, and Emission of Light by Small Particles* (Cambridge University Press, 2002).

15. M. J. Berg, C. M. Sorensen, and A. Chakrabarti, "Extinction and the optical theorem. Part I. Single particles," *J. Opt. Soc. Am. A* **25**, pp. 1504-1513 (2008).

16. M. Born and E. Wolf, *Principles of Optics* (Cambridge University Press, Cambridge 1999).

17. P. Kulkami, P. A. Baron, and K. Willeke, *Aerosol Measurement: Principle, Techniques, and Applications*, 3rd ed. (Wiley, 2011).

18. M. J. Berg and N. R. Subedi, "Holographic interferometry for aerosol particle characterization," *J Quant Spectrosc Radiat Transf*, **150**, pp. 36-41 (2015).

19. M. J. Berg and S. Holler, "Simultaneous holographic imaging and light-scattering pattern measurement of individual microparticles," *Opt. Lett.* **41**(14), pp. 3363-3366 (2016).

20. T. Colomb and J. Kühn, *Digital holographic Microscopy* (Spinger, 2011).

21. P. Memmolo, L. Miccio, F. Merola, O. Genari, P. A. Netti, and P. Ferraro, "3D morphometry of red blood cells by digital holography," *Cytometry Part A* **85**(12), pp. 1030-1036 (2014).

22. X. Yu, J. Hong, C. Liu, and M. K. Kim, "Review of digital holographic microscopy for three-dimensional profiling and tracking," *Opt. Eng.* **53**(11), pp. 112306-1-22 (2014).

23. A. Ashkin, J. M. Dziedzic, J. E. Bjorkholm, and S. Chu, "Observation of a single-beam gradient force optical trap for dielectric particles," *Opt. Lett.* **11**(5), pp. 288-290 (1986).

24. R. Omori, K. Kobayashi, and A. Suzuki, "Observation of a single-beam gradient-force optical trap for dielectric particles in air," *Opt. Lett.* **22**(11), pp. 816-816 (1997).

25. D. G. Grier and Y. Roichman, "Holographic optical trapping," *App. Opt.* **45**(5), pp. 880-887 (2006).

26. B. Sun, Y. Roichman, and D. G. Grier, "Theory of holographic optical trapping," *Opt. Exp.* **16**(20), pp. 15765-15776 (2008).

27. A. Farré, M. Shayegan, C. López-Quesada, G. A. Blab, M. Montes-Usategui, N. R. Forde, and E. Martin-Badosa, "Positional stability of holographic optical traps," *Opt. Express* **19**(22), pp. 21370-21384 (2011).

28. M. Reicherter, J. Liesener, T. Haist, and H. J. Tiziani, “Advangaes of Holographic Optical Tweezers,” in *Novel Optical Instrumentational for Biomedical Applications*, A Boccara, ed., Vol. **5143** of Proc. SPIE (Optical Society of America), pp. 5143-5176 (2003).

APPENDIX A

RECONSTRUCTION ALGORITHM & CALIBRATION OF THE SCALE

The Mathematica codes used to reconstruct the image of the particle using Fresnel-Kirchhoff diffraction theory and calibrate the scale factor of the measurement are presented here. The following "sample" code is intended to illustrate the Mathematica methods required to replicate the experimental results described in this dissertation work.

A.1 Reconstruction of image

The reconstruction code in Mathematica is

Setting Directory

» *SetDirectory["E:\\Backscatter_holography\\June\\06-10-2016\\Ragweed_pollen\\trial-2"];*

Parameters

» $um=1.0*10^{-6}$;

» $\lambda=0.351*um$;

» $k=2.0*\pi/\lambda$;

» *pix=5.4*um;*

» $\gamma=2.0$;

» $\alpha=15.4/1.5$;

» *numFrame=5;*

Importing files from computer

» *import1=Import["raw1.fit", "Data"][[1]];*

» *import2=Import["raw2.fit", "Data"][[1]];*

» *import3=Import["raw3.fit", "Data"][[1]];*

» *import4=Import["raw4.fit", "Data"][[1]];*

» *import5=Import["raw5.fit", "Data"][[1]];*

» *import6=Import["ref1.fit", "Data"][[1]];*

» *import7=Import["ref2.fit", "Data"][[1]];*

» *import8=Import["ref3.fit", "Data"][[1]];*

» *import9=Import["ref4.fit", "Data"][[1]];*

» *import10=Import["ref5.fit", "Data"][[1]];*

» *import11=Mean[{import1, import2, import3, import4, import5}];*

» *import22=Mean[{import6, import7, import8, import9, import10}];*

Contrast hologram

» *contrast=import11-import22;*

» *holoDat=contrast;*

» *dimX=Dimensions[holoDat][[1]]/2;*

» *dimY=Dimensions[holoDat][[2]]/2;*

» *holo1=ListInterpolation[holoDat, {{-dimX, dimX}, {-dimY, dimY}}];*

» *holoDat1=Table[holo1[x, y], {x, -dimX, dimX}, {y, -dimX, dimX}];*

» *dim=Length[holoDat1];*

» *window=(dim*pix)/2;*

» *aveDat=TrimmedMean[Flatten[holoDat1], 0.33];*

» *holoDat2=holoDat1-aveDat;*

» *hologram1=ListInterpolation[holoDat2, {{1, dim}, {1, dim}}];*

» *p1=DensityPlot[holo1[x, y], {x, -dimX, dimX}, {y, -dimX, dimX}, PlotPoints→300,*

ImageSize→600, ColorFunction→GrayLevel, PlotRange→All,

AspectRatio→Automatic, Frame→True, FrameLabel→{"x[pix]", "y[pix]]", "contrast

hologram", None}, BaseStyle→{FontFamily→Times, FontSize→30},

RotateLabel→True];

Reconstruction of image

» *z=0.81450;*

» *recon1=Table[Chop[hologram1[i, j]*Exp[$\frac{i*\pi}{\lambda*z}$ *((i-1)^2*pix^2+(j-1)^2*pix^2)]],*

{i, 1, dim}, {j, 1, dim}];

» *recon=Fourier[recon1, FourierParameters→{0, -1}];*

» *window=dim/2;*

» *view1=ListInterpolation[Abs[recon]^2, {{-window, window}, {-window, window}}];*

» *p2=DensityPlot[-view1[x, y], {x, -window, window }, {y, -window, window },*

PlotPoints→300, ImageSize→600, ColorFunction→GrayLevel, PlotRange→All,

AspectRatio→Automatic, Frame→True, FrameLabel→{"x[pix]", "y[pix]",

"reconstructed image", None}, BaseStyle→{FontFamily→Times, FontSize→30},

RotateLabel→True];

Exporting image *for calibration*

» *Export[“reconstruction.tiff”, p2];*

A.2 Calibration of the holographic image

The calibration code in Mathematic is

Setting Directory

» *SetDirectory["E:\\Backscatter_holography\\June\\06-10-2016\\Ragweed_pollen\\trial-2"];*

Calibration of scale factor on standard-sized particle

» *image1Dat=Import["E:\\Backscatter_holography\\June\\06-10-2016\\Ragweed_pollen\\trial-2\\microscope_image.jpg", "Data"];*

» *α=306/135;*

» *imgX=Dimensions[image1Dat][[1]];*

» *imgY=Dimensions[image1Dat][[2]];*

» *dat1=Table[image1Dat[[i, j, 3]], {i, 1, imgX}, {j, 1, imgY}];*

» *image1Temp=Table[Reverse[dat1[[i]]], {i, 1, imgX}];*

» *image1=ListInterpolation[image1Temp, {{1, imgX*α}, {1, imgY*α}}];*

» *g1=DensityPlot[image1[x, y], {y, 1, imgY*α}, {x, 1, imgX*α}, PlotPoints→300, ImageSize→600, ColorFunction→GrayLevel, PlotRange→All, AspectRatio→Automatic, BaseStyle→{FontFamily→Times, FontSize→30}, RotateLabel→True, Frame→True, FrameLabel→{"x[μm]", None, "(c) calibrated image", None}];*

Using above calibrated scale factor on random particle

» *image2Dat=Import["G:\\Backscatter Holography\\June\\06-10-2016\\Ragweed pollen\\trial-2\\reconstruction.tiff","Data"];*

» *α=306/135;*

» *imgA=Dimensions[image2Dat][[1]];*

» *imgB=Dimensions[image2Dat][[2]];*

» *dat2=Table[image2Dat[[i ,j ,3]], {i, 1, imgA}, {j, 1, imgB}];*

» *image2Temp=Table[Reverse[dat2[[i]]], {i, 1,imgA}];*

» *image2=ListInterpolation[image2Temp, {{1, imgA*α}, {1, imgB*α}}];*

» *g2=DensityPlot[image2[x,y], {y,1,imgB*α}, {x, 1, imgA*α}, PlotPoints→300,*

ImageSize→600, ColorFunction→GrayLevel, PlotRange→All,

AspectRatio→Automatic, BaseStyle→{FontFamily→Times, FontSize→30},

RotateLabel→True, Frame→True, FrameLabel→{"x[μm]", "y[μm]",

"(c) reconstructed image", None}];

Image zoom-in

» *g3=DensityPlot[image2[x, y], {y,375, 675}, {x, 425, 725}, PlotPoints→300,*

ImageSize→600, ColorFunction→GrayLevel, PlotRange→All,

AspectRatio→Automatic, BaseStyle→{FontFamily→Times, FontSize→30},

RotateLabel→True, Frame→True, FrameLabel→{"x[μm]", "y[μm]",

"(c) reconstructed image", None}, FrameTicks→{{{{425, "-150"}, {500, "-75"}, {575,

"0"}, {650, "150"}, {725, "150"}}, None}, {{{375,"-150]"}, {450, "-75"}, {525, "0"},

{600, "150"}, {675, "150"}}, None}}];

Exporting calibrated image

» *Export["Calibrated _image.tiff", g3];*

Arranging images

» *g4=GraphicsGrid[{{raw hologram, contrast hologram}, {holographic image, microscope image}}, Spacing →{5.0, 5.0}, Frame→False];*